DIFFERENTIATION OF NORMAL AND CANCEROUS HUMAN LIVER TISSUE

THE IDENTIFICATION AND DIFFERENTIATION BETWEEN NORMAL AND SECONDARY COLORECTAL CANCER IN HUMAN LIVER TISSUE USING X-RAY INTERACTION TECHNIQUES

By

SAHAR DARVISH MOLLA, B.Sc, M.Sc

A Thesis

Submitted to the School of Graduate Studies

in Partial Fulfilment of the Requirements

for the Degree

Master of Science

McMaster University

MASTER OF SCIENCE (2012) McMaster University

Medical Physics & Applied Radiation Sciences Hamilton, Ontario

TITLE:	The Identification and Differentiation between Normal and Secondary Colorectal Cancer in Human Liver Tissue Using X-ray Interaction Techniques
AUTHOR:	Sahar Darvish Molla, B.Sc M.Sc
SUPERVISOR:	Professor Michael J Farquharson
NUMBER OF PAGES:	xvi , 119

Abstract

As secondary colorectal liver cancer is the most widespread malignancy in patients with colorectal cancer, the main aim of this study is to identify and differentiate between benign and malignant secondary colorectal liver cancer tissue. Low energy X-ray interaction techniques were used (X-ray Fluorescence and coherent scatter). XRF and coherent scattering data were collected for all 24 normal and 24 tumour matched pair tissues. Measurements of these parameters were made using a laboratory experimental set-up comprising a ^{42}Mo X-ray tube, Si Drift detector and Scintillation (NaI) detector.

Twelve elements of interest (P, S, K, Ca, Cr, Fe, Cu, Zn, As, Se, Br and Rb) were statistically explored for normal and tumour samples. Comparing normal and tumour tissues, statistically significant differences have been determined for K ($p = .046$), Ca ($p = .040$), Cr ($p = .011$), Fe, Cu, Zn, Br and Rb ($p < .01$). However, for P, S, As and Se, no statistically significant differences have been found ($p > .05$).

Coherent scatter profiles were collected and fitted for all the samples and three peaks were observed at momentum transfer values: adipose peak: 1.1 nm^{-1}, fibrous peak: 1.6 nm^{-1} and water content peak: 2.2 nm^{-1}. The Amplitude, FWHM and area under these peaks were statistically analysed. These parameters were found to be significantly higher in secondary colorectal liver tumour compared to surrounding normal liver tissue ($p < .05$) for both fibrous and water content peaks. However, no significant differences were found for adipose peak parameters ($p > .05$).

Multivariate analysis was performed using the XRF, coherent scatter and elemental ratios data separately and the accuracy of classification results of 20 unknown samples was found to be 50%, 30% and 80% respectively. However when all the variables were combined together, the classification models were improved. 17 out of 20 unknown samples were classified correctly. This study has shown that the XRF and coherent scatter data of normal and secondary colorectal liver cancer are statistically different and the combination of these variables in multivariate analysis has the potential to be used as a method of distinguishing normal liver tissue from the malignant tumour tissue.

Acknowledgements

March, my birth month, is Colorectal Cancer Awareness month and I started to write my thesis which is related to secondary colorectal liver cancer, in this month. And I was writing the whole month of April, when people wear the yellow Daffodil to show their supports for fighting against cancer. Daffodil is the March birth flower meaning of rebirth, hope, respect, regard and unrequited love. I do not know, may be all were by incidence, but thank GOD that all these made my inspiration to work hard towards this thesis. It has been my dream so that one day I can have a contribution in fighting against cancer. Therefore I would like to print this yellow daffodil here at the beginning of my thesis, as an indication of remembrance and support for those affected by cancer. We will all work hard to find solutions for fighting back cancer.

I owe a debt of gratitude to a number of people who assisted me materially and spiritually during two years of being in Canada, studying, researching and writing my thesis.

First among equals, is Dr. Michael Farquharson, my experienced caring supervisor who has supported me during these two years with his immense knowledge, patience and motivation. Thank you for giving me a unique opportunity to work on such an important interesting topic. Alia Al-Ebraheem, for sharing her experience and knowledge with me through this thesis frankly, who was abundantly helpful and offered invaluable assistance, support and guidance.

Dr. Fiona McNeil and Dr. Joanne O'Meara, my committee supervisors, for offering valuable advice and help. Fiona Ahlang, Linda Ellis, Nancy Brand and Wendy Malarek, the medical physics department staff, for their motherly support during the past two years of being in McMaster University. All my friends (Phanisree, Olga, Natalia, Ibrahim, Farshad, …) for keeping me company so not to feel lonely and for being there for me.

Vasy and Jim Daniolos my beloved people for their great support and compassion. Thank you for accepting me in your home and heart, the time that I was really helpless and alone here in Canada. Thank you for being my Canadian family.

Dr. Iraj Hormozdiari, my best teacher in life, for not only teaching me physics but also teaching me how to live and think, for generously sharing all of his prominent experiences that only decades of living can reveal them. Indeed without his great and valuable efforts, advice and sympathy I would not have been able to come to Canada and pursue my education. Thank you for being with me in all my grief and happiness.

My only brother, Saman, for his supportive gracious spirit and for all his computer help. Thank you for being with me in my hard parts of life, which indeed without you and your accompaniment and compassion it would not be possible to leave them all behind.

I would like to express my special gratitude and indebtedness to my lovely caring parents: to my mother whose continuous uncountable sacrifices, encouragement and support were unremitting source of inspiration for me. Being away from her is a real torture in my life, but thank you for being virtually with me through internet early mornings and late nights. Thank you for being my "maman Soheila". To my father, who I don't know if I would be able to thank him with any words, for his true love and advice. Thank you for putting hard on yourself to make my life comfortable. Thank you for all you gave me materially and spiritually. Thank you for being my "baba Bijan".

And lastly to my love, Fariborz, for his unquestioning support, patience and love. Thank you for your countless trust, positive attitude and soothing words. Thank you for believing in me and being with me every moment no matter how far we are from each other. Loyalty forever.

Table of Contents

List of Figures

List of Tables

Chapter 1

Introduction

Introduction

Cancer is a disorder that initiates in the cells. The human body consists of various tissues and organs and each of them are made up of millions of cells. Each cell grows, functions, replicates and dies with the help of genes inside them. As long as the cells follow these orders normally, the organs and subsequently the whole body remain healthy. Once they disobey the routines, tumours start to form and in worse cases spread through the bloodstream to other organs. However, tumours can be either benign or malignant. The latter ones are invasive and can cause damage to nearby tissues and in advanced stages spread to other organs and lead to metastases. (Canadian Cancer Society)

The abnormal growth of cells that line the inside of the colon and rectum is known as "Colorectal Cancer". It is known to be the fourth most common cancer worldwide among men and women (Jemal *et al*, 2009) and the third most commonly diagnosed cancer in Canada according to Canadian Cancer Society statistics in 2011. Out of 177,800 new cases of cancer reported in 2011 in Canada, 22,200 cases were due to Colorectal Cancer and 8,900 deaths were estimated (12% of all type). Newfoundland and Labrador have the highest colorectal cancer incidence rates among men and women and British Columbia has the lowest rates for both sexes (CCS, 2011).

In 30% of patients with colorectal cancer, the liver is the only site of metastasis which leads to the death of these patients (Pawlik and Choti, 2007). Hepatic resection is the well known therapeutic modality for most patients with colorectal liver metastasis (CRLM). However, it is difficult to define the surgical margin with 100% accuracy prior to the surgery, and if a narrow surgical margin is noted on a pathology report after the initial surgery, this may lead to a second and even in some cases multiple surgeries. One of the success factors in surgical oncology is the safe removal of all tumor tissue while preserving as much healthy tissue where possible, and this means accurately determining surgical margins. Surgical margin is a tumor free margin which is visible to the surgeon with naked eye.

Hence, there is a need for a rapid, accurate diagnostic tool that can differentiate between benign and malignant tissue at the time of surgery. The objective of this study is to develop a technique, which measures low energy X-ray interaction data that is modelled to tissue classification, and used as a method of predicting clear margins. For this end two main X-ray interactions with soft tissue; X-ray Fluorescence (XRF) and Coherent Scattering are used to identify trace elements and structural composition respectively. XRF analysis is a non destructive method and is independent of chemical bonding of the element in the sample, and has been widely used to estimate the elemental content of human tissues. On the other hand, the pattern of the scattered X-rays contains

information about the molecular structure of the tissue. Some of these studies and their results will be reviewed in this chapter.

The physics of these two interactions are discussed in detail in the next sub sections and are followed by an overview of studies using these X-ray techniques in human soft tissue. The behaviour of trace element and diffraction patterns are compared in the healthy and cancerous tissues according to previous studies and literature.

In the second chapter, the methodologies used for sample preparation, data collection, peak fitting, statistical analysis and multivariate analysis will be introduced. All the results are presented in the third chapter followed by a complete discussion.

1.1 Interactions of X-rays with Matter

X-rays, a form of electromagnetic waves, have been widely used for research and medical purposes since the German scientist, Wilhelm Conrad Rontgen, accidentally discovered them while experimenting with vacuum tubes. As an X-ray beam passes through a material, it can interact with that material. It can interact with the matter and be completely absorbed by depositing its energy (Photoelectric Absorption). It can also interact and be scattered or deflected from its original direction (Scattering).

1.1.1 Photoelectric Absorption

In a photoelectric interaction, the incident photon with energy $h\upsilon$, interacts with an inner shell electron such as a K or L shell. If the photon energy is higher than the binding energy of the shell (E_b), the electron is ejected from the atom with the kinetic energy of E_e given by:

$$E_e = h\nu - E_b \qquad (1\text{-}1)$$

The interaction cross section of photoelectric absorption is proportional to $(h\upsilon)^{-3}$ (incident photon energy) and Z^5 (atomic number) (Knoll, 1979), therefore the less the energy of incident photon and the higher the atomic number of material, the higher the probability of photoelectric absorption occurring.

After this interaction the atom is excited. The de-excitation process following the photoelectric absorption can occur through two main mechanisms; Characteristic X-ray Emission and Auger Electron Emission.

1.1.1.1 Characteristic X-ray Emission

In a photoelectric absorption process, when the incident photon energy overcomes the binding energy of the inner shell such as the K shell, and has all of its energy absorbed by the electron of that shell, it causes that electron to be ejected from the atom. This leads to a vacancy in K shell which is filled by an electron from another orbit, such as the L or M shell. This transition results in the emission of an X-ray photon. If the vacancy occurs in the K shell and is subsequently filled with an electron from the L shell, the emitted X-ray photon is called a K_α characteristic X-ray and its energy is equal to:

$$E_{x-ray} = (E_b)_{Kshell} - (E_b)_{Lshell} \qquad (1\text{-}2)$$

In quantum mechanics there are four quantum numbers which specify the state of the electron. According to Pauli's exclusion principle, it is impossible for two electrons in an atom to have the same quantum numbers. The quantum numbers for the three first inner shells: K, L and M are shown in table 1 (Lachance, Claisse, 1995).

Shell	n	l	m_l	m_s	# of orbits	# of e in shell
K	1	0	0	± 1/2	1	2
L	2	0 , 1	0 , 1 , -1	± 1/2	3	8
M	3	0 , 1 , 2	0 , 1 , -1 , 2 , -2	± 1/2	5	18

Table 1-1. Quantum numbers of K, L mad M shells

Where:

n: Principle quantum number

l: Orbital angular momentum: from 0 to n-1

m_l: Magnetic orbital quantum number: $-l < m_l < l$

m_s: Magnetic spin quantum number: ± 1/2

The transition between shells is subjected to the quantum selection rule, which determines the permitted and forbidden transitions. Among all, those transitions are allowed that satisfy the conditions stated in equations (1-3) and (1-4):

$$\Delta L = \pm 1 \tag{1-3}$$

$$\Delta J = 0, \pm 1 \tag{1-4}$$

Where L is the total orbital angular momentum of the atom and J is the total angular momentum of atom.

Thus, K_α characteristic X-ray indicates that the photoelectron ejected from the K shell and subsequently the hole is originated in K shell. It is called α because it is filled from the outer orbit, L shell. Since each element has different and unique binding energies due to the unique atomic number, the emitted X-ray is the characteristic of that particular atom; hence it is called a characteristic X-ray.

There is another possibility that the vacancy in the K shell is filled from the electron of the next outer orbit, M shell. In this case the emitted X-ray photon is called K_β characteristic X-ray, and the photon energy would be:

$$E_{x-ray} = (E_b)_{Kshell} - (E_b)_{Mshell} \tag{1-5}$$

Clearly, the energy of K_β X-ray is higher than the K_α one, since the binding energy of the L shell is higher than the M shell and increases with atomic number of element.

1.1.1.2 Auger Electron Emission

The second mechanism that can occur following the photoelectric absorption interaction is the emission of an Auger electron, in which the energy is not carried away by the characteristic X-ray emission but by the electron from one of the outer shells of the atom. The kinetic energy of the Auger electron is the difference between the atomic ionization energy and the binding energy of the shell from which the Auger electron was ejected. In low Z atoms, due to the smaller electron binding energies, Auger electron emission is most likely to happen. In the low Z materials the probability of the Auger electron emissions is higher than the characteristic X-rays emission. (Knoll, 1979)

Considering the fact that all the incident photon does not result in X-ray fluorescence, the fluorescent yield, ω, is defined as the fraction of all cases in which the excited atom emits a characteristics X-ray photon in its deexcitation. Fluorescent yield depends on the atomic number Z and it increases as Z increases (Knoll, 1979). The K fluorescence yield ω_k is given by the number of photons emitted by all K lines during a given time interval divided by the number of K level vacancies created during the same time interval. For instance ω_k for Mg and Zn is about 0.022 and 0.490 respectively (Lachance and Claisse, 1995).

1.1.2 Scattering

Scattering is another resultant mechanism of interaction of an incident photon with an atom. Considering the energy before and after scattering, it is categorized into coherent scattering and incoherent scattering. The former one, which is also called Rayleigh scattering, is an elastic scattering in which there is no loss of energy after scattering. In incoherent scattering, also known as Compton scattering, the scattered photon has less energy than the incident photon, so it is called inelastic scattering. In this study we will only use coherent scattering and Compton scattering is beyond the purpose of this study. Therefore only the coherent scattering is discussed in more details in the following subsection.

1.1.2.1 Coherent Scattering

In the coherent scattering process, also called elastic scattering or Rayleigh scattering, the incident photon interacts with the whole atom, and causes the electrons in the atom to oscillate and accelerate and in the process of decelerating emit the scattered photon at an angle θ, while, there is no loss of energy. Therefore, the recoiled atom is not ionized or excited. X-ray diffraction occurs when these scattered photons constructively interfere at certain angles. This is also known as the Bragg effect (Fig. 1). The Bragg condition is an equation relating the angle θ_B, at which the interference between the waves takes place, and X-ray wavelength, λ, and the interplanar distance, d:

$$n\lambda = 2d\sin\theta_B \qquad (1\text{-}6)$$

Where n = 1, 2, 3,... is the order of reflection.

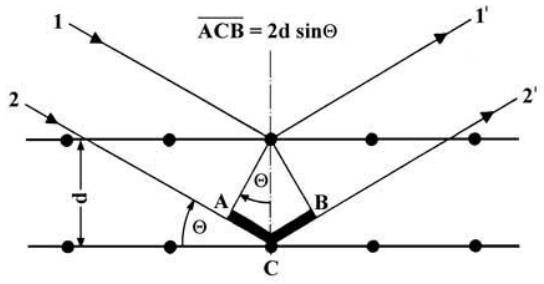

Fig 1-1. Bragg's Law (Schlot R and Uhlig S, 2000-2006)

When the photon energy is much less than the rest mass energy of the electron and the target is a free electron the classical Thompson differential cross section is used:

$$\frac{d\sigma}{d\Omega}=\left(\frac{d\sigma_T}{d\Omega}\right)F^2(x)=\frac{r_e}{2}=\left(1+\cos^2\theta\right)F^2(x) \qquad (1\text{-}7)$$

Where r_e is the classical electron radius and dΩ is the differential solid angle. The Thompson differential cross section for coherent scattering, in which the target is the whole atom, is modified with a form factor. In this case the atomic electrons act as scattering centres and the result is the coherent superposition of the amplitudes of these contributions. The differential cross section per solid angle for coherent scattering is given by:

$$\frac{d\sigma}{d\Omega}=\left(\frac{d\sigma_T}{d\Omega}\right)F^2(x)=\frac{r_e}{2}=\left(1+\cos^2\theta\right)F^2(x) \qquad (1\text{-}8)$$

This form factor depends on the momentum transfer which is generally defined as:

$$q^2=k^2+(k')^2-2kk'\cos\theta \qquad (1\text{-}9)$$

Where k and k' are the wave numbers for the incident and scattered photon respectively. In the coherent scattering case it is considered that $k=k'$, therefore eq. (1-9) is reduced to:

$$q=2k\sin\left(\frac{\theta}{2}\right) \qquad (1\text{-}10)$$

In the spectroscopy field the incident photon on the sample deflected through an angle θ, due to the momentum transferred variable defined as a function of wave length and scattered angle θ and its unit is the inverse of length (Ryan and Farquharson, 2007):

$$q = \frac{1}{\lambda}\sin\left(\frac{\theta}{2}\right) \qquad (1\text{-}11)$$

1.1.3 Attenuation of X-Rays

Passing through material, X-rays undergo attenuation. For instance, bones absorb more X-rays than biological soft tissues, meaning that X-rays are attenuated more in bone than in tissue. The transmitted intensity for a parallel monochromatic X-ray beam with an incident intensity of I_0 is given by equation (1-12):

$$I_x = I_0 e^{(-\mu_l x)} \qquad (1\text{-}12)$$

Where μ_l is the linear attenuation coefficient of the material and has the unit of inverse length. For convenience, the mass attenuation coefficient is used instead of linear absorption coefficient:

$$\mu_m = \frac{\mu_l}{\rho} \qquad (1\text{-}13)$$

where ρ is the density of material in g/cm^3. We can rewrite equation (1-12) with substituting (1-13):

$$I_x = I_0 e^{(-\mu_m \rho x)} \qquad (1\text{-}14)$$

where ρx is mass thickness, the mass per cm^2. The main advantage of mass attenuation coefficients is that they are directly comparable. It is an atomic property of each element and depends on the wavelength. It is the fraction of the intensity that is not transmitted in the same direction as the incident beam. At the energy ranges in this study, the loss of intensity is due to two processes, which were discussed in previous sections: absorption and scatter (coherent and incoherent scattering).

1.2 Overview of using X-ray techniques in human soft tissues

As mentioned in the previous section, X-ray Fluorescence and Coherent Scattering are the two main interactions of X-rays with matter in this study. Each of these methods can reveal information on composition and structure of the matter. Hence, scientists and researchers have used these techniques for human tissue analysis to identify the differences between normal and malignant tissues in various organs in the body.

In the next two subsections, an overview of trace element and X-ray coherent scatter studies in human soft tissues; such as breast, kidney, prostate, lung and liver, are presented.

1.2.1 Trace element behaviour in healthy and cancerous tissue

XRF has been widely used to measure the elemental content of materials. Particularly, XRF has been used for trace element analysis in healthy and cancerous biological tissues, such as breast, prostate, kidney, lung and liver. Benign and malignant neoplastic breast tissue trace elements were analysed by Majewska *et al* (2007) with TXRF. They found significant differences of Fe and Se concentration distribution between benign and malignant neoplastic breast tissue, whereas no significant differences observed for Cu and Zn. However, Geraki *et al* (2002, 2004) reported elevated amount of Fe, Cu and Zn in the cancerous tissue compared to benign. Likewise, Poletti *et al* (2002, 2004) reported significantly higher amount of K, Ca, Cu and Zn in neoplastic breast tissue compared to the healthy tissue. They concluded that XRF using synchrotron radiation seems to be an appropriate method to study trace elements in breast tissues and as a strong cancer diagnostic tool. Similarly, the results of Silva *et al* (2009) showed statistically significant ($p < .001$) higher concentration levels of Ca, Fe, Cu and Zn in neoplastic tissue than in normal surrounding breast tissue. They also found the concentration level of Fe and Cu are correlated in malignant breast tissue as well as the level of Ca and Zn. In 2010 Magalhaes *et al* using TXRF, revealed the same trend of results. P, S, K, Ca, Cu, Zn, Fe, Ni, Br, Se and Rb were all observed to be higher in the cancerous breast tissue compared to the healthy tissue. Farquharson *et al* (2009) worked particularly on Zn presence in invasive ductal carcinoma of breast and reported a significant increase of Zn in tumour regions with ER+ve (Estrogen Receptor) compared to surrounding tissues and non significant increase in tumour regions with ER-ve samples.

Using XRF Spectroscopy, Carvalho and Marques (2001) found an increased amount of Zn in Kidney tissue from patients with cirrhosis. In 2002 Dobrowolski *et al* quantified trace element distribution in Renal Cell Carcinoma (RCC) depending on stage of disease using Synchrotron Radiation Induced X-Ray Emission (SRIXE). K, Ca, Zn, Se, Br and Rb contents were found lower in RCC tissue compared to the healthy kidney cortex, however Cr, Fe and Cu contents were higher in RCC tissue. Their results indicated that with the progress of malignant disease the concentration of trace elements were changed. For instance, the concentration of S and Fe were decreased, whereas the concentration of Ca, Zn and Se were increased in both RCC and kidney cortices. Kwiatek *et al* (2002) also compared the trace elements in cancerous and non-cancerous kidney tissue. Cd, Cr, Ti, V, Cu, Se and Zn were found at a lower concentration level in the cancerous tissue compared to the non-cancerous tissue. Contrarily, Fe concentration level was observed higher in cancerous tissue. Al-Ebraheem *et al* (2008) have measured the level of Fe, Cu, Zn and K in malignant and normal kidney tissue. Fe, Cu and K were reduced in tumour tissue by 150%, 8% and 90% respectively, while Zn was found to increase in tumour by 26% compared to normal tissue.

There are few trace element studies in Prostate tissue determining the differences between benign and cancerous tissue, which the final results are consistent with each other. Kwiatek *et al* (2004) quantified higher concentration levels of Fe, Cr, Mn and Ca and a lower level of Zn in cancerous prostate tissue compared to benign. Pereira *et al* (2010) observed lower amount of Fe and Cu and higher amounts of Zn in prostate tissue with HPB, using an XRF microtomography method. Shilstein *et al* (2006) proposed a new diagnostic method for prostate cancer based on in vivo prostatic Zn mapping by XRF trans-rectal probe. In their study they presented higher levels of Zn in BPH (benign) and CAP (cancerous) tissue and they summarised that the Zn concentration level is more indicative parameter than PSA level for the prostate cancer.

An early trace element study on the lung tissue was carried out by Drake and Sky-Peck in 1989 using Ultramicro Energy Dispersive X-ray Fluorescence. They accomplished a discriminant analysis of trace element distribution in normal and malignant breast, colon and lung tissues. Cr, Fe, Cu, Zn, Rb and As concentration were found elevated and Ca, Br and Sr concentrations were suppressed in normal lung tissue in comparison with the malignant tissue. They presented Fe, Mn and Cu as the most substantial elements in discerning between malignant and normal lung tissue. Kuala-Kukus *et al* (1999), quantified the concentration of P, S, K, Ca, Ti, Cr, Mn, Fe, Cu, Zn, Se, Sr, Hg and Pb in 65 squamous lung cancer tissues and in 5 benign lung tissues with two different methods of PIXE and TRXRF. Ti, Cr and Mn concentration levels were found higher, whereas concentrations of Sr and Pb were found lower in female cancerous

lung tissue compared to male cancerous tissue. In 2007 Majewska *et al* determined the Cu and Zn concentrations in malignant and benign lung tissue using TXRF. They also found lower amount of Cu and Zn in malignant neoplastic lung tissue compared to the normal tissue. Recently, Zhange *et al* (2011) quantified 15 trace elements in 60 lung tissue samples from residents of Xuanwei and Fuyuan, two counties with extremely high lung cancer incidences in Yunnan province, China, of which only 8 trace elements were found to be significantly different between cancerous and benign tissues. Ni, Cu, Se and Pb were found to be higher while V, Fe, Zn and Cd were found to be lower in lung cancerous tissue than those in the benign ones.

XRF work on secondary colorectal liver cancer has been carried out by Gurusamy *et al* (2008) using synchrotron radiation. Unlike the breast tissue, the amount of Fe, Cu and Zn were reported lower in the cancerous tissue than in the normal surrounding liver tissue. Farquharson *et al* (2009) quantified the concentration level of Fe, Cu, Zn and K in colorectal liver metastasis by XRF using synchrotron radiation. Lower levels of Fe, Cu, Zn and K were observed in the cancerous tissue. They performed Receiver Operator Characteristic (ROC) analysis for all the four elements and only Zn was demonstrated to be a reliable indicator of tissue classification. Likewise, Al-Ebraheem *et al* (2008) have measured the level of Fe, Cu, Zn and K in healthy and malignant liver tissue. A significant reduction was found for all the elements in tumour tissue compared to the normal tissue by 72%, 29%, 63% and 43% respectively.

1.2.2 X-ray Diffraction Studies in healthy and cancerous tissue

X-ray diffraction allows the exploration of the atomic or molecular structure of tissue (Theodorakou and Farquharson, 2002). The pattern of the scattered X-rays has information on the molecular structure of the tissue. The number of coherently scattered photons depends on the scattering angle, thus each diffraction pattern is a signature of a unique molecular structure. Hence, coherent scattering is a well known and standard method in quantitative and structural analysis of tissues and it has been widely used for several decades. In 1987 Kosanetzky *et al* presented diffraction patterns for some plastics and several biological samples using the small angle X-ray scattering technique. Their results demonstrated that fat and bone have different forms of scattering profile from water, liver and muscle. Theodorakou and Farquharson (2009) investigated four peaks in the X-ray diffraction profile of normal and secondary colorectal liver metastasis tissues: adipose peak at 1.1 nm^{-1}, fibrous peak at 1.6 nm^{-1}, water content peak at 2.2 $nm^{-1}$and a peak due to incoherent scattered radiation at 3.4 nm^{-1}. Since the peak values were shown

to be dependent on material characteristics, any differentiation can be mainly due to the type of sample material.

Most studies have been carried out on malignant breast and normal breast tissue. Results of some of these studies are presented here. Kidane *et al* (1999) measured scattering properties of breast tissue with Energy Dispersive X-ray Diffraction (EDXRD). They found a correlation between the peak height of adipose and fibrous tissues, with the histologically estimated amount of adipose and fibrous tissue. Furthermore, Changizi *et al* (2005) studied the application of Small Angle X-ray Scattering (SAXS) for differentiation between normal and cancerous breast tissue using EDXRD. They found a sharp, high intensity peak at low momentum transfer region, about 1.1 nm^{-1} for adipose tissue. Fernandez *et al* (2002) reported that the average intensity of scattering from tumour parts is an order of magnitude higher than the intensity from healthy regions. Poletti *et al* (2002a, 2002b) and Ryan and Farquharson (2004) also studied the X-ray diffraction patterns for healthy and cancerous breast tissue using Angular Dispersive X-ray Diffraction (ADXRD). ADXRD is more accurate than EDXRD, since the momentum transfer only depends on the angular resolution of the set up of experiment, whereas in EDXRD, it also depends on the resolution of the detection system and polychromatic spectrum. The results of both of these studies also showed that adipose tissue has a sharp peak at low momentum transfer (1.1 nm^{-1}), while carcinoma has a sharp peak at higher momentum transfer region, at about 1.6 nm^{-1}. The scattering signatures of fibroadenoma, carcinoma, fibrocystichange and other benign diseases were found to be similar to water spectra and peak position. This is expected because of the high water content of these tissues.

In 2005 Castro *et al* studied the X-ray scattering patterns for healthy and neoplastic uterus and kidney. Similar patterns were observed for healthy and cancerous tissue in both uterus and kidney, consisting of a peak at momentum transfer of about 1.57 nm^{-1} followed by a broad low intensity region. They measured the peak heights relative to background ratios and they showed that this parameter is higher in healthy tissues than in cancerous tissue for both uterus and kidney.

Theodorakou and Farquharson (2009) used their ADXRD data and multivariate analysis technique and classified secondary colorectal liver cancer tissue and surrounding normal liver tissue. They declared that X-ray diffraction data can be used as a tissue classifier. Recently, Sidhu *et al* (2011) carried out measurements with SAXS and used the diffraction data and multivariate analysis to differentiate between tissue types in breast tissue. The principal component analysis results indicated that, the amplitude of the fifth-order axial Bragg peak, the magnitude of the integrated intensity and the full-width at

half-maximum of the fat peak were significantly different between tissue types. Their discriminant analysis showed that the best classification result would be achieved if all the 16 parameters were used.

1.3 Colon Anatomy and Colorectal Cancer

The digestive system in our body consists of different organs where the intake food is processed to produce energy and the waste is stored until it passes out from the body. The colon and rectum are the last parts of this system and have important role to end the digestion process. Together, they make up a long, muscular tube called the large intestine. The colon is the first 6 feet of the large intestine, and the rectum is the last 8 to 10 inches.

The colon consists of four parts namely the ascending colon, transverse colon, the descending colon, and the sigmoid colon (see Fig. 1-2). The rectum and the anus are under the sigmoid colon. The rectum is about eight inches and is a connection between the sigmoid colon with the anal canal. The anal canal is 2.5 - 4 cm long and is located between the rectum and anus.

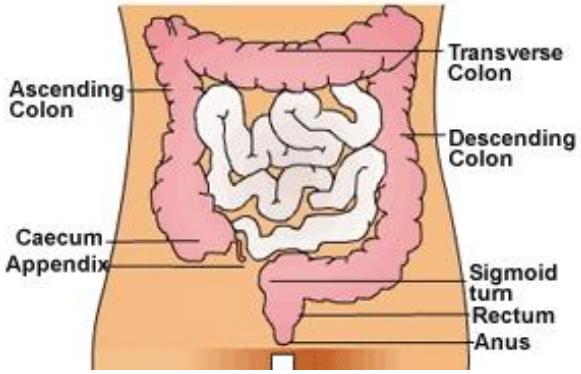

Fig 1-2. Colon and Rectum Anatomy (from Medindia)

The main function of the colon is to extract water, salts, and nutrients from partially digested food, and to propel the residue to the rectum and anus for expulsion.

Cancer is uncontrollable growth of abnormal cells which forces out the normal cells and replaces them. The walls of the colon and rectum have several layers of tissues. Most colorectal cancers start in the innermost layer and slowly spread to the other layers as the disease progresses. Many cases of the colorectal cancers initiate as polyps which are small and non cancerous growth on the inner wall of the colon. If left untreated they may develop a cancerous one.

Cancer cells can sometimes break away from a tumour and spread to other organs through the bloodstream or lymph system. Cancer that has spread in this way is called metastatic cancer. It is named a recurrence, if cancer comes back in a person who appeared to be free of the disease after treatment. In 30% of patients with colorectal cancer, the liver is the only site of metastasis which leads to the death of these patients (Pawlik and Choti, 2007). In the next section liver anatomy and secondary colorectal liver metastasis are discussed briefly.

1.4 Liver Anatomy and Secondary Colorectal Liver Metastasis

The largest organ in the body is known to be the liver with approximately 1.5 kg weight. It is situated in the upper right corner of the abdomen, lies close to the colon, the intestines and the right kidney. The liver performs over 500 metabolic functions and processed about 720 litres of blood per day. In the metabolic processes and subsequently in the absorption of nutrients, liver is the organ that plays an essential role. Secretion of bile, storing various nutrients such as fat, carbohydrate, proteins and vitamins, producing substances required for the clotting of blood, detoxification processes and clearing the body of harmful substances are some of the major functions of the liver in the body.

The liver has eight functionally independent segments, and each segment has its own vascular flow, outflow and biliary drainage. Due to this self-contained anatomy, each segment can be resected without damaging the remaining parts (see Fig. 1-3).

The abnormal growth of cells in the liver causes liver cancer, which is categorized into two types of cancer: primary liver cancer or secondary liver cancer. The former one originates from the cells in the liver; however the latter one originates in some other organs of the body such as in our case, originates in the colon and spreads to the liver. In this case it is called secondary colorectal liver Metastases (CRLM).

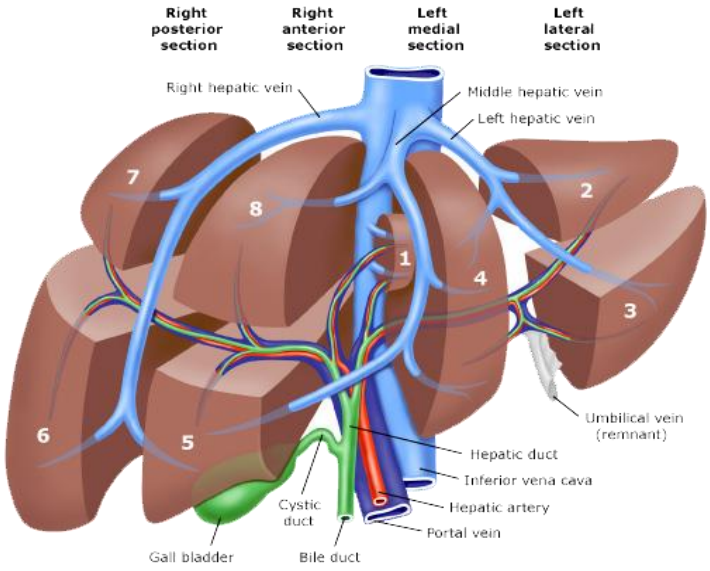

Fig. 1-3 Liver Anatomy and eight independent segments (from Health Metz)

Chapter 2

Methodology

2.1 X-ray Fluorescence Spectroscopy

The goal of X-ray Fluorescence (XRF) is to measure the characteristic emissions and determine the chemical elements in the sample quantitatively and qualitatively. To this end, the sample should be irradiated, and some amount of energy (more than the binding energy of the inner shell) should be added to the innermost atomic shell. In the transition process of electron from the outer shell to the vacancy, characteristic X-rays arise. Irradiation of the sample can be done through different methods such as irradiation using elementary particles of sufficient energy (electrons, protons, α-particles, etc.), irradiation using X- or gamma rays from radionuclides and irradiation using X-rays from an X-ray tube. Due to safety and protection aspects, using an X-ray tube is technically the most straightforward method compared to the other methods.

In this study, The X-ray source is a molybdenum micro focus tube source that is monochromated to approximately 17.5 keV and focused to deliver a 1.8mm × 1.8mm beam of approximately 3.5×10^6 photons per second on to the sample, achieved using a multi layer x-ray optics device (see Fig 2-1). The light elements in the range of 1.88 keV to 13.7 keV consisting of P, S, K, Ca, Cr, Fe, Cu, Zn, As, Se, Br and Rb are excited by the ^{42}Mo X-ray source. The resulting XRF spectrum shows the intensity of X-rays at different energies. Energy of K_α for these elements is represented in table 2-1.

Region	Element	K_α Energy [keV]	Region	Element	K_α Energy [keV]	Region	Element	K_α Energy [keV]
ROI 1	^{15}P	2.010	ROI 2	^{24}Cr	5.410	ROI 3	^{33}As	10.538
	^{16}S	2.311		^{26}Fe	6.049		^{34}Se	11.221
	^{19}K	3.315		^{29}Cu	8.050		^{35}Br	11.927
	^{20}Ca	3.692		^{30}Zn	8.642		^{37}Rb	13.395

Table 2-1. K_α Energy for the elements of interest

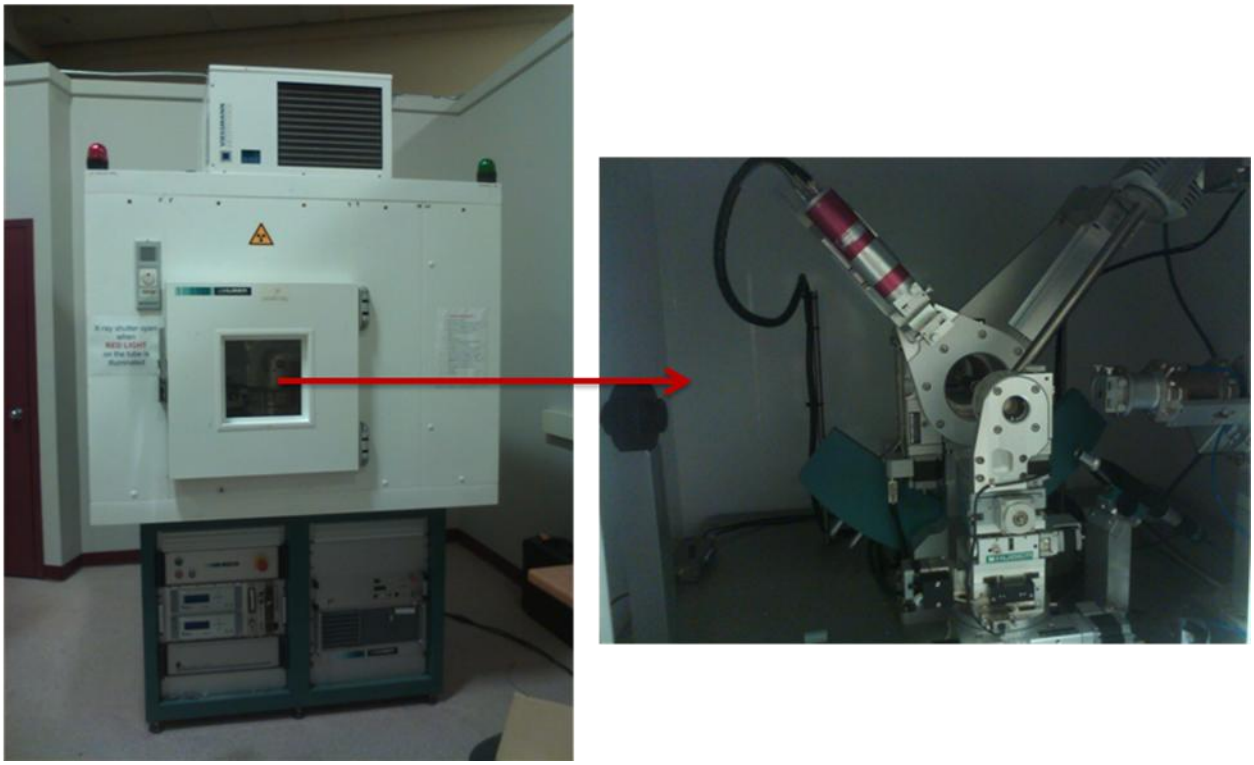

Fig. 2-1 XRF and Coherent scatter measurement system

2.2 Sample Preparation

A total of 58 samples were used in this study, 29 being secondary colorectal liver cancer tissues and 29 normal liver tissues. After resection, all samples were kept frozen at -80°C. At the time of measurement, the samples were defrosted and mounted in sample holders made from high-density polyethylene. The holders are cylindrical in shape with a recess cut into the end that is 4 mm diameter and 2 mm deep. The walls of the recess are 100 μm thick (see Fig. 2-1). To avoid contamination, the sample holders were cleaned by storing them in nitric acid over night followed by washing with de-ionised water in an ultrasound bath for approximately 3 hours. The sample holders were then stored in 70% ethanol until needed for measurement. Sample preparation was carried out in a bio-cabinet and all the tools being used were cleaned with 70% ethanol beforehand. Each sample was transferred from the freezer to the air flow cabinet to be defrosted. The samples were placed into a sample holder using sterile surgical blades and tweezers, and

were then sealed in place using a small piece of 4 μm XRF Ultralene film and secured using an O ring that had been cleaned in the same manner as the sample holders.

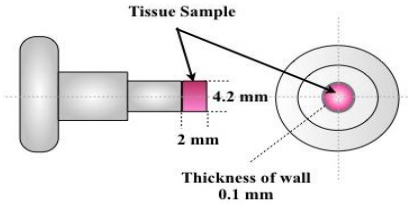

Fig. 2-2 Schematic and Dimension of Sample Holder

2.3 Data Collection

XRF and X-ray scattering data were collected and analysed respectively. In order to prevent degeneration of the sample, a refrigeration unit encapsulates the experimental apparatus in order to maintain a constant sample temperature. Since the concentration level of trace elements in human tissues are quite low, long measurement times are required to obtain reasonable counting statistics.

2.3.1 XRF Measurement

The experimental set up for the XRF measurements is shown in Fig. 2-3. The detector used is a silicon drift detector (SDD) that is collimated to have an active area of 10 mm^2 (XFlash LE SDD, Bruker AXS, GmbH, Karlsruhe, Germany) and is a distance of 5 mm from the end of the sample, to avoid the air path attenuation of the XRF response. A 90° geometry between the incident X-ray beam and detector was used in order to minimise the scattered radiation reaching the detector. The sample is rotated in the beam about a central axis during the measurement so that all of the tissue is probed by the incident X-ray beam and the inhomogeneity effect is eliminated. Measurements were made during the day or overnight with the x-ray tube operating at the voltage of 50 kV and current of 500 mA with a counting time of 26100 seconds (during the day), or at 50 kV and 320 mA with a counting time of 52200 sec (overnight). These voltage and current settings were chosen to have approximately the same x-ray beam intensity during the day and overnight measurements. The energy dispersive XRF spectrum is recorded using a software package (QM100) supplied by Bruker-AXS and data can be exported in excel format for processing. A typical XRF spectrum with all the elements of interest within the energy region of 1.88 to 18 keV is shown in Fig. 2-4. The Ar peak shown in the spectrum is due to the ionization of air in the radiation beam and it is not from the sample tissue.

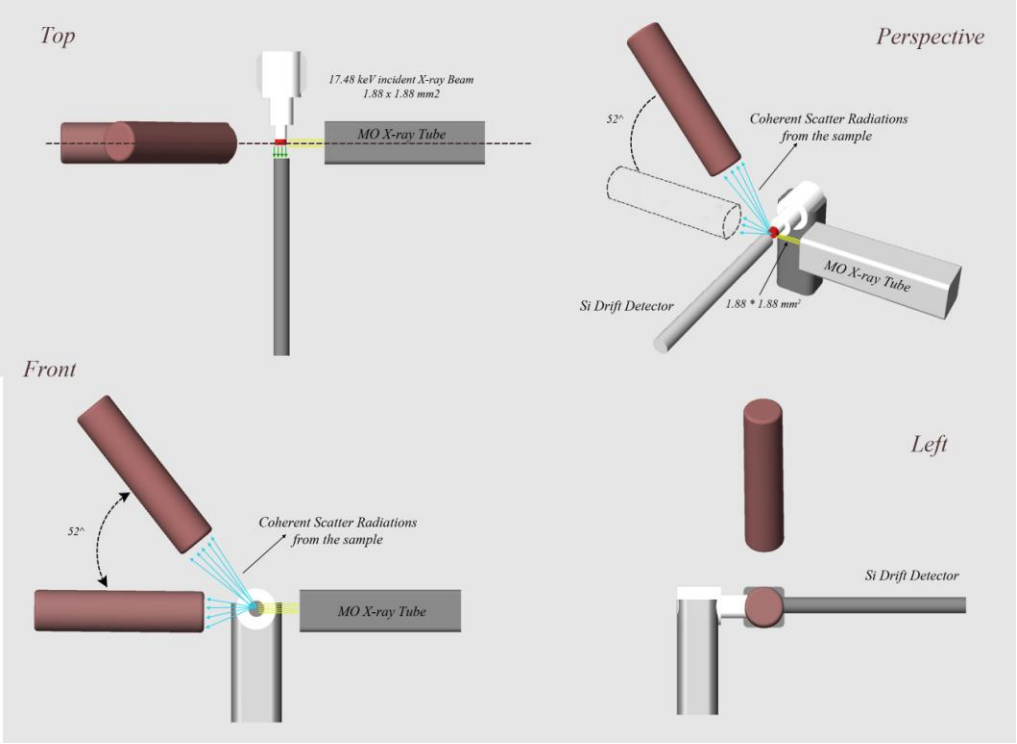

Fig. 2-3 Schematic of Experimental Geometry for the XRF and coherent scatter measurements

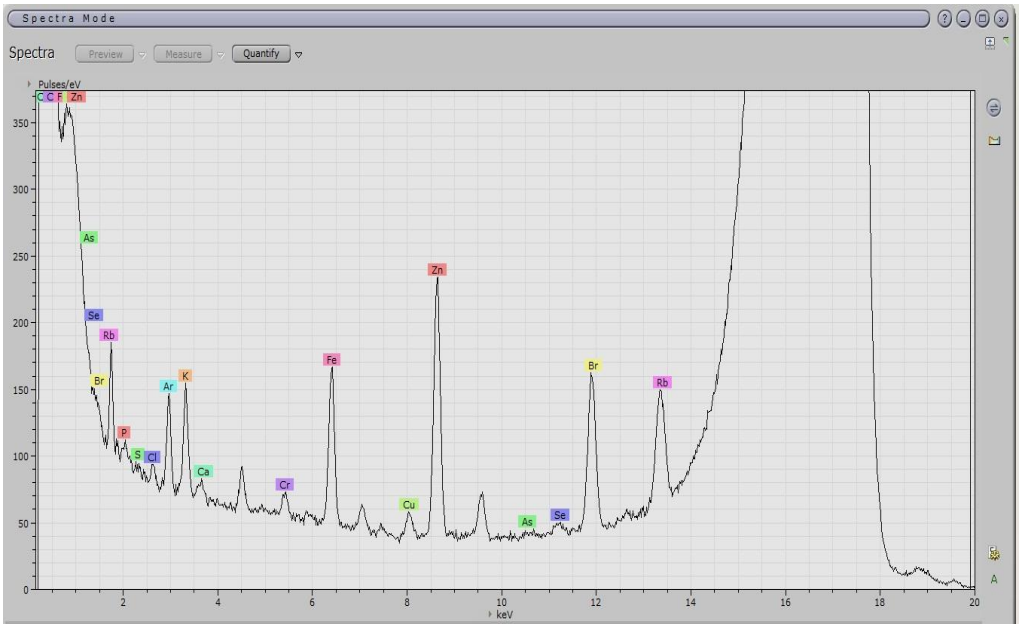

Fig 2-4 Typical XRF Spectrum for one of the Samples with the K_α of elements of interest within ROI 1.88 keV to 18 keV

Fig. 2-5 shows the averaged spectrum (all data; tumour and normal) for the ROI of 1.88 keV to 4 keV and the K_α and K_β X-rays of the elements in this region (P, S, K, Ca). Fig. 2-6 depicts the averaged spectrum (all data; tumour and normal) for the ROI of 5 keV to 10 keV and the K_α and K_β X-rays of the elements in this region (Cr, Fe, Cu, Zn).

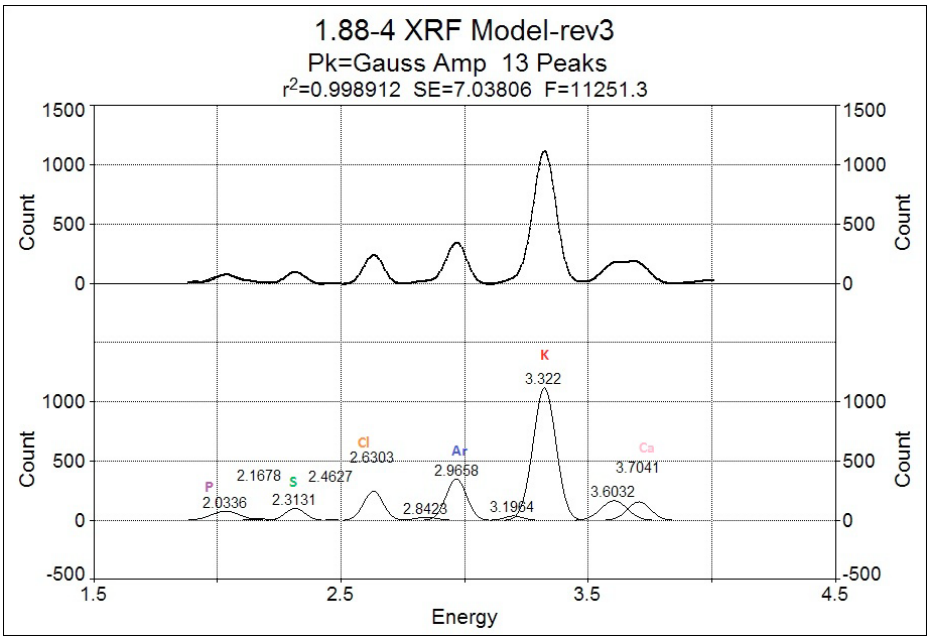

Fig 2-5. Typical peaks fitted in ROI 1

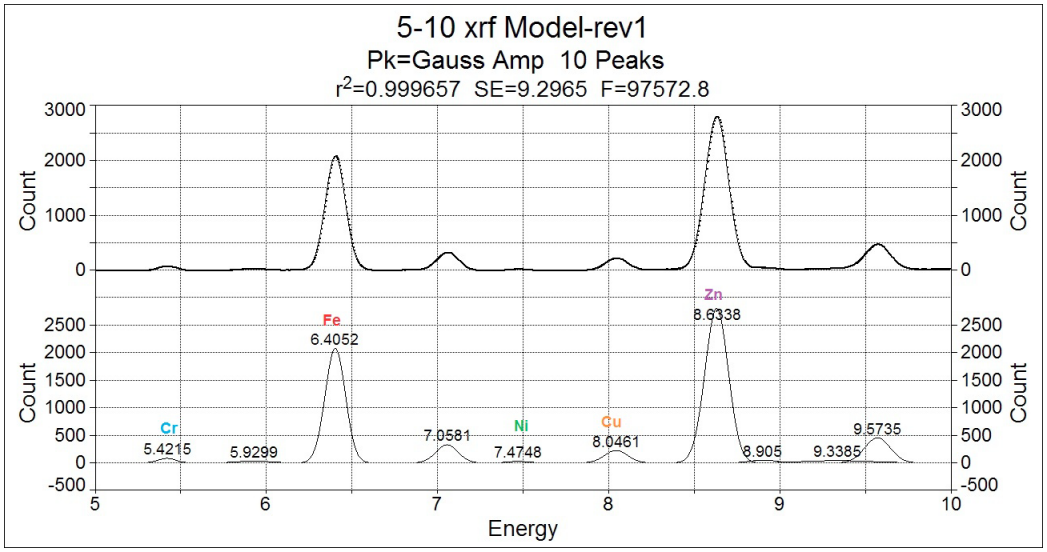

Fig 2-6. Typical peaks fitted in ROI 2

Fig. 2-7 shows the averaged spectrum (all data; tumour and normal) for the ROI of 10.35 keV to 13.7 keV and the K_α and K_β X-rays of the elements in this region (As, Se, Br, Rb).

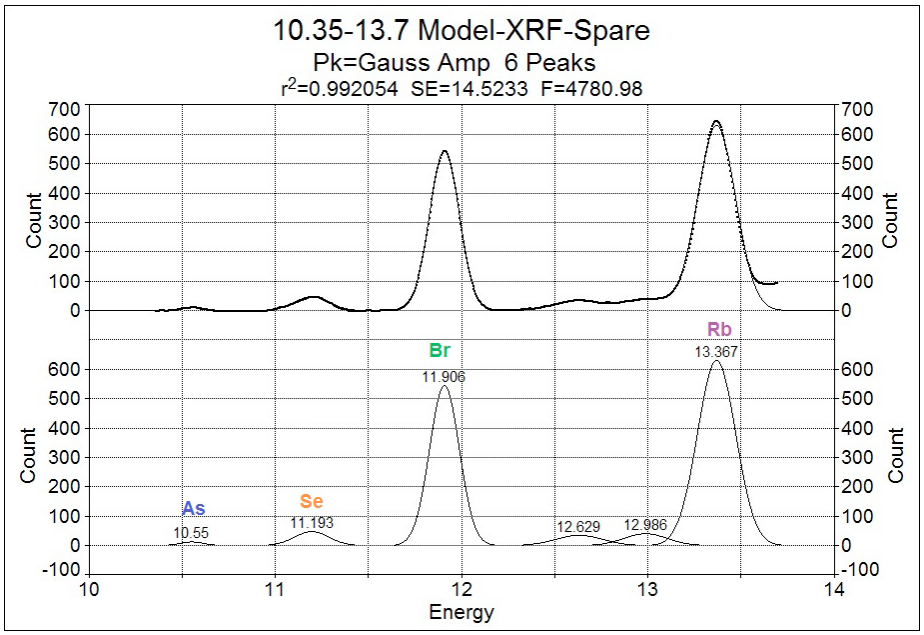

Fig 2-7. Typical peaks fitted in ROI 3

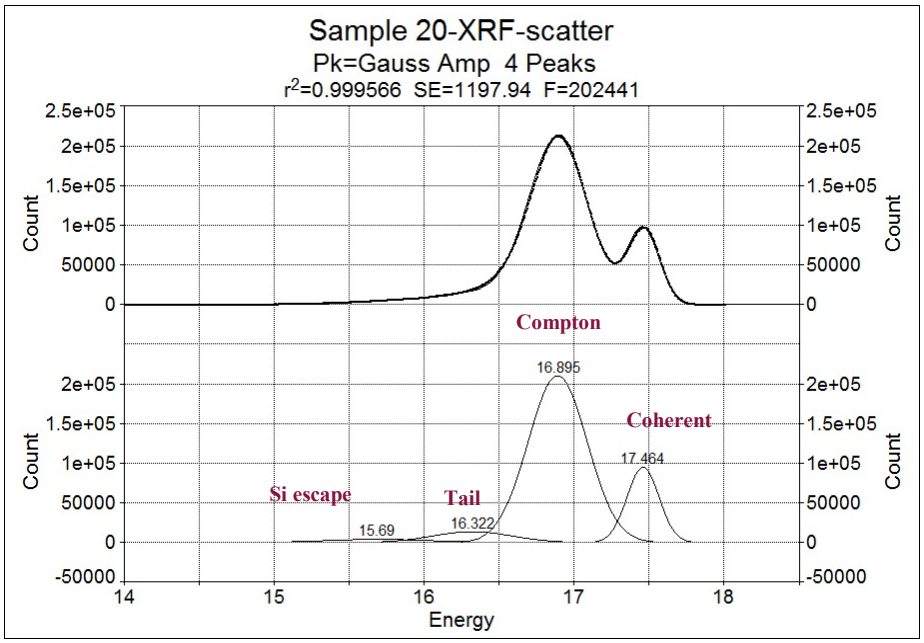

Fig. 2-8 Averaged Spectra for the ROI 14 keV to 18 keV (scattered region)

Fig. 2-8 shows the scatter region including the Si escape peak, tail, Compton (inelastic scattering) and coherent (elastic scattering) scatter peaks. Theoretically, the Si escape peak is the effect related to the characteristic X-ray generated by the interaction of incident radiation within the detector. A small X-ray escape peak is observed 1.8 keV below the full-energy peak. The tail is due to incomplete charge collection at the detector surface.

2.3.2 Coherent Scattering Measurement

In this study, coherent scatter was measured using an angular dispersive technique. Fig. 2-3 shows a schematic of the experimental set up. The range of angles at which data was collected was from 5° to 25° at interval steps of 0.5° and then from 28° to 52° in steps of 3°. This set up is due to the fact that, the peaks which shows the structural composition of a tissue are mostly over an angular range of 5° to 24.5° corresponding to a momentum transfer range of 0.615 nm^{-1} to 2.991 nm^{-1}. After this range there is no structural information, therefore in order to save time and hard memory and to end the spectrum properly the interval steps of 3° are selected for this range. This can be seen in Fig. 2-9 clearly. The Fourth peak at 3.395 nm^{-1} is due to the incoherent scattering radiation which is not in the scope of our research. The sample rotation is programmed such that the sample undergoes one complete rotation for each angular measurement in 500 sec during the day and in 1000 sec overnight measurements with the total counting time of 26100 sec and 52200 sec respectively. The result is a spectrum of photon counts as a function of momentum transfer (see Fig. 2-9).

All the data are normalised to unity to remove any effects of changing in X-ray source flux and time of measurement. Since self attenuation correction was needed for the diffraction data, before each coherent scatter measurement, incident flux and transmitted flux from the sample were measured. The ratio of the transmitted and incident flux was used for the self attenuation correction of coherent scatter data for each sample. The averaged count of all the samples (normal and tumour) versus momentum transfer plot is illustrated in the Fig. 2-9.

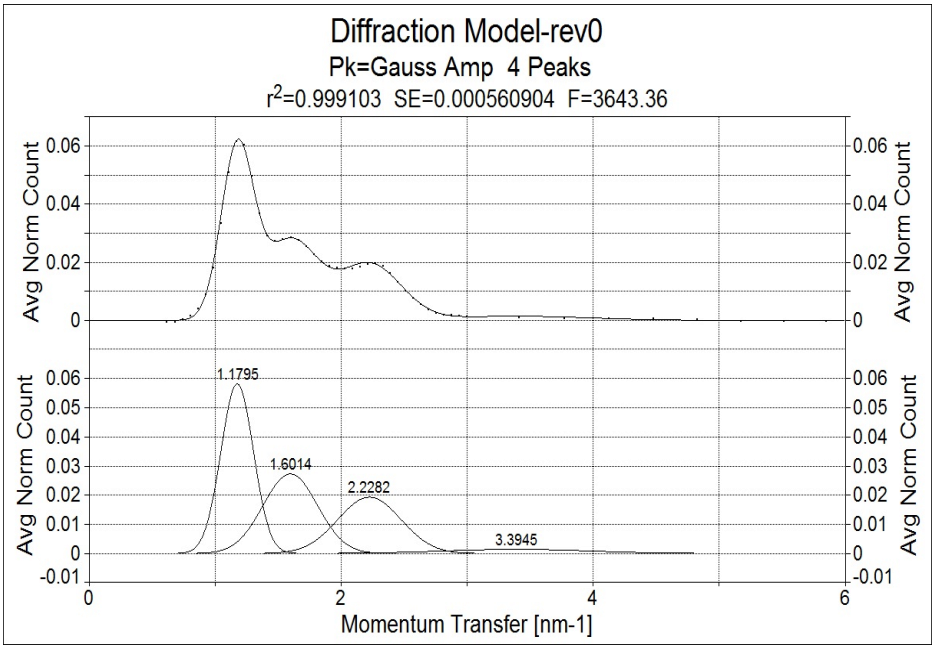

Fig. 2-9 A typical coherent scattering profile

2.4 Peak Fit

All the collected spectra were analysed using Peak Fit software (PeakFit™ v. 4.12, Seasolve Software Inc.). For peak fitting, first the background was subtracted followed by smoothing procedure. Smoothing of peak is done in order to suppress any statistical fluctuations which may be associated with the uncertainty of each channel contents. The peaks for each sample spectrum were fitted with peakfit's Gaussian amplitude version separately, and the peak parameters (amplitude, FWHM, area under the peaks) were determined.

For the XRF part, each peak of the elements of interest in the 3 ROIs was fitted for all normal and tumour samples and the amplitude, FWHM, integrated area under the peak were determined. As an example, two fitted samples using the models shown in Figs. 2-5 to 2-8, one normal and one tumour sample, are illustrated in Fig. 2-10 and Fig. 2-11, respectively.

The areas obtained from peak fit, were normalised to the incident scatter counts by dividing the elements' integral area by the total integral area of the scatter region to remove any effects of changing in X-ray source flux and time of measurement.

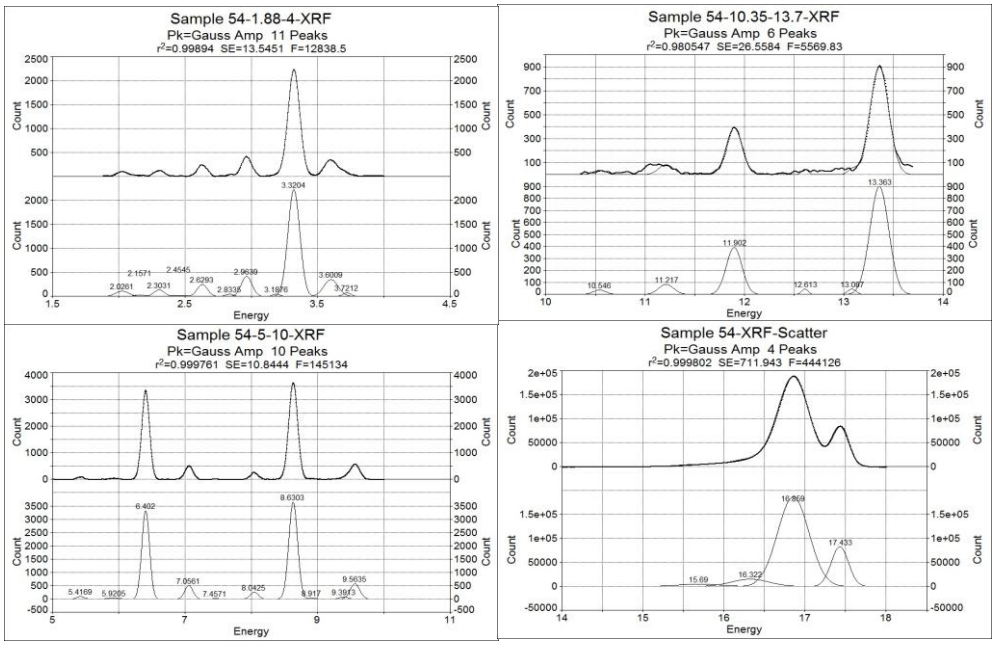

Fig. 2-10 Peak Fitting for 3 ROIs for sample # 54 (Normal Sample)

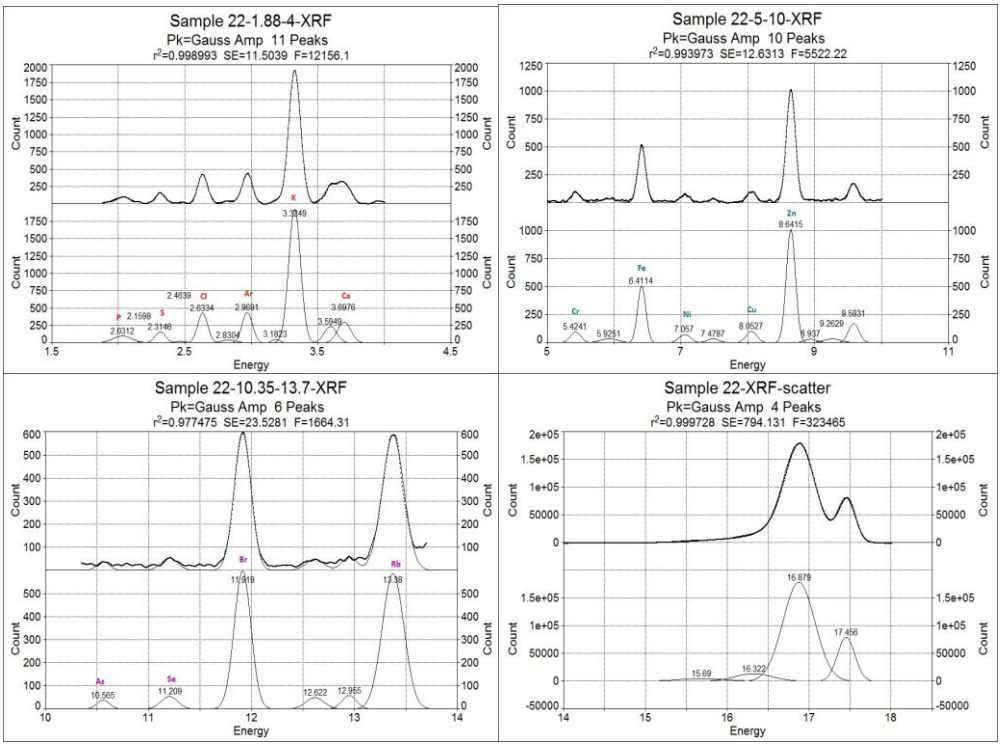

Fig. 2-11 Peak Fitting for 3 ROIs for sample # 22 (Tumour Sample)

For the coherent scatter part, the fitted coherent scattering spectra of one normal and one tumour sample using the model shown in Fig. 2-9, are shown in Fig. 2-12 and Fig. 2-13, respectively.

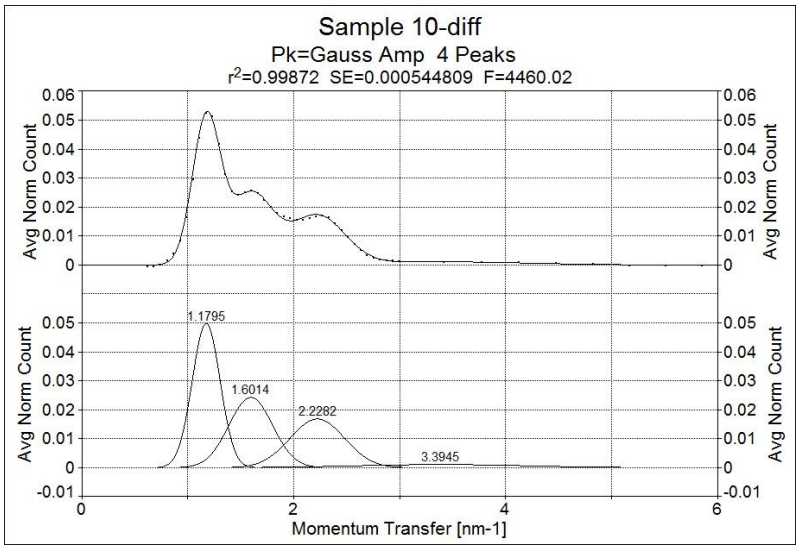

Fig. 2-12 A typical fitted coherent scatter spectrum for a normal liver sample

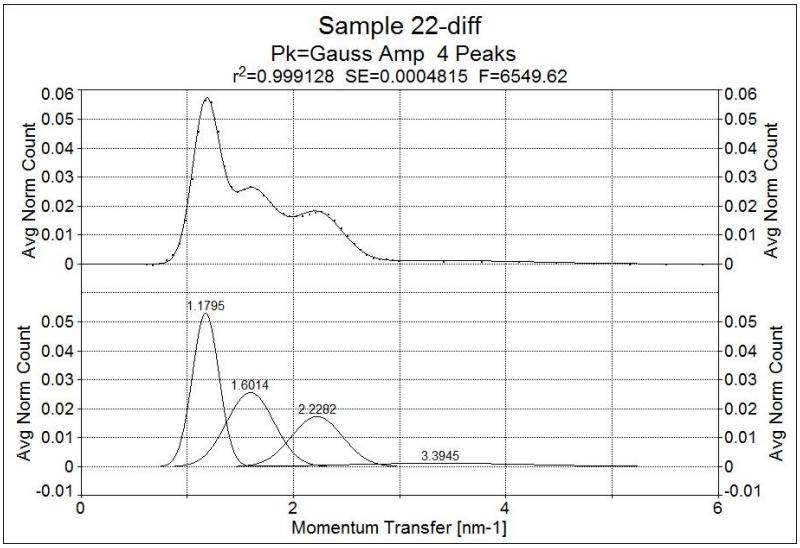

Fig. 2-13 A typical fitted coherent scatter spectrum for a tumour liver sample

Information presented on top of each plots are: type of peak (Gaussian), number of peaks fitted, Fit Standard Error (SE) and F-statistic (F).

2.5 Statistical Analysis Methodology

The XRF and coherent scattering data were statistically analysed using statistical software SPSS v.19 (SPSS Inc.) and the level of 12 elements of interest and coherent scattering parameters were compared respectively between all the 29 matched pair tumour and normal liver tissues. It was found that 5 matched pair samples had high amount of Fe and Zn, thus as outliers, they were excluded from the data for the rest of the analyses. Descriptive statistics was performed to find out the mean and standard deviation values for all the variables. Shapiro-Wilk test was used as a method of normality check. For all the elements and coherent scattering parameters of which data were normally distributed, the paired-samples T-Test was used with 95% confidence level in order to investigate the significant parameters. For those which were not normally distributed Wilcoxon test was used. These tests assess whether the means of the normal and tumour groups are statistically different from each other.

In order to investigate more statistically significant parameters between cancerous and normal liver tissue, forty six ratios of elements were examined. Out of forty six ratios, three ratios were normally distributed, and forty three were not normally distributed. Twenty one ratios were found to be statistically significant with $p < .001$.

In order to have a better visualization of the statistical results, box plots were used. It has advantages in that it displays the median, interquartile range and the smallest and largest values for a group of samples. A typical box plot of concentrations of Br, Rb for tumour and normal tissues is shown in Fig 14. The black horizontal lines show the median and each box extends from the 25^{th} to the 75^{th} percentile. Whiskers extend to the largest and smallest observed values within 1.5 box lengths. The circles are samples with values between 1.5 and 3 box lengths from the upper or lower edge of the box. Samples shown with stars are called extreme values, which are samples with values of more than 3 box lengths from the upper and lower edge of the box.

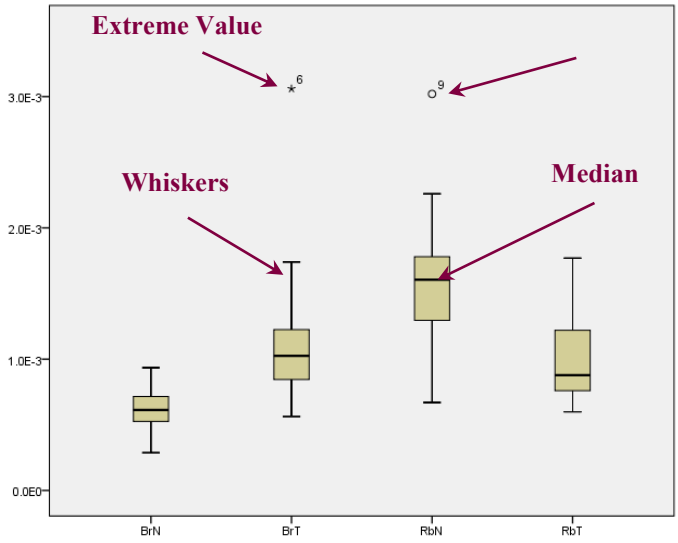

Fig. 2-14 A typical annotated Box Plot

2.6 Multivariate Analysis and Modelling Methodology

The objectives of multivariate analysis are data description, discrimination and classification. Principal Component Analysis (PCA) is a useful method used for the first objective; descriptive and explorative data structure modeling. Discrimination copes with the separation of groups of data. Soft Independent Modeling of Class Analogy (SIMCA) is used for the classification. The main objective of classification is to assign new samples to the class to which they demonstrate the largest similarity.

Multivariate analysis software, Unscramble v. 9.8 (CAMO Software Inc.) was used for the data modelling. In order to perform SIMCA classification PCA must be carried out on the data set for each individual class of samples. Hence, firstly, PCA was carried out for all the normal and tumour samples and two PCA models were built to assess if samples fall into separate clusters and to determine significant variables and outlier samples. Samples were categorized as 24 normal, 24 tumour liver tissues. Four subgroups, each consisting of 5 samples, randomly, picked out of all the samples and treated as the unknown samples. These models were used in SIMCA approach to classify the unknown samples.

These procedures were performed four times with different variables. The first run was with the XRF elemental variables. Eight elements: K, Ca, Cr, Fe, Cu, Zn, ^{35}Br and ^{37}Rb, which showed a significant difference in tumour and normal liver tissues, were

selected for the PCA modelling. The samples in four unknown subgroups were classified according to these set of variables. The second run was carried out with six coherent scattering variables: amplitude, FWHM and area under the fibrous peak and all those for water content peak. Once more, the samples in four subgroups were classified according to these six variables. The poor classification results of these two runs, lead to the selection of other variables which are strongly significant between tumour and normal tissues. As it was mentioned before, twenty one ratios of different elements were found to be prominently significant and therefore PCA was carried out once again with this new set of variables. The unknown samples in four subgroups were classified and the accuracy of the results was improved. Ultimately all these variables were combined together and the final PCA was performed. SIMCA classification procedure was carried out with these amalgamated variables for all the unknown samples of four subgroups. In all the cases 4 PCs were used for the best and optimum results.

In the following subsections PCA and SIMCA procedures will be briefly presented (from Esbensen, 2006 guide book).

2.6.1 What is PCA?

Principal component Analysis (PCA) is a mathematical transformation of data which entails breaking up X data matrix into a structure part and a noise part. X matrix is a n by p matrix, which n is the objects and p is the variables. The objects in this research are all the tumour and normal liver tissue samples while the variables are the measurements for each object, which in this case the variables are all the elemental contents (elements and their ratios) and structural composition of tissues from coherent scattering parameters (amplitude, FWHM, area of adipose, fibrous and water peak). All these variables unanimously characterise each and all of the samples. The main advantage of PCA is that there is no limitation on the number of variables for the characterisation of the samples. It is difficult to visualise more than 3 variables in the variable spaces, therefore to simplify this, assume that p = 3. Therefore the variable space has three axes; x_1, x_2 and x_3 and each sample can be characterised by its coordinates (x_1, x_2, x_3). In Fig. 2-15*a* which is the plot of all the samples in the Cartesian co-ordinate, a prominent trend can be seen. The swarm of data is positioned along the direction of maximum variance (spread of samples) of the direction represented by the central axis. This central axis is called the first principal component or PC1. Least squares fit is the mathematical method to find out the principal components. For this purpose all the points are projected perpendicularly down onto the central axis, which this can be seen in Fig. 2-15*a*. This perpendicular distance of the sample i from the line is called sample residual, e_i. PC1 is

then the line that minimises $\sum (e_i)^2$. The large object residual is the implication of poor fitting, meaning that the model does not represent the original data very well.

Usually the swarm of samples shows a trend in more than one direction. In this case the higher-order principal components can be defined. The second principal component (PC2) is the line perpendicular to the PC1 and in the direction of the second largest variance (see Fig. 2-15*b*). The process of finding these orthogonal axes is continued until the final set of PCs has the ability to completely describe any variation within the data set. In most of the cases the total variation in data can be described about 99% only with PC1 and PC2. Thus, a transformation into a more relevant co-ordinate system and a reduction in dimensionality are the major objectives of PCA.

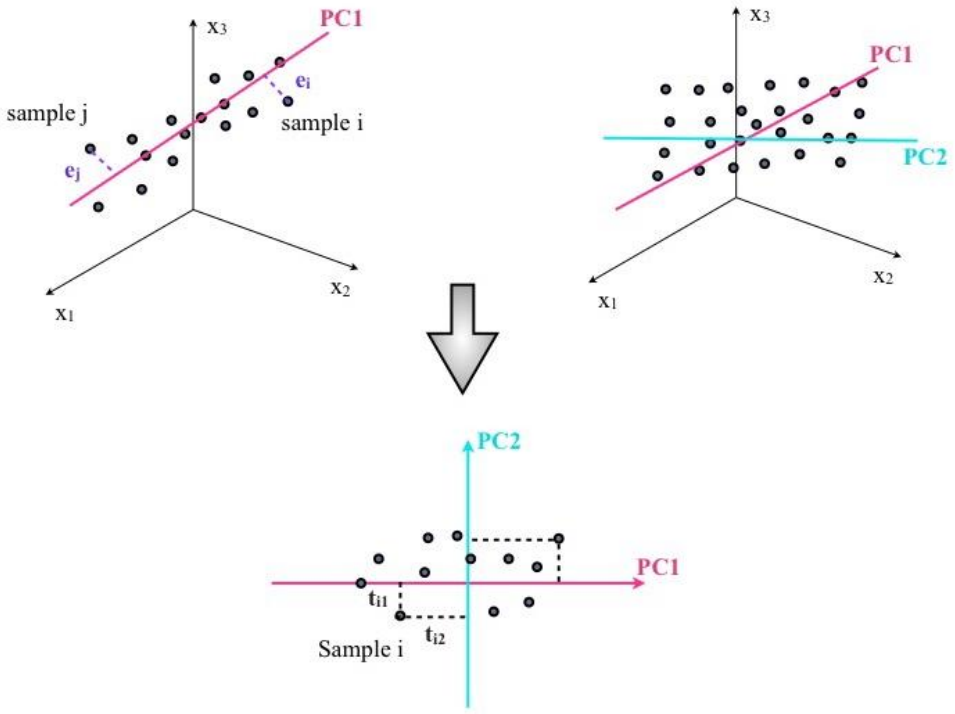

Fig. 2-15 a. Samples' co-ordinates in Cartesian space and data swarm with PC1. **b.** Data swarm with two PCs. **c.** Scores as PC-coordinates (Esbensen, 2006)

The coordinate of a sample in PC space is called a score which in Fig. 2-15*c* is designated as t_{i1} and t_{i2}. This transformation to PC space is the result of PCA and it would be visualised by the score plot. Indeed, a score plot is the map of samples and can be viewed as how the objects are related to one another. The most commonly used plot in analysis is the score plot of PC1 versus PC2. A typical score plot of samples is illustrated

in Fig. 2-16. This is the plot of all the samples, and it is clear normal samples are separated from the tumour ones; however there is an overlap around the origin. Two numbers can be seen at the bottom of Fig. 2-16, which correspond to explained variance, computed as the complement to residual variance, divided by total variance and it is expressed as a percentage. In this example, PC1 explains 52% of variance in original data and PC2 explains 20%. This indicates that 52% of the variation in the data is described by the model while the remaining 48% are noise. Moreover, PC1 and PC2 together can describe 72% of the total variation in data.

The relationship between the original *p* variables and the Principal Components is the information that can be obtained from the loading plot. Loadings build the direction of each PC relative to the original co-ordinate system and refer to variable space where the origin of variable co-ordinate space is moved to the average object. A typical loading plot is shown in Fig. 2-17. Simply, loading plot is the map of variables and it indicates how much each variable contributes to each PC. PCA-loadings are usually normalised to the interval (-1, 1). The mathematical representation of PCs can be given by equation (2-7):

$$\vec{p}_{\alpha} = \sum_{k} p_{ka} \vec{e}_{k} \qquad (2\text{-}7)$$

where loadings are the coefficients (p_{ka}) in this linear combinations of the original unit vectors.

Studying the score plot together with the loading plot gives the most valuable information about both the samples and the variables, and makes the data interpretation easier and more feasible. As it can be observed in Fig. 2-17 some of the variables fell into the right-hand side of PC1 and some into the left-hand side. The former ones correspond to a similar group of normal samples on the right-hand side of score plot (Fig. 2-16) and the latter ones correspond to a similar group of samples, mainly tumour samples, on the left-hand side of score plot. It can be interpreted that the normal samples have higher amount of Fe, Cu, Zn and Rb, whilst tumour samples have higher amount of Br and coherent scattering peaks parameters.

In this research, the variables are of different types and the data consequently appear in significantly different ranges. Hence, to study and analyse them together, scaling or weighting variables was performed using the standard deviation, before any PCA. This prevents the influence of units of measurement variable for each data value, and makes all the variables to get the same variance.

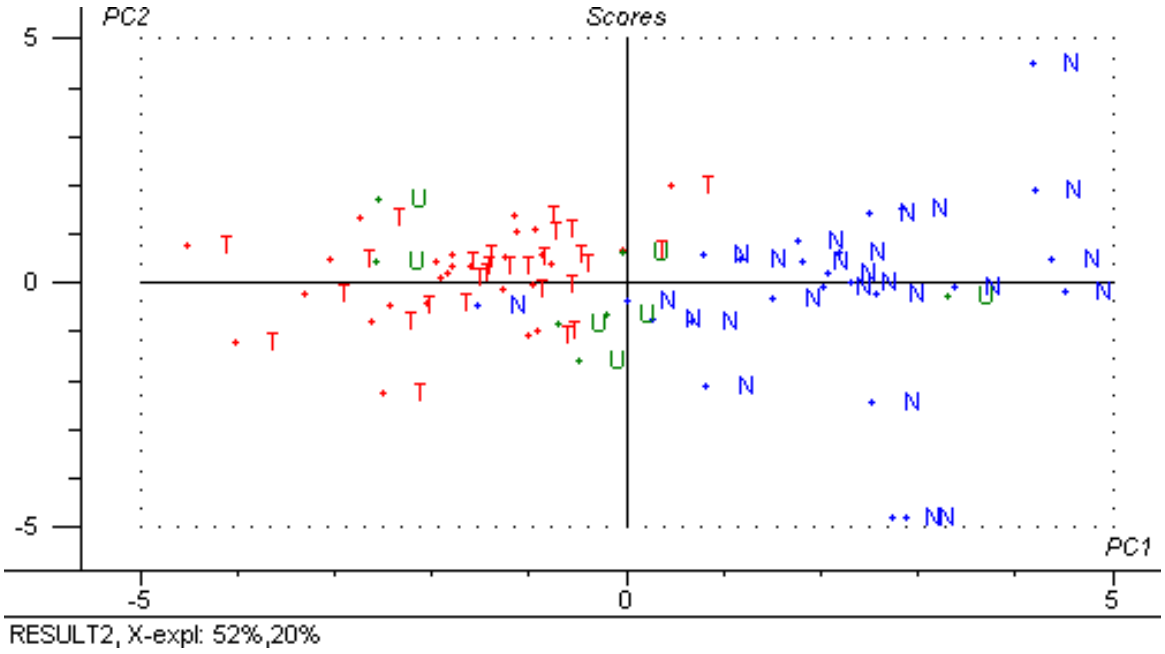

Fig. 2-16 A typical score plot. T (red), N (blue), U (green) denote tumour, normal and unknown samples respectively

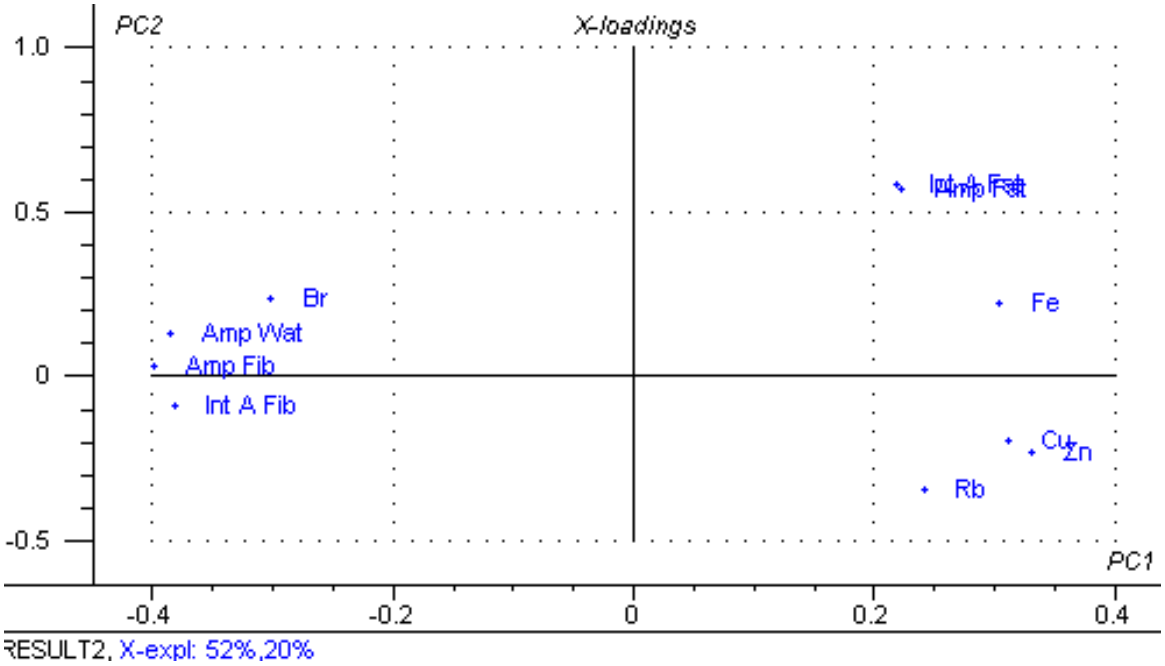

Fig. 2-17 A typical loading plot.

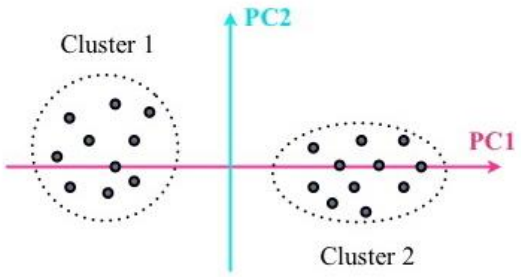

Fig. 2-18 Clustering as founded in the overview score plot, samples in cluster 1 are similar, and are dissimilar to samples in cluster 2 (Esbensen, 2006)

2.6.2 What is SIMCA?

Soft Independent Modelling of Class Analogy (SIMCA) is the classification method, simply based on similarities using separate bilinear modelling for each bona fide data class. Basically, a complete SIMCA classification model mainly made up of several PC models, one for each individual class identified. Each SIMCA class consists of similar samples, and those in different groups are essentially dissimilar (see Fig. 2-18). One of the purposes of using SIMCA classification is to identify the objective groups and to investigate the characteristics of each such class. The substantial goal of SIMCA classification is to assess whether a new sample is similar to the other samples, in order to assign this new sample to the class to which it shows the largest similarity.

In this research, the SIMCA system combines the information for each tissue type, plotting the PCA models for all tissue types back into a common set of axes with units of standard deviation. Each new sample is tested against the individual PCA models in turn. A residual is calculated as the sum of the distance between the sample variable value and the predicted value for each PC. Comparing this sample variable error with the class membership limit (confidence level) determines whether a sample may belong to a particular class or not. The ability of system to predict unknown sample membership accurately is dependent on how far apart each of the PCA models is. The further apart the component models are, the greater ability they have to distinguish between samples. Ideally no membership limits should overlap, as this allows samples to be able to belong to more than one class.

There are different plots available in this software helping to interpret the object class-model relationship. Coomans plot is the most useful plot that could reveal compressed valuable information about the class membership to any two models simultaneously. It shows the transverse distances from all new samples as well as the

calibration samples to two built PC models. A typical Coomans plot is illustrated in Fig. 2-19. The samples in blue colour represent the calibration samples in normal model and those in red are calibration samples from tumour model. The new and unknown samples are shown in green colour being classified. If a sample genuinely belongs to a model, it must fall within the membership limit, i.e. in this example if a sample is normal it should fall into the left side of vertical line, and if it is tumour it should fall below the horizontal line. These two lines are the cut-off class membership limits, as it can be seen in Fig. 2-19. Indeed if a sample falls outside of these limits, i.e. in the upper right corner, it belongs to neither of models, while samples that are within both limits, i.e. close to the origin, should be classified as belonging to both models.

The discrimination power plot is another informative plot that gives useful information about the ability of variables to discriminate between any two models. The discrimination power value of 1 is an indication that the variable has no discrimination ability and the values of higher than 3 is the indication of good discrimination of a specific variable. A typical discrimination power plot is shown in Fig. 2-20 for eight elements as the variables and two normal and tumour models.

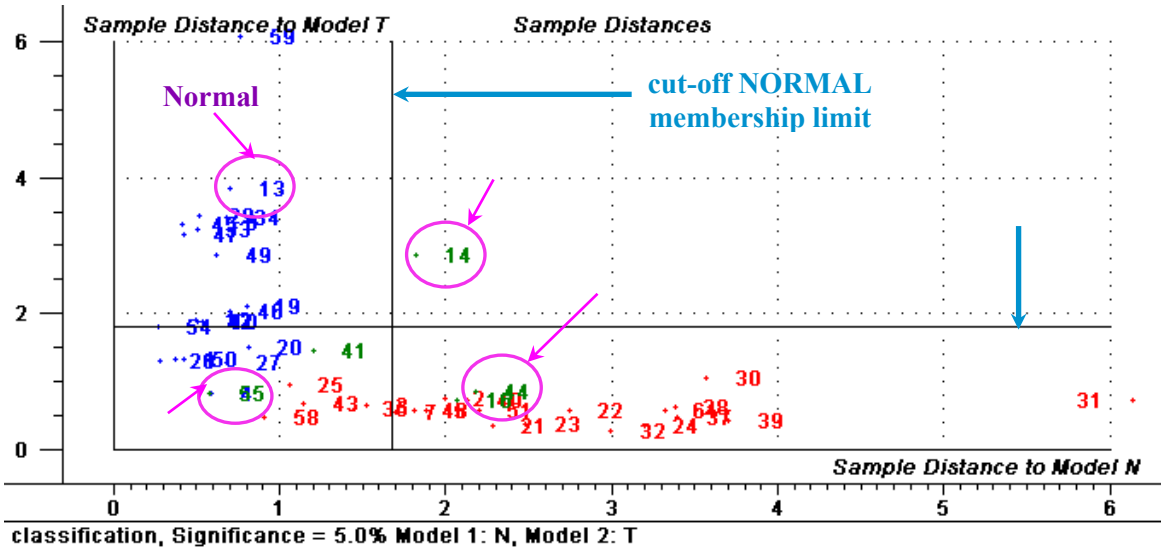

Fig. 2-19 A typical annotated Coomans plot

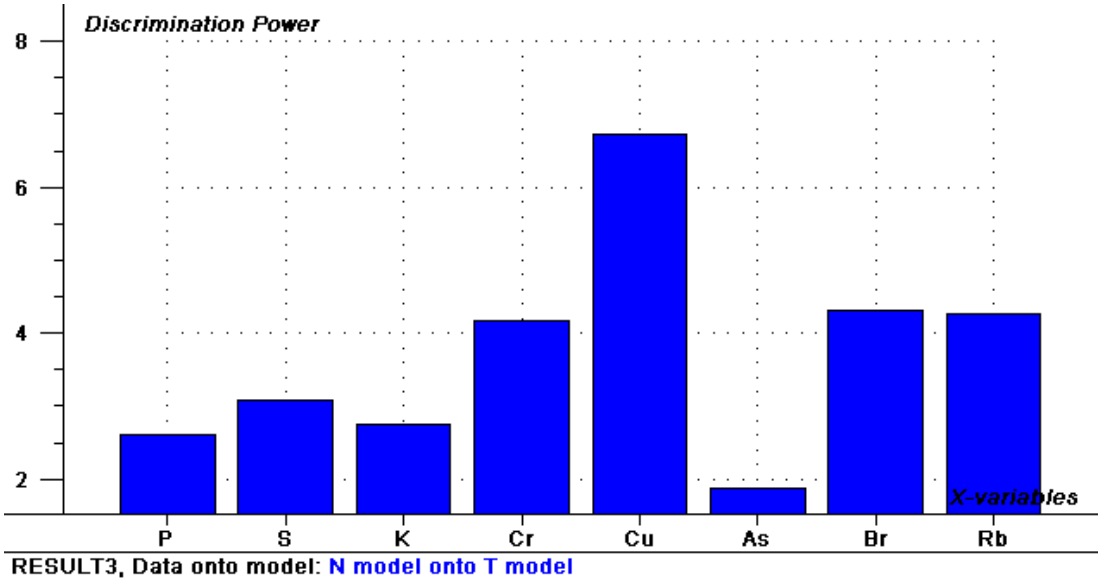

Fig. 2-20 A typical discrimination power plot for eight elemental variables

In Fig. 2-20, the data from the normal model are projected onto the tumour model. This plot demonstrates which elements are the most important in distinguishing between these two models. It can be seen that P, K and As have a discrimination power of less than three and therefore may not be useful in the overall classification.

In order to have information about the relevance of each variable in modelling of the individual models, there is a modelling power plot in SIMCA, indicative of the importance of a given variable for a given model and this can lead to the improvement of each model. Those variables which have a large influence on the model are those that have a large modelling power (more than 0.3). Those variables with a low modelling power (less than 0.3) are not useful and may make the model under perform. As it is shown in Figs. 2-21 and 2-22, all the elements have the modelling power of more than 0.3.

In some cases with poor classification results excluding the variables with low discrimination power and modelling power can help to improve the models and consequently the classification results.

For a full description of both PCA and SIMCA the reader is pointed to Esbensen, 2006.

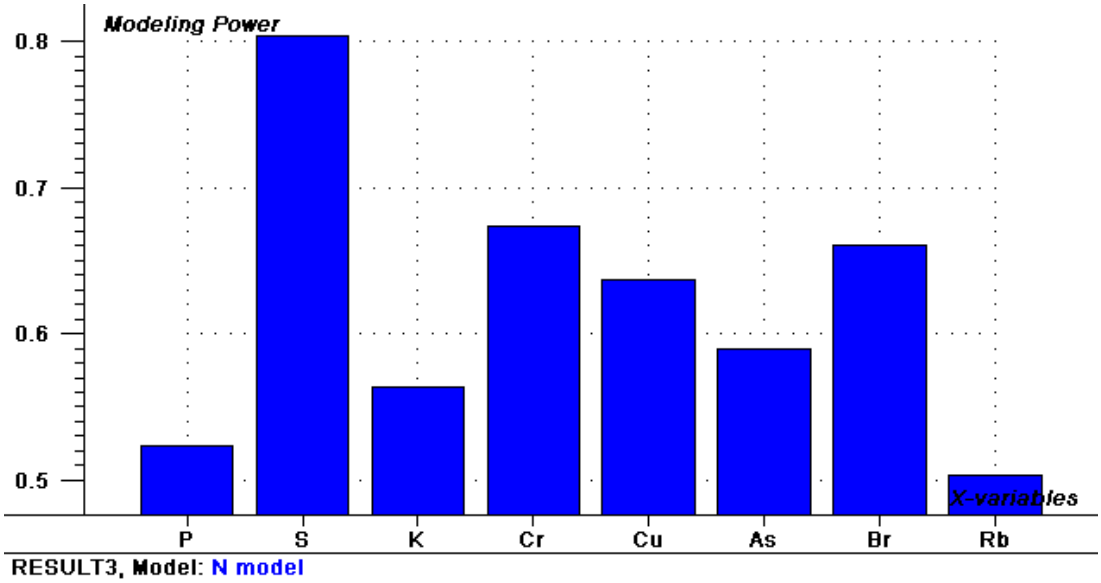

Fig. 2-21 A typical modelling power plot for eight elemental variables for normal model

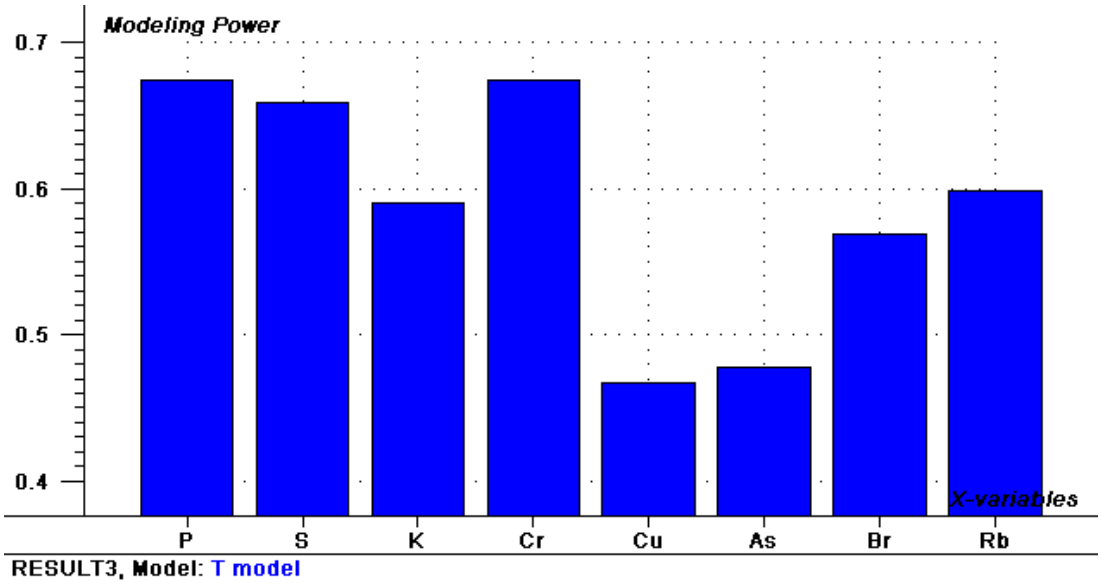

Fig. 2-22 A typical modelling power plot for eight elemental variables for tumour model

Chapter 3

Results

3.1 XRF Study

The average concentration levels of 12 elements in the energy range of 1.88 keV to 13.70 keV are calculated for both 24 normal and 24 tumour tissue samples. The mean amounts of all the elements in normal samples are compared with those in tumour samples in Fig. 3-1.

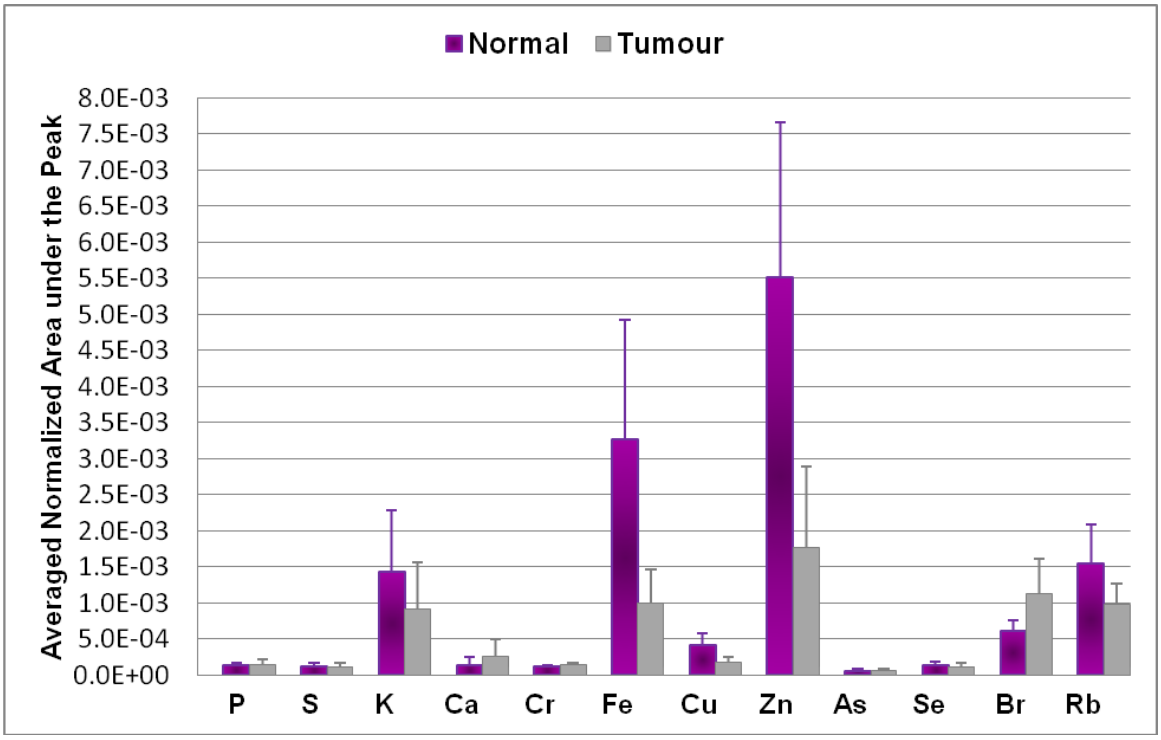

Fig. 3-1 Average concentration level of 12 elements compared in tumour and normal liver tissue

The statistical analyses were performed for all the elements and the results shown. Using elements, those that vary significantly between normal and tumour tissues, in building the normal and tumour models, SIMCA modelling is carried out and the classification results for four subgroups of unknown samples will be presented.

3.1.1 Statistic Results

Descriptive statistic results for 24 matched-pair samples are shown in table 3-1 for the first four elements. Mean values are compared in normal and tumour tissues. Only K and Ca are statistically significant between normal and tumour tissue, with p-value of 0.046 and 0.040, respectively.

Element	# of Samples	Mean	Std. Deviation	P Value
P_N	24	0.000131	0.000040	0.228
P_T	24	0.000151	0.000066	
S_N	24	0.000128	0.000049	0.527
S_T	24	0.000117	0.000060	
K_N	24	0.001435	0.000843	0.046
K_T	24	0.000912	0.000655	
Ca_N	24	0.000144	0.000108	0.040
Ca_T	24	0.000266	0.000213	

Table 3-1 Statistic results of four elements in ROI 1 for normal and tumour liver tissue (Mean ± std. of normalised peak area for each element)

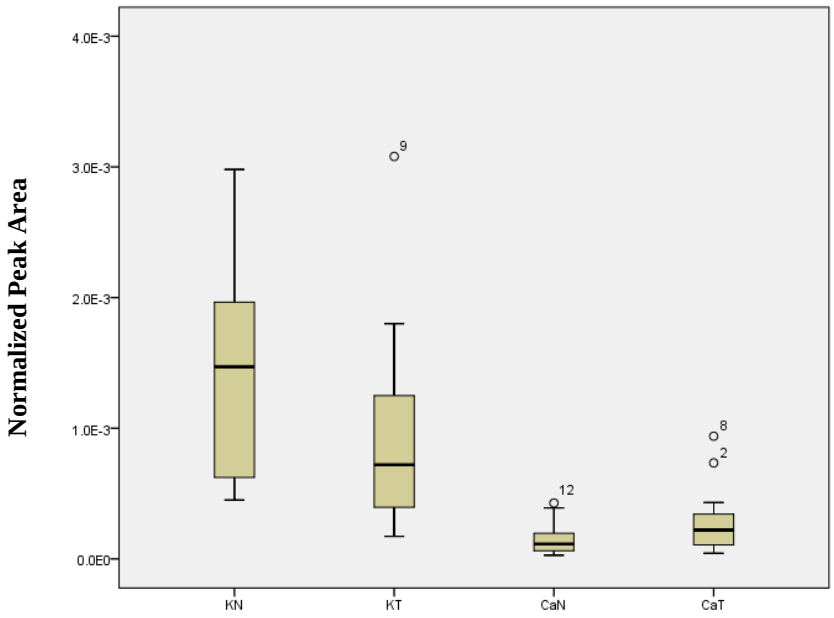

Fig. 3-2 Box Plot of K and Ca for normal and tumour liver tissue

To have a better visualisation of these results, a box plot is presented for the two significant elements; K and Ca (Fig. 3-2). It is apparent from the box plot that the Concentration level of K is lower in the tumor tissue, unlike the Ca concentration level which is higher in tumor tissue compared with the normal tissue.

Descriptive statistic results for the second ROI containing four elements are shown in table 3-2. Box plot is shown in Fig 3-3. From these, it is possible to observe that Fe, Cu and Zn are found to be significantly higher in concentration in normal tissue ($p<.01$) compared to tumour tissue. While, Cr is the element that is found significantly lower in normal tissue ($p = .011$) compared to the tumour tissue.

Element	# of Samples	Mean	Std. Deviation	P Value
Cr_N	24	0.000121	0.000020	0.011
Cr_T	24	0.000144	0.000032	
Fe_N	24	0.003262	0.001655	< 0.01
Fe_T	24	0.000997	0.000460	
Cu_N	24	0.000414	0.000164	< 0.01
Cu_T	24	0.000176	0.000078	
Zn_N	24	0.005519	0.002144	< 0.01
Zn_T	24	0.001762	0.001124	

Table 3-2 Statistic results of four elements in ROI 2 for normal and tumour liver tissue (Mean ± std. of normalised peak area for each element)

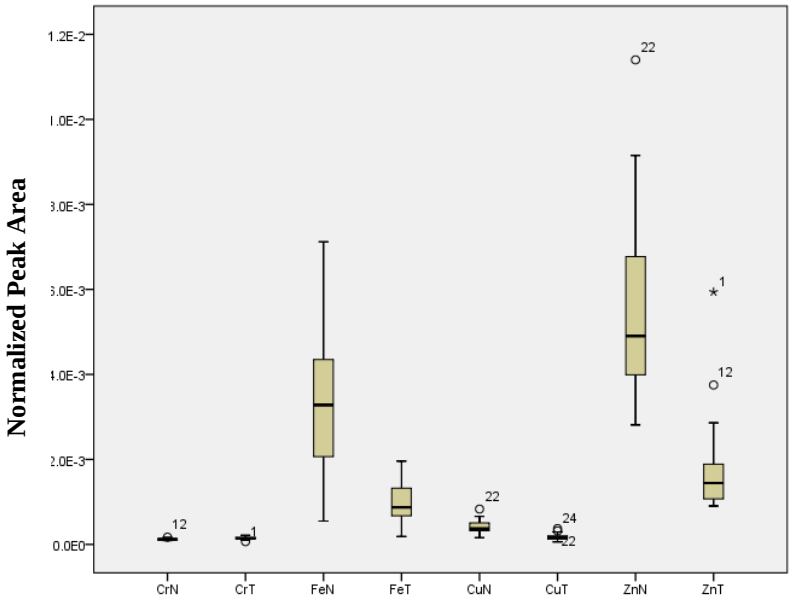

Fig. 3-3 Box Plot of Cr, Fe, Cu and Zn for normal and tumour liver tissue

The descriptive statistic results for the last four elements of interest (ROI 3) are presented in table 3-3. It is observed that As and Se are not significantly different in tumour and normal liver tissue (p=.219 and p=.137, respectively). However, Br is significantly higher (p<.01) in tumour and Rb is significantly lower (p<.01) in tumour tissue compared to the normal liver tissue. These results are visualized graphically with box plot in Fig. 3-4.

Element	# of Samples	Mean	Std. Deviation	P Value
As_N	24	0.000062	0.000020	0.219
As_T	24	0.000069	0.000025	
Se_N	24	0.000131	0.000059	0.137
Se_T	24	0.000116	0.000054	
Br_N	24	0.000612	0.000148	< 0.01
Br_T	24	0.001133	0.000492	
Rb_N	24	0.001544	0.000541	< 0.01
Rb_T	24	0.000974	0.000301	

Table 3-3 Statistic results of four elements in ROI 3 for normal and tumour liver tissue (Mean ± std. of normalised peak area for each element)

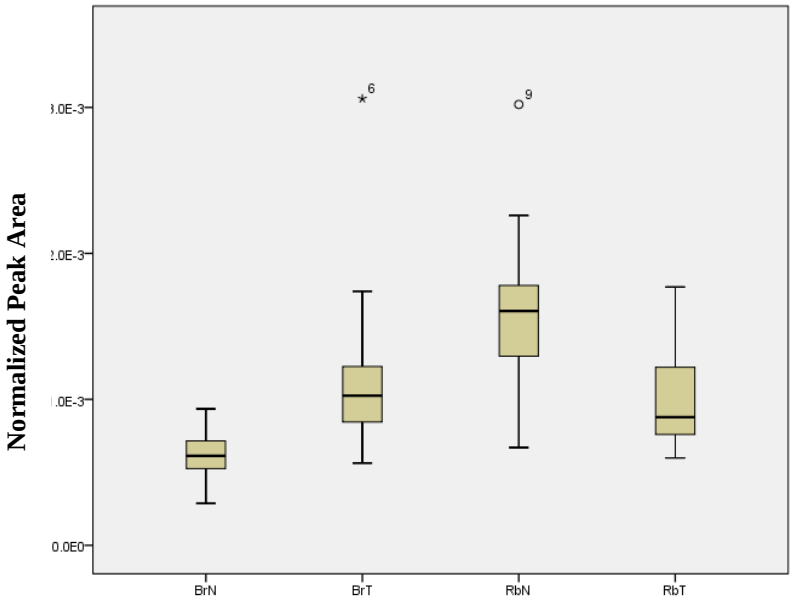

Fig. 3-4 Box Plot of Br and Rb for normal and tumour liver tissue

3.1.2 Multivariate Results

Multivariate analysis and classification modelling were conducted for four different subgroups of unknown samples, with the elemental content data, (those which were statistically significant) using Unscramble version 9.8 (CAMO Ltd). The four subgroups, which are chosen randomly from all the samples, and their type were identified by histopathology, are presented in table 3-4 by the sample number.

Subgroup	Normal	Tumour
1	19 , 33 , 1	24 , 48
2	13 , 20	7 , 28 , 51
3	14 , 41 , 55	16 , 44
4	12 , 47	21 , 30 , 5

Table 3-4 Four subgroups of samples for classification given by sample number

From the statistics analysis, Ca, K, Cr, Fe, Cu, Zn, Br and Rb were found to vary significantly between tumour and normal liver tissue. Therefore, only these eight elements were included in the modelling process and the remaining elements were excluded.

Multivariate analysis, consisting of PCA and SIMCA modelling, using elemental data as variables were carried out for each subgroup separately and the results are presented as following.

3.1.2.1 First subgroup classification results

PCA was carried out for all the normal, tumour and unknown samples in order to obtain a clear visualization of the overall data set structure and to observe a clear grouping in the PC1-PC2 plot. The score plot of all the samples is illustrated in Fig 3-5. From the score plot, which is the map of samples, two distinct clusters of normal and tumour, with a small overlap in the middle can be seen. Normal samples are mostly on the right hand side of PC1 and tumour samples are mostly on the left hand side of PC1. It is clear that three of the unknown samples are among normal cluster and two of them among tumour cluster. PC1 explains 46% variation of raw data matrix and PC2 explains 14% and both together can explain 60% variation of data.

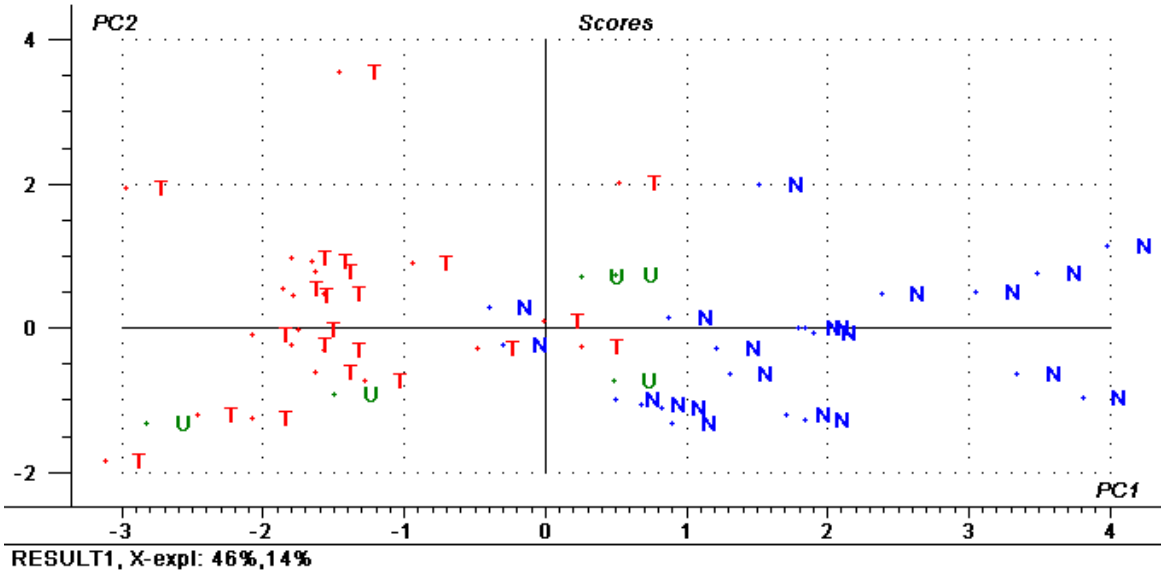

Fig. 3-5 Score Plot of PC1 vs. PC2 (first subgroup)

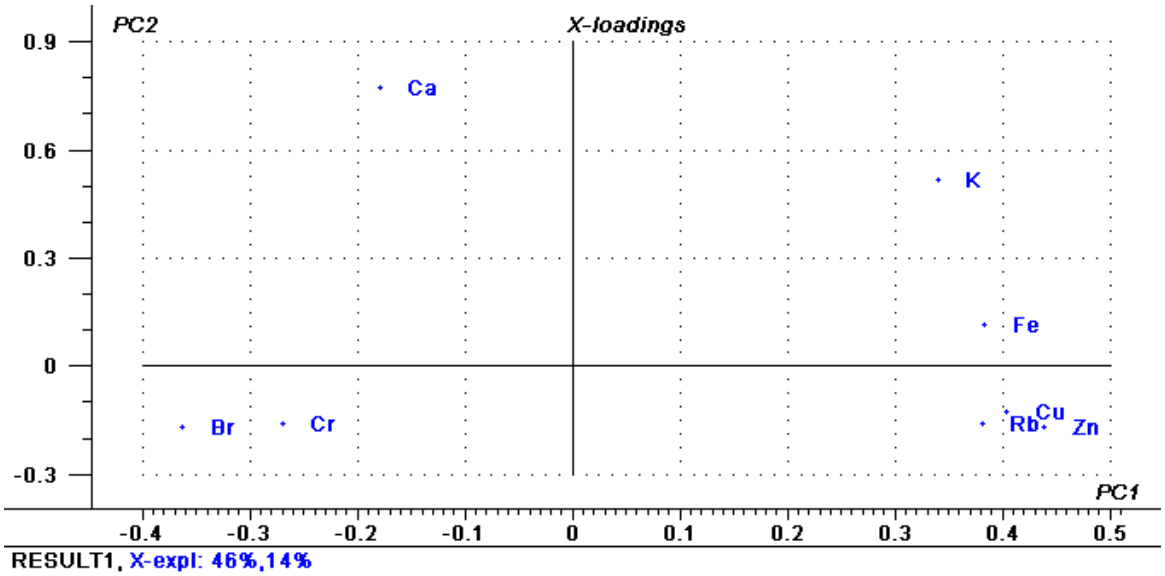

Fig. 3-6 Loading Plot of PC1 vs. PC2 (elements as variables-first subgroup)

Fig 3-6 is showing the loading plot for all the samples. It indicates the map of variables, in this case eight statistically significant elements: K, Ca, Cr, Fe, Cu, Zn, Br and Rb. It can be interpreted that the normal samples have higher amount of Fe, Cu, Zn and Rb, whilst tumour samples have higher amount of Br, Ca and Cr. These results are in

agreement with statistical results (see Fig. 3-1). This plot shows how much each element contributes to each PC. As it can be observed, Cu, Cr, Fe, Cu, Zn, Br and Rb contribute strongly to PC1 and slightly to PC2, while Ca mostly contributes to PC2 and K contributes to both PC1 and PC2.

In next step, PCA was carried out for normal and tumour samples separately and the models were saved and used in the SIMCA modelling process to classify the unknown samples as normal or tumour. Samples 1 and 48 were marked as both normal and tumour, showing that it had a distance that is within the critical limits of both models simultaneously. Samples 19 and 33 are uniquely allocated to the normal class and samples 24 to the tumour class. Thus, three out of five samples were classified correctly. The result of the SIMCA classification for the first unknown subgroup is demonstrated with the Coomans plot in Fig 3-7. If a sample truly belongs to a model it should fall within the membership limit. This can be conspicuously seen in the graph for samples19 and 33, they both fall in blue region and for sample 24 falls in red region.

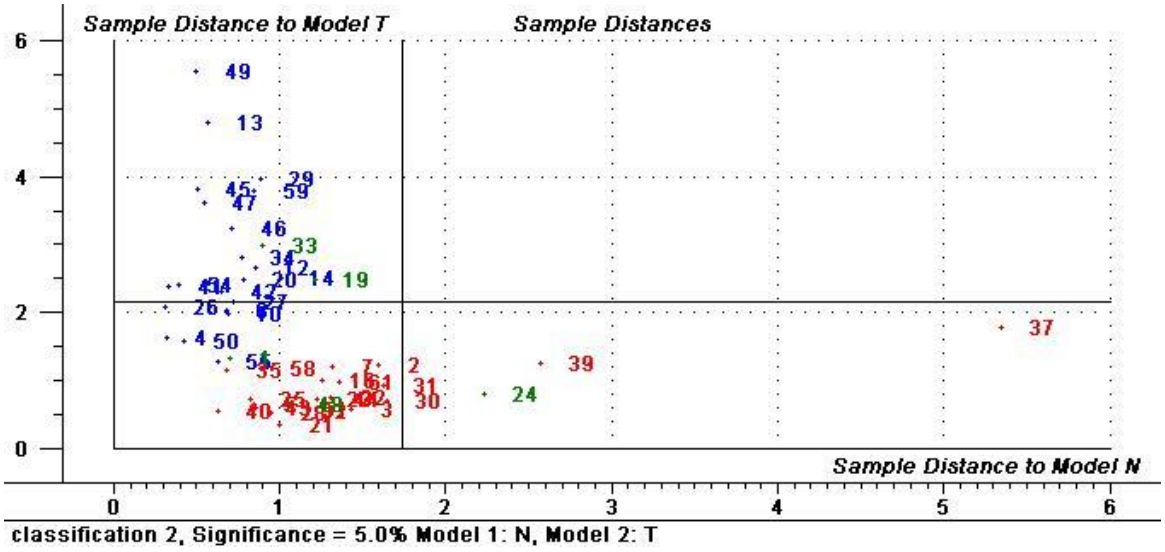

Fig. 3-7 Coomans Plot, classification result (elements as variables-first subgroup)

The discrimination power plots of each element of interest for each subgroup and SIMCA modelling is presented in Fig. 3-8. It is clear that Fe has the highest discrimination power, since all the four subgroups it has a discrimination power of more than 5.

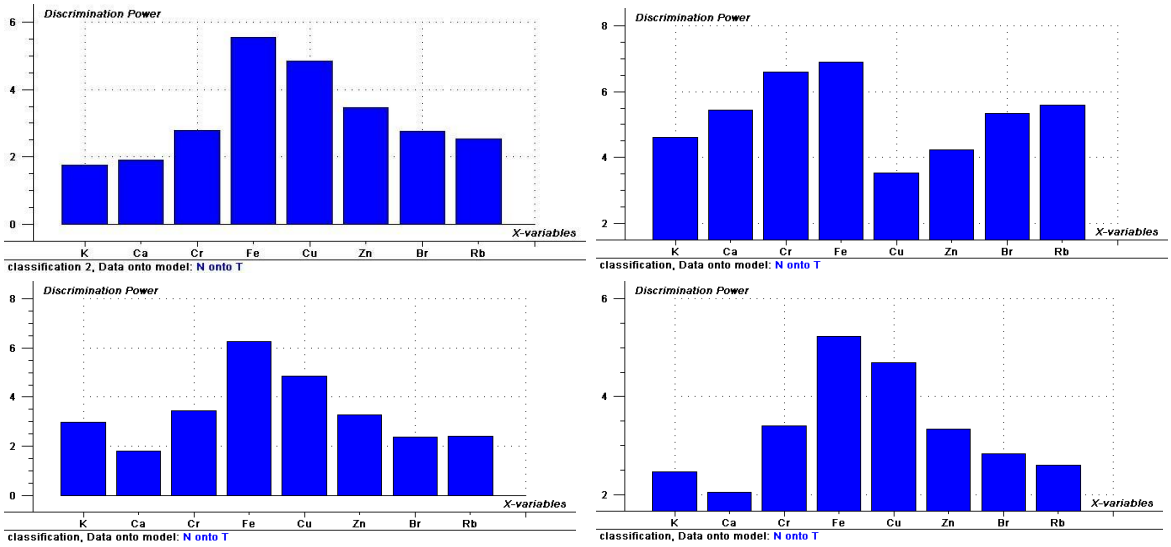

Fig. 3-8 Discrimination Power Plots of eight elements for each four subgroups (from top left to bottom right: subgroup one, two, three and four respectively)

The modelling power plots for the eight elements in the four subgroups for normal and tumour models are illustrated in Figs. 3-9 and 3-10 respectively. All the eight elements have a modelling power of more than 0.3 in normal model. While in the tumour model, most of the elements have a very low powering model. Hence, PCA and SIMCA were performed with the four elements (Ca, Fe, Zn and Br) with a relatively high discrimination power. The results are presented in the next part.

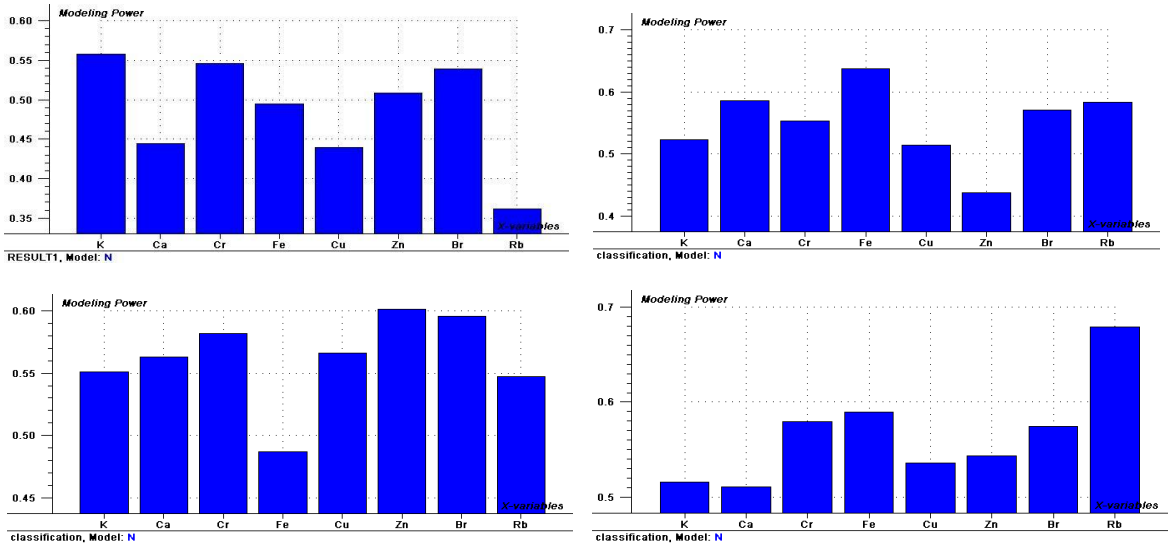

Fig. 3-9 Modelling Power Plots, for the coherent scatter variables for four subgroups for Normal model (from top left to bottom right: subgroup one, two, three and four respectively)

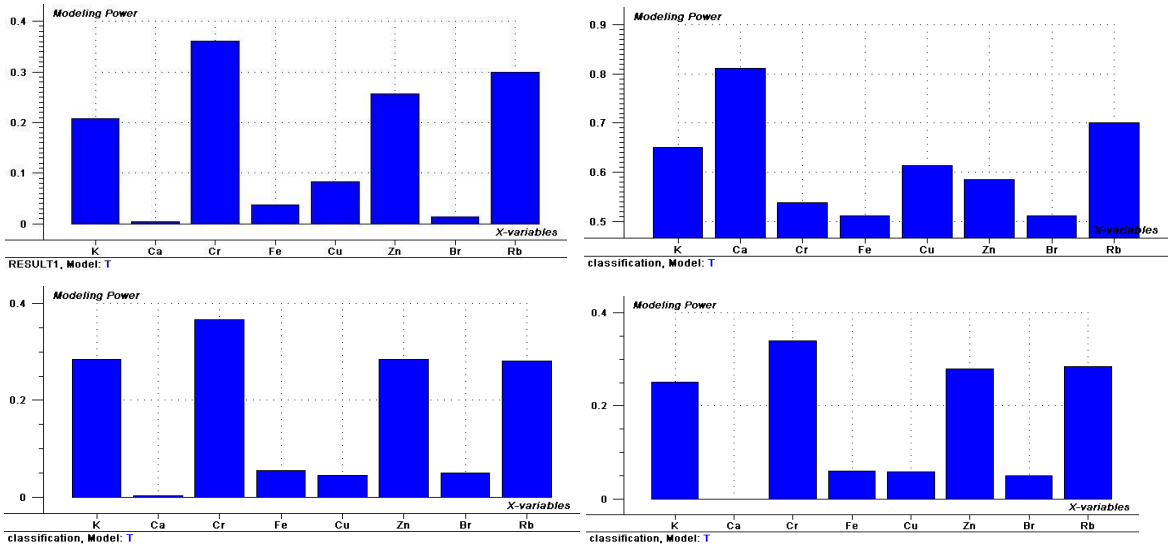

Fig. 3-10 Modelling Power Plots, for the coherent scatter variables for four subgroups for Tumour model (from top left to bottom right: subgroup one, two, three and four respectively)

Summary of all four subgroups classification results for the elemental data analysis with 5% confidence level are reviewed in table 3-5:

Eight Elements as Variables					
Subgroup	Sample	Classification Result		Histopathological Result	
		Normal	Tumour	Normal	Tumour
1	19	*		*	
	33	*		*	
	1	*	*	*	
	24		*		*
	48	*	*		*
2	13			*	
	20	*		*	
	7	*			*
	28	*	*		*
	51	*	*		*
3	14	*		*	
	41			*	
	55	*	*	*	
	16		*		*
	44	*	*		*
4	12	*		*	
	47	*		*	
	21		*		*
	30		*		*
	5	*	*		*

Table 3-5 Summary of the classification results with eight elemental variables (K, Ca, Cr, Fe, Cu, Zn, Br, Rb) and 5% confidence level

The PCA and SIMCA modelling were performed using Fe and Zn, both of which show high discrimination power (more than 3) and they are both higher in normal liver tissue compared to tumour tissue, and Ca and Br, both of which are higher in tumour liver tissue compared to normal liver tissue. The discrimination power plots are demonstrated in Fig. 3-11. Explicitly, these four elements have a large discrimination power (≥ 3).

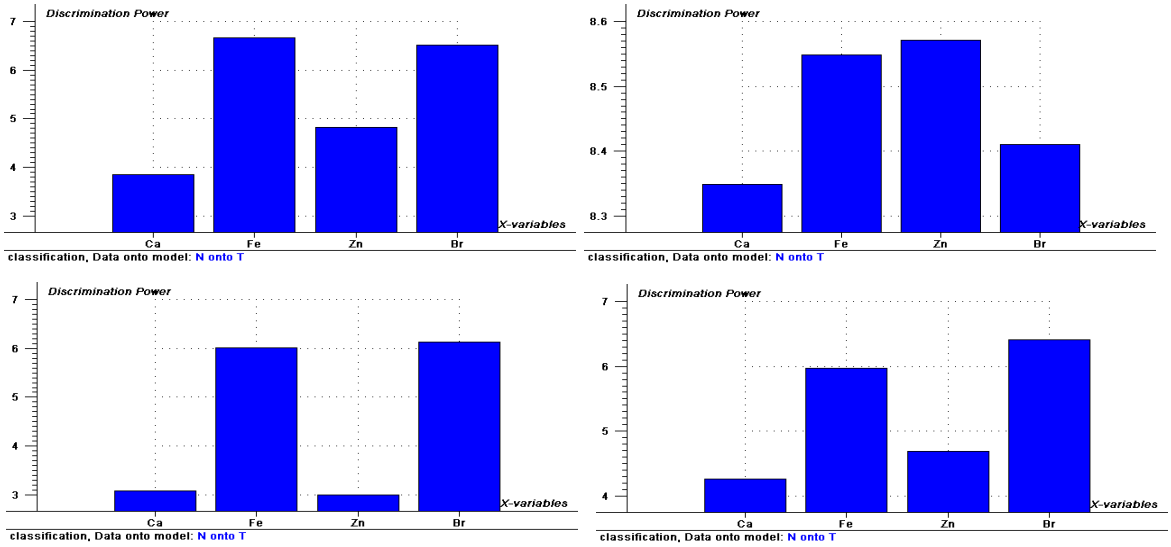

Fig. 3-11 Discrimination Power Plots of four elements for each four subgroups (from top left to bottom right: subgroup one, two, three and four respectively)

The Summary of classification results for the twenty unknown samples is shown in table 3-6. It is found that with these four elements as PCA variables, 14 samples were classified correctly out of 20 samples with 95% confidence level.

Four Elements as Variables					
Subgroup	Sample	Classification Result		Histopathological Result	
		Normal	Tumour	Normal	Tumour
1	19	*		*	
	33	*		*	
	1	*	*	*	
	24		*		*
	48		*		*
2	13			*	
	20	*		*	
	7	*			*
	28		*		*
	51		*		*
3	14	*		*	
	41	*		*	
	55	*	*	*	
	16		*		*
	44	*	*		*
4	12	*		*	
	47	*		*	
	21		*		*
	30	*			*
	5		*		*

Table 3-6 Summary of the classification results with four elemental variables (Ca, Fe, Zn, Br) and 5% confidence level

The discrimination power of the SIMCA modelling was checked with the Fe as an element significantly higher in normal liver tissue compared to tumour tissue and Br as an element significantly higher in the tumour tissue. The discrimination power plots for these two elements and for the four subgroups are illustrated in Fig. 3-12.

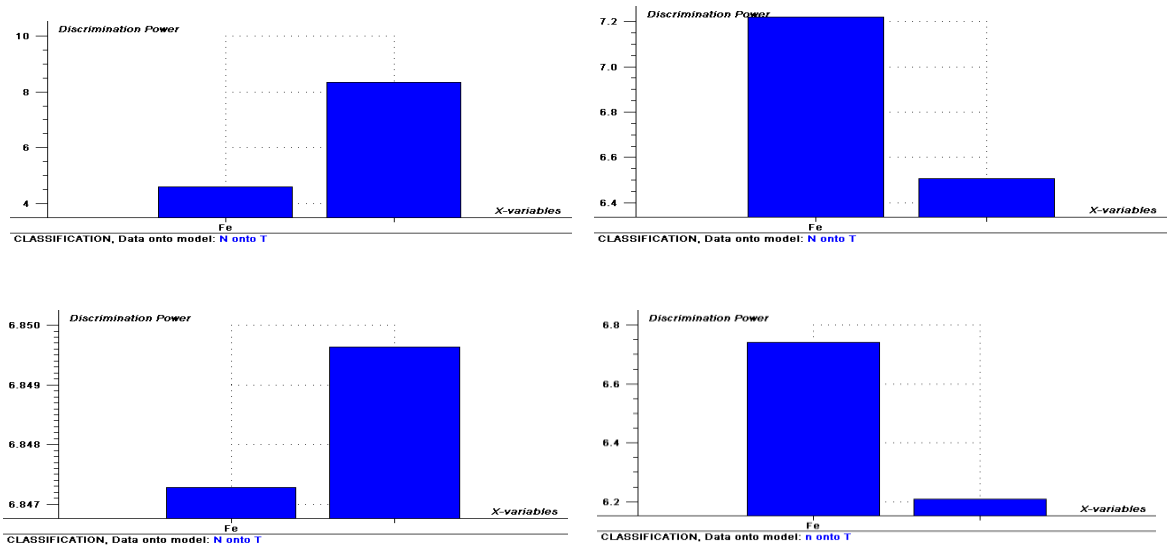

Fig. 3-12 Discrimination Power Plots of two elements for each four subgroups (from top left to bottom right: subgroups: one, two, three and four respectively)

The summary of the classification results for all the 20 unknown samples is presented in table 3-7, and indicates that 15 samples were classified correctly.

Two Elements as Variables					
Subgroup	Sample	Classification Result		Histopathological Result	
		Normal	Tumour	Normal	Tumour
1	19	*		*	
	33	*		*	
	1	*	*	*	
	24		*		*
	48		*		*
2	13	*		*	
	20	*		*	
	7	*	*		*
	28		*		*
	51		*		*
3	14	*	*	*	
	41	*		*	
	55	*	*	*	
	16		*		*
	44		*		*
4	12	*		*	
	47	*		*	
	21		*		*
	30		*		*
	5	*	*		*

Table 3-7 Summary of the classification results with two elemental variables (Fe, Br) and 5% confidence level

The score, loading and Coomans plots for the three other subgroups are presented in Appendix III.

3.2 Coherent Scatter Study

The averaged scatter profile spectra for both 24 normal and 24 tumour samples are shown in Fig. 3-13. It is observed that the first peak is slightly lower in tumour, unlike the second and third peaks which are higher in tumour. This observation is approved numerically by the statistical analysis results which will be presented in the following subsection (see table 3-8).

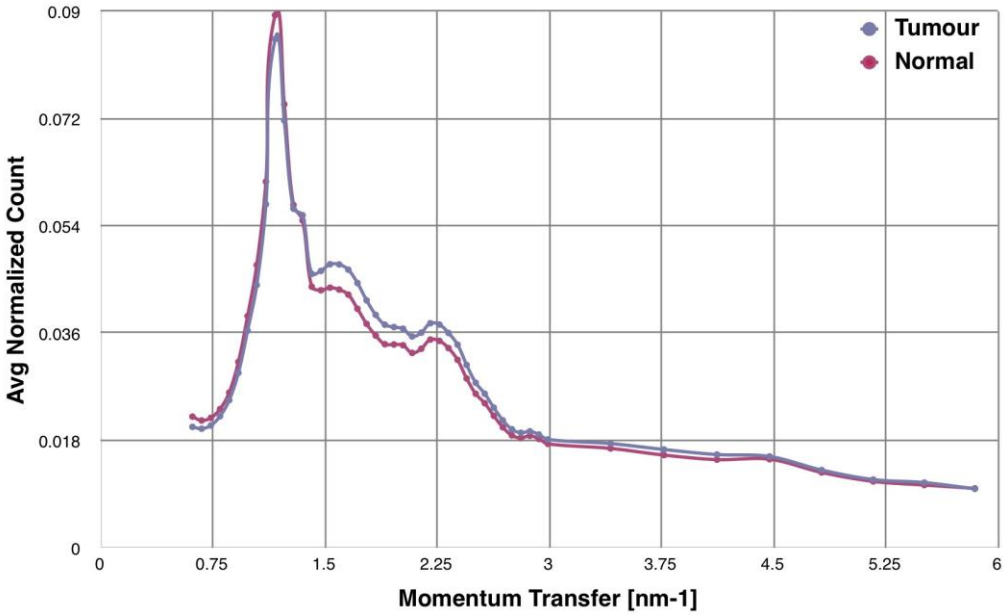

Fig. 3-13 Averaged normalized coherent scatter profile for tumour and normal samples

Four peaks were fitted to the data and demonstrated in Fig. 3-14: Adipose peak at 1.1 nm^{-1}, Fibrous peak at 1.6 nm^{-1}, Water content peak at 2.2 nm^{-1} and a peak at 3.4 nm^{-1} due to the incoherent scattered radiation which are in agreement with the results previously reported by Geraki *et al* (2004). The fourth peak is not due the coherent scattering and also it does not carry any structural information, hence, for the rest of analyses it is excluded from the data and the parameters of the first three peaks are analysed only.

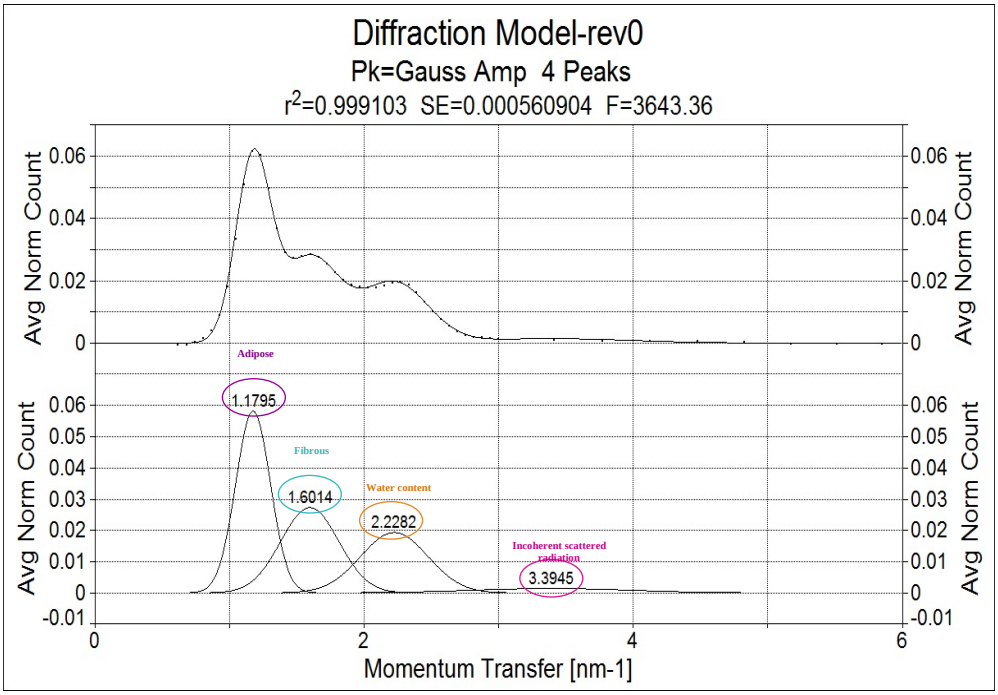

Fig. 3-14 Four peaks were fitted with background subtraction for average diffraction spectra from the normal and the tumour samples

Using this model, all the sample data were fitted and three peak parameters; the amplitude, FWHM and area under the peak are extracted. The statistical analysis and multivariate analysis for the scattered data will be presented in the next two subsections.

3.2.1 Statistic Results

The descriptive statistics are shown in table 3-8 for 24 matched pair samples. All the parameters except FWHM of adipose peak were normally distributed; hence the paired T-Test was used. Wilcoxon test was used for the FWHM of Adipose peak. The results in the table indicate that the three parameters associated with adipose peak are not seen to vary significantly between normal and tumour tissue ($p>.05$). Whereas, the amplitude and integrated area for both fibrous and water content peaks are statistically significant ($p<.01$), the same for FWHM with p value of .039 and .027 respectively.

Peak	Peak Parameter	Type of Tissue	# of Samples	Mean	Std. Deviation	P Value
Adipose Peak	Amplitude	Normal	24	0.0519	0.00135	0.051
		Tumour	24	0.0487	0.00085	
	FWHM	Normal	24	0.3003	0.00104	0.549
		Tumour	24	0.3004	0.00212	
	Int Area	Normal	24	0.0166	0.00042	0.053
		Tumour	24	0.0156	0.00026	
Fibrous Peak	Amplitude	Normal	24	0.022	0.00065	< 0.01
		Tumour	24	0.0271	0.00049	
	FWHM	Normal	24	0.5185	0.00472	0.039
		Tumour	24	0.5339	0.00584	
	Int Area	Normal	24	0.0122	0.00043	< 0.01
		Tumour	24	0.0154	0.00037	
Water Content Peak	Amplitude	Normal	24	0.0151	0.00036	< 0.01
		Tumour	24	0.0181	0.00029	
	FWHM	Normal	24	0.552	0.00468	0.027
		Tumour	24	0.566	0.00432	
	Int Area	Normal	24	0.0089	0.00026	< 0.01
		Tumour	24	0.0109	0.00024	

Table 3-8 Statistic results of coherent scatter data for normal and tumour liver tissue (Mean ± std. of normalised peak area)

These results can be better interpreted from the box plots. In Figs. 3-15 to 3-17 box plots for the amplitude, FWHM and integrated area of three peaks are shown. A similar trend can be observed from these plots. All three parameters for fibrous and water content peaks are higher in tumour than in the normal liver tissue, while those are slightly lower in tumour for the adipose peak.

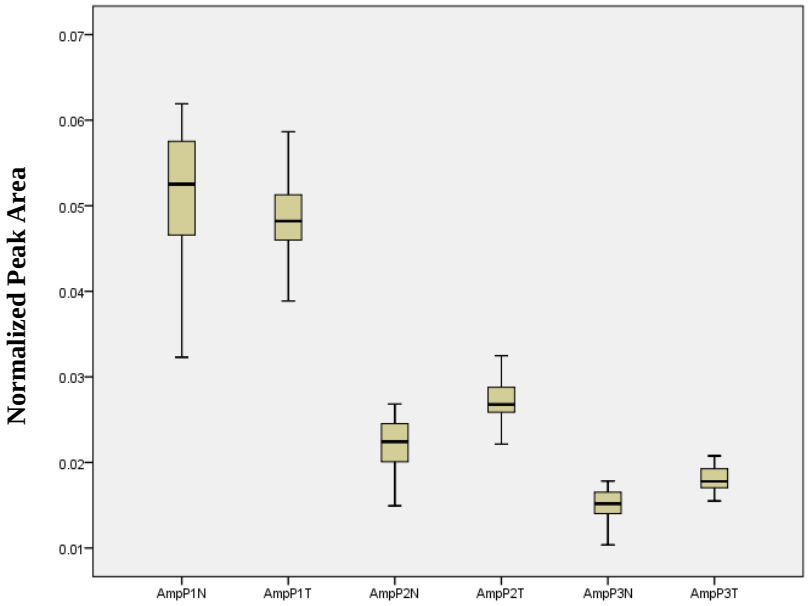

Fig. 3-15 Box Plot of amplitude of adipose, fibrous and water peaks for normal and tumour liver tissue

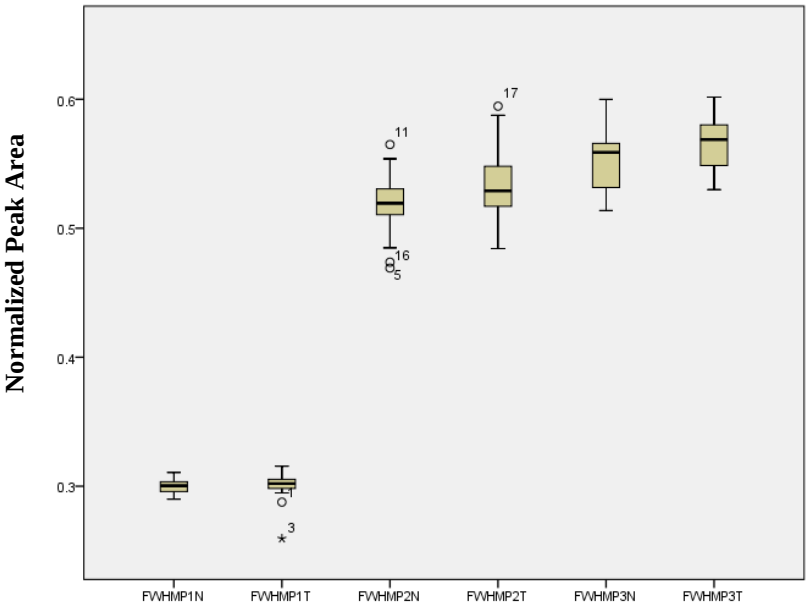

Fig. 3-16 Box Plot of FWHM of adipose, fibrous and water peaks for normal and tumour liver tissue

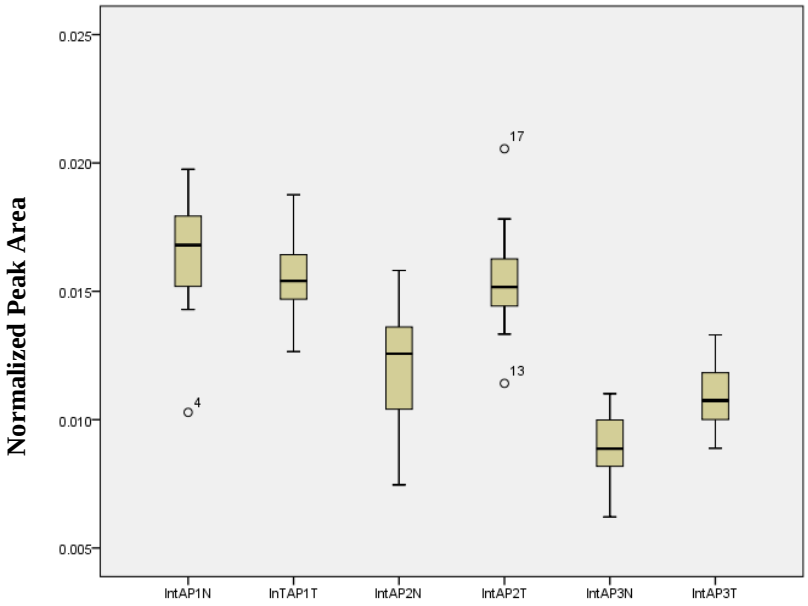

Fig. 3-17 Box Plot of area under the adipose, fibrous and water peaks for normal and tumour liver tissue

3.2.2 Multivariate Results

Multivariate analyses were carried out using the coherent scattering variables. With respect to the statistic analysis it was shown that the adipose peak parameters were not significantly different between tumour and normal liver tissue. Therefore, these three parameters were not included in the modelling process. Total of six parameters: amplitude, FWHM and integrated area of the other two peaks were selected as the modelling variables. The analyses were performed for the same subgroups mentioned in table 3-1 and the results are presented in the following subsections.

3.2.2.1 First subgroup classification results

The score and loading plots of all the 21 normal, 22 tumour and 5 unknown samples are shown in Fig 3-18 and 3-19, respectively. It can be seen that the two clusters of normal and tumour are not as clear as in the score plots of previous sections (elemental data). In this case there is more overlap.

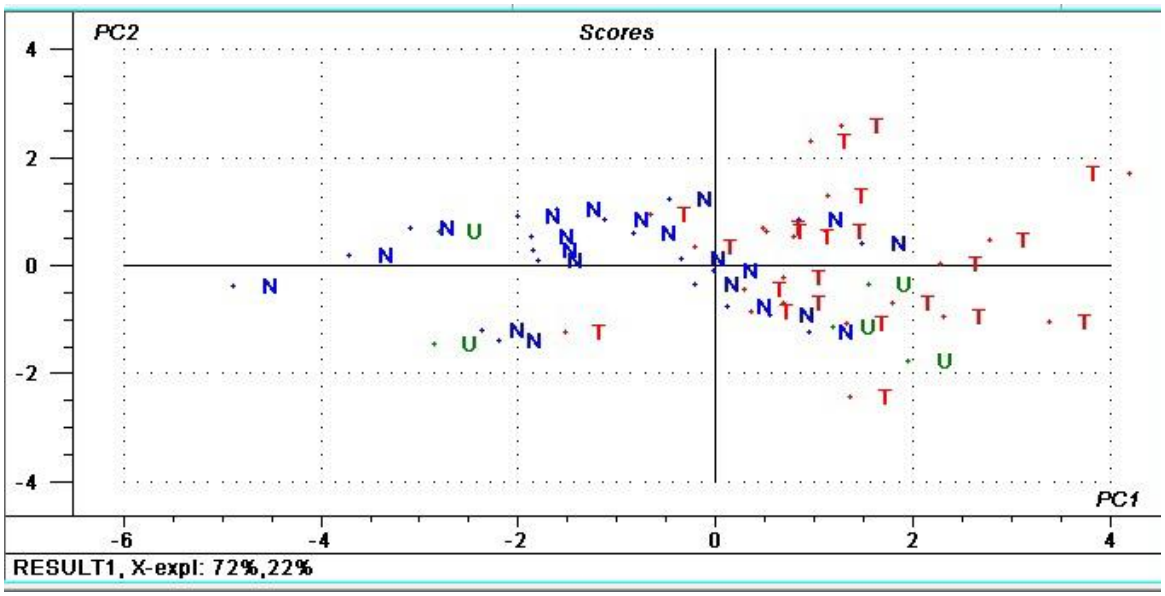

Fig. 3-18 Score Plot of PC1 vs. PC2 (first subgroup)

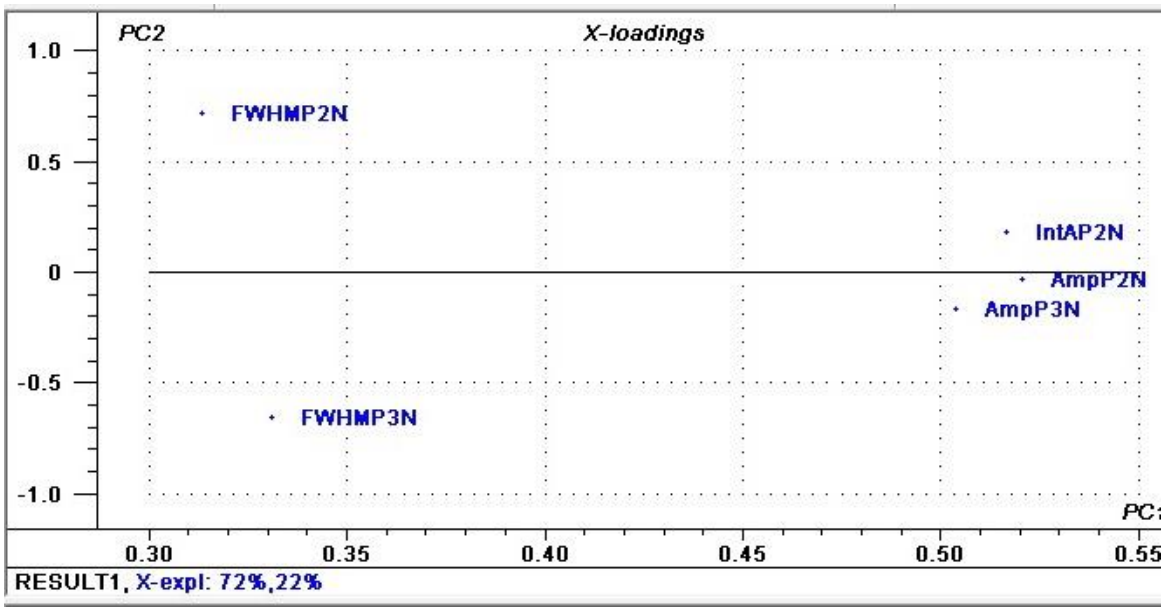

Fig 3-19 Loading plot of PC1 vs. PC2 (coherent scatter data as variables-first subgroup)

SIMCA modelling results show that samples 19 and 33 are allocated to normal model and sample 24 to tumour model, while samples 1 and 48 could belong to both normal and tumour models. The Coomans plot is shown in Fig 3-20. Therefore, three out of five samples were classified correctly.

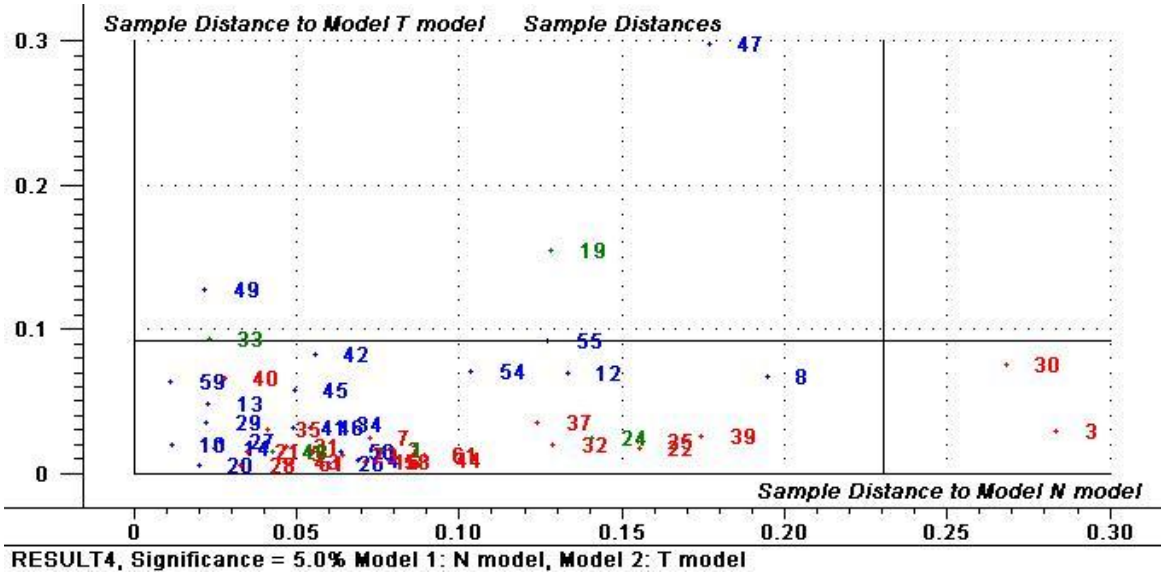

Fig 3-20 Coomans plot, classification results (coherent scatter data as variables-first subgroup)

The discrimination power plots for coherent scatter variables for the four subgroups are shown in Fig 3-21.

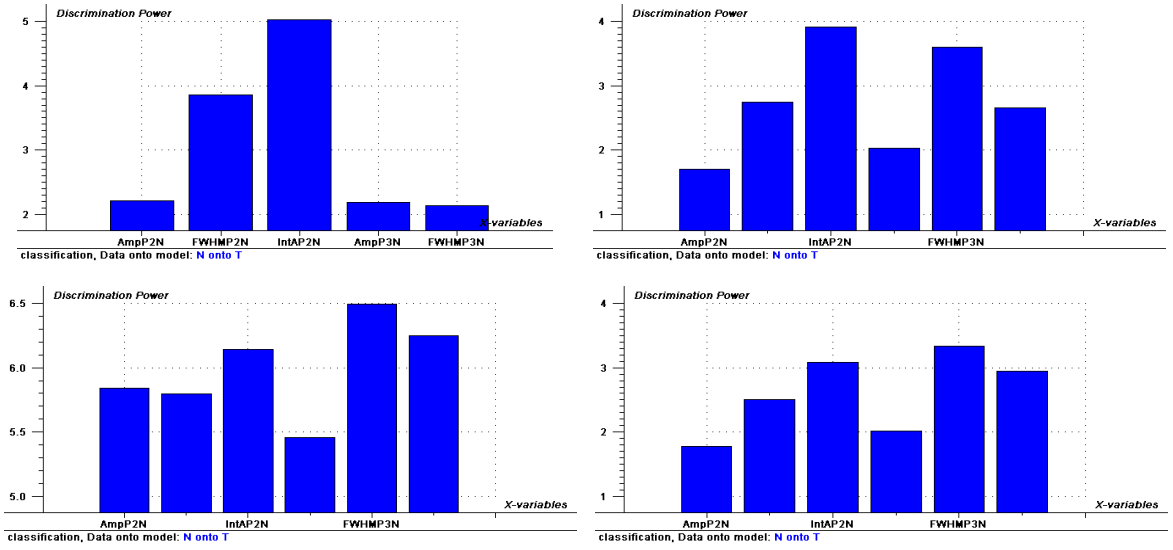

Fig 3-21 Discrimination Power Plots, for the coherent scatter variables for four subgroups (from top left to bottom right: subgroup one, two, three and four respectively)

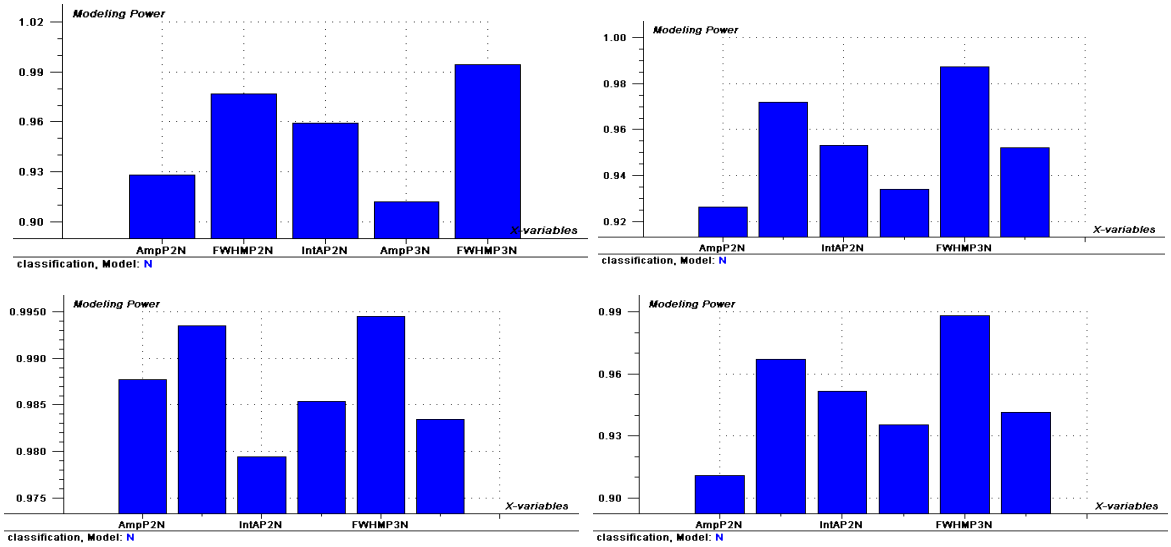

Fig 3-22 Modelling Power Plots, for the coherent scatter variables for four subgroups for Normal model (from top left to bottom right: subgroup one, two, three and four respectively)

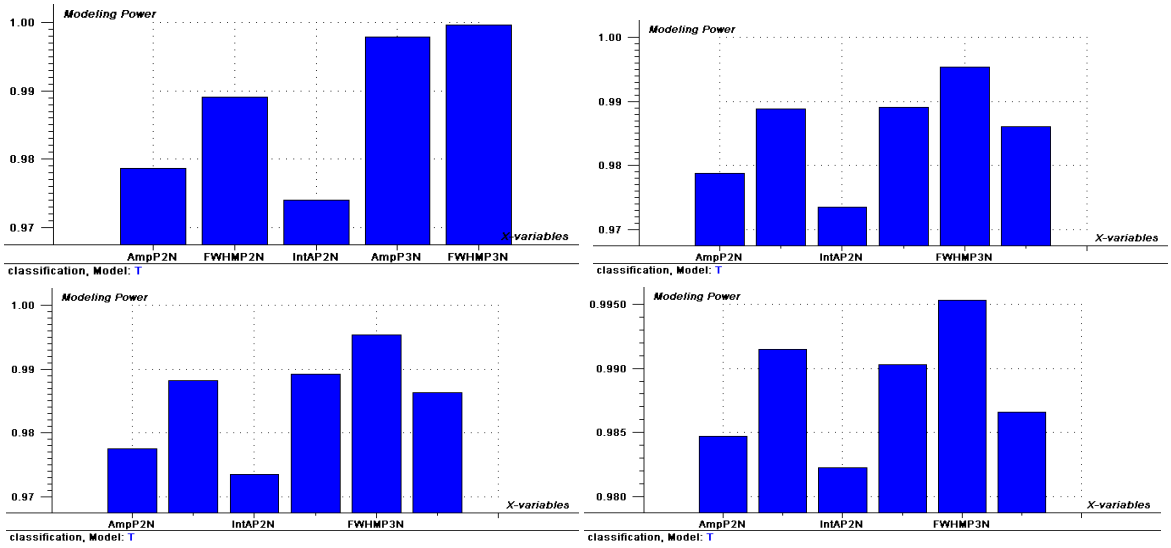

Fig 3-23 Modelling Power Plots, for the coherent scatter variables for four subgroups for Tumour model (from top left to bottom right: subgroup one, two, three and four respectively)

Modelling power plots for the coherent scatter variables for normal and tumour models in all the four subgroups imply that although these variables have low discrimination power, they have a very large modelling power (>>0.3), meaning that they are helpful for building normal and tumour models but not very helpful for the discrimination goal.

Summary of all four subgroups classification results for coherent scattering data analysis with 5% confidence level are reviewed in table 3-9:

Coherent scattering parameters as Variables					
Subgroup	Sample	Classification Result		Histopathological Result	
		Normal	Tumour	Normal	Tumour
1	19	*		*	
	33	*		*	
	1	*	*	*	
	24		*		*
	48	*	*		*
2	13	*	*	*	
	20	*	*	*	
	7	*	*		*
	28	*	*		*
	51	*	*		*
3	14			*	
	41	*	*	*	
	55	*	*	*	
	16		*		*
	44		*		*
4	12	*		*	
	47			*	
	21	*	*		*
	30				*
	5	*	*		*

Table 3-9 Summary of classification results with coherent scatter variables (Amplitude, FWHM and Area under the fibrous and water content peaks) and 5% confidence level

The score, loading and Coomans plots for the three other subgroups are presented in Appendix IV.

3.3 Elemental Ratio Study

In order to investigate more significant variables between normal and tumour liver tissue, for the purpose of better multivariate analysis and modelling, the ratios of twelve elements were determined. Forty six ratios were statistically analysed and the results will be presented in the next subsection. Afterward, the most statistically significant ratios will be selected to implement the PCA and SIMCA modelling. The results of multivariate analyses will be reported in subsection 3.3.2.

3.3.1 Statistic Results

The statistical results for the 46 ratios of elements are shown in table 3-10.

Ratio	P Value	Ratio	P Value
$(K/Cr)_N$ - $(K/Cr)_T$	0.024	$(Fe/Zn)_N$ - $(Fe/Zn)_T$	0.903
$(K/Fe)_N$ - $(K/Fe)_T$	0.007	$(Fe/As)_N$ - $(Fe/As)_T$	0.000
$(K/Cu)_N$ - $(K/Cu)_T$	0.123	$(Fe/Se)_N$ - $(Fe/Se)_T$	0.000
$(K/Zn)_N$ - $(K/Zn)_T$	0.002	$(Fe/Br)_N$ - $(Fe/Br)_T$	0.000
(K/As)N - $(K/As)_T$	0.049	$(Fe/Rb)_N$ - $(Fe/Rb)_T$	0.000
$(K/Se)_N$ - $(K/Se)_T$	0.219	$(Cu/Zn)_N$ - $(Cu/Zn)_T$	0.002
$(K/Br)_N$ - $(K/Br)_T$	0.003	$(Cu/As)_N$ - $(Cu/As)_T$	0.000
$(K/Rb)_N$ - $(K/Rb)_T$	0.822	$(Cu/Se)_N$ - $(Cu/Se)_T$	0.000
$(Ca/Cr)_N$ - $(Ca/Cr)_T$	0.141	$(Cu/Br)_N$ - $(Cu/Br)_T$	0.000
$(Ca/Fe)_N$ - $(Ca/Fe)_T$	0.000	$(Cu/Rb)_N$ - $(Cu/Rb)_T$	0.021
$(Ca/Cu)_N$ - $(Ca/Cu)_T$	0.000	$(Zn/As)_N$ - $(Zn/As)_T$	0.000
$(Ca/Zn)_N$ - $(Ca/Zn)_T$	0.000	$(Zn/Se)_N$ - $(Zn/Se)_T$	0.000
$(Ca/As)_N$ - $(Ca/As)_T$	0.199	$(Zn/Br)_N$ - $(Zn/Br)_T$	0.000
$(Ca/Se)_N$ - $(Ca/Se)_T$	0.034	$(As/Se)_N$ - $(As/Se)_T$	0.040
$(Ca/Br)_N$ - $(Ca/Br)_T$	0.786	$(As/Br)_N$ - $(As/Br)_T$	0.002
$(Ca/Rb)_N$ - $(Ca/Rb)_T$	0.011	$(As/Rb)_N$ - $(As/Rb)_T$	0.004
$(Cr/Cu)_N$ - $(Cr/Cu)_T$	0.000	$(Se/Br)_N$ - $(Se/Br)_T$	0.000
$(Cr/Zn)_N$ - $(Cr/Zn)_T$	0.000	$(Se/Rb)_N$ - $(Se/Rb)_T$	0.044
$(Cr/As)_N$ - $(Cr/As)_T$	0.368	$(Br/Rb)_N$ - $(Br/Rb)_T$	0.000
$(Cr/Se)_N$ - $(Cr/Se)_T$	0.004	$(Rb/Br)_N$ - $(Rb/Br)_T$	0.000
$(Cr/Br)_N$ - $(Cr/Br)_T$	0.000	* $(Cr/Fe)_N$ - $(Cr/Fe)_T$	0.000
$(Cr/Rb)_N$ - $(Cr/Rb)_T$	0.000	* $(Zn/Rb)_N$ - $(Zn/Rb)_T$	0.000
$(Fe/Cu)_N$ - $(Fe/Cu)_T$	0.162	* $(K/Ca)_N$ - $(K/Ca)_T$	0.001

Table 3-10 Mean comparison between normal and tumour tissue

Forty three ratios were normally distributed, thus the Paired-Sample T-Test was carried out to compare the mean values in normal and tumour samples and find out the most significant ones. However, the ratios with asterisk in the table 3-8 are the ratios that were not normally distributed, thus Wilcoxon Test was used to compare the mean values.

Clearly it can be observed in table 3-10 that thirty four ratios are significantly different between normal and tumour samples. Amongst these, only those that have p-value less than 0.001 were selected. Descriptive analyses were performed for these ratios and the results are presented in table 3-11:

Element	# of Samples	Mean	P Value	Element	# of Samples	Mean	P Value
$(Ca/Fe)_N$	24	0.0583	< 0.001	$(Cu/As)_N$	24	7.9598	< 0.001
$(Ca/Fe)_T$	24	0.3120		$(Cu/As)_T$	24	2.7668	
$(Ca/Cu)_N$	24	0.4202	< 0.001	$(Cu/Se)_N$	24	3.4671	< 0.001
$(Ca/Cu)_T$	24	1.6682		$(Cu/Se)_T$	24	1.7508	
$(Ca/Zn)_N$	24	0.0298	< 0.001	$(Cu/Br)_N$	24	0.7420	< 0.001
$(Ca/Zn)_T$	24	0.1883		$(Cu/Br)_T$	24	0.1764	
$(Cr/Cu)_N$	24	0.3375	< 0.001	$(Zn/As)_N$	24	105.2628	< 0.001
$(Cr/Cu)_T$	24	0.9396		$(Zn/As)_T$	24	28.7967	
$(Cr/Zn)_N$	24	0.0245	< 0.001	$(Zn/Se)_N$	24	44.4463	< 0.001
$(Cr/Zn)_T$	24	0.1052		$(Zn/Se)_T$	24	18.6847	
$(Cr/Br)_N$	24	0.2070	< 0.001	$(Zn/Br)_N$	24	9.8375	< 0.001
$(Cr/Br)_T$	24	0.1413		$(Zn/Br)_T$	24	1.8095	
$(Cr/Rb)_N$	24	0.0911	< 0.001	$(Se/Br)_N$	24	0.2296	< 0.001
$(Cr/Rb)_T$	24	0.1619		$(Se/Br)_T$	24	0.1176	
$(Fe/As)_N$	24	57.4961	< 0.001	$(Br/Rb)_N$	24	0.4734	< 0.001
$(Fe/As)_T$	24	16.3616		$(Br/Rb)_T$	24	1.2702	
$(Fe/Se)_N$	24	28.6352	< 0.001	$(Cr/Fe)_N$	24	0.0528	< 0.001
$(Fe/Se)_T$	24	10.6365		$(Cr/Fe)_T$	24	0.1965	
$(Fe/Br)_N$	24	5.7418	< 0.001	$(Zn/Rb)_N$	24	3.9335	< 0.001
$(Fe/Br)_T$	24	0.9581		$(Zn/Rb)_T$	24	1.9162	
$(Fe/Rb)_N$	24	2.4240	< 0.001				
$(Fe/Rb)_T$	24	1.0981					

Table 3-11 Mean comparison between normal and tumour tissue for the most significantly different ratios

3.3.2 Multivariate Results

Multivariate analysis was carried out using twenty one ratios mentioned in table 3-11 as the significant variables between normal and tumour samples. PCA and SIMCA classification results for the four unknown subgroups mentioned in table 3-4 will be reported in next subsections.

3.3.2.1 First subgroup classification results

PCA was carried out for all the samples and the result is shown in score plot (see Fig. 3-24). Two separate clusters of samples, one normal and one tumour can be seen seemingly. The unknown samples fell into one of the clusters distinctively. PC1 explains 52% variation of raw data matrix and PC2 explains 12% and both together can explain 64% variation of data.

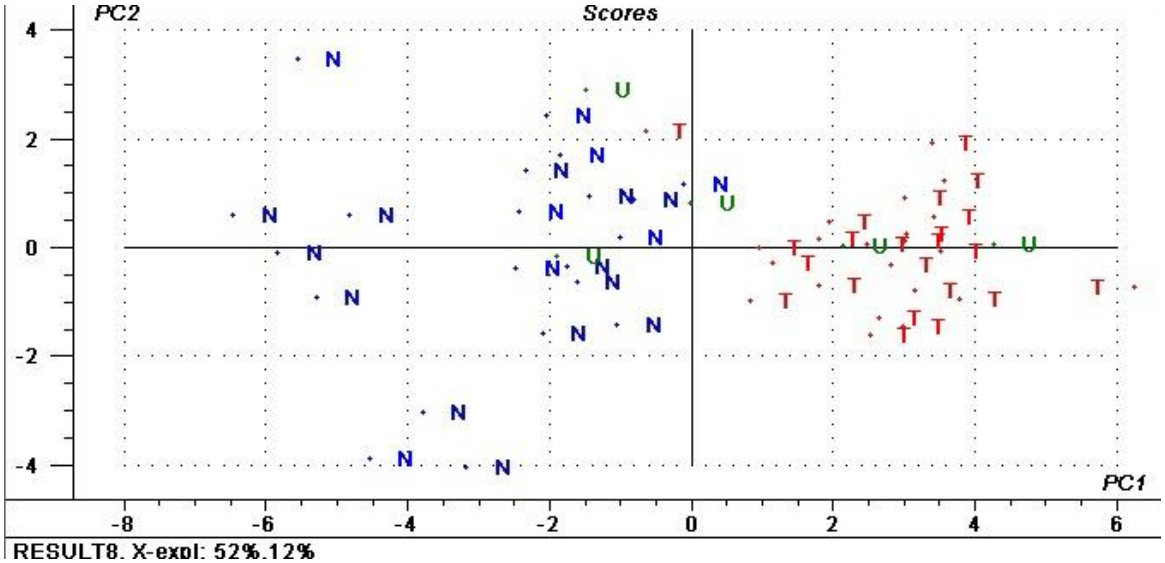

Fig. 3-24 Score Plot of PC1 vs. PC2 (first subgroup)

The map of variables is shown in Fig. 3-25. Studying loading plot together with score plot may give us useful information. It can be seen in the Fig 3-24 that all the variables that are on the right-hand side of loading plot have higher values in the tumour samples and all the variables on the left-hand side of loading plot correspond to normal samples in the score plot. It is evident that all the variables have contribution to PC1, while some of the variables, i.e. those on the PC1 axis or close to that, only have contribution to PC2.

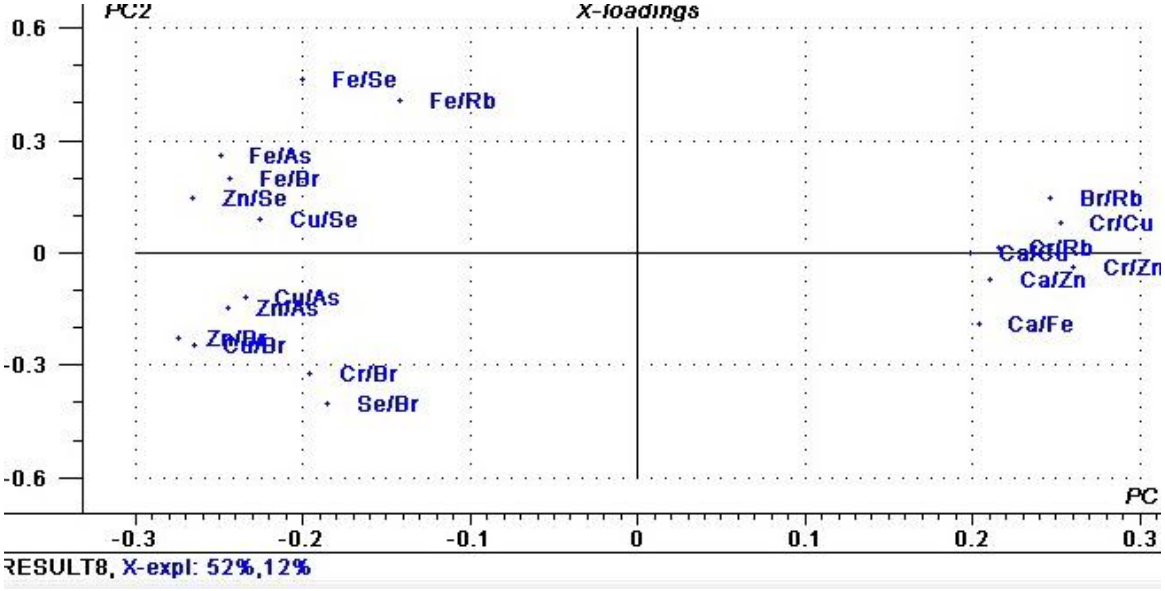

Fig. 3-25 Loading Plot of PC1 vs. PC2 (elemental ratios as variables-first subgroup)

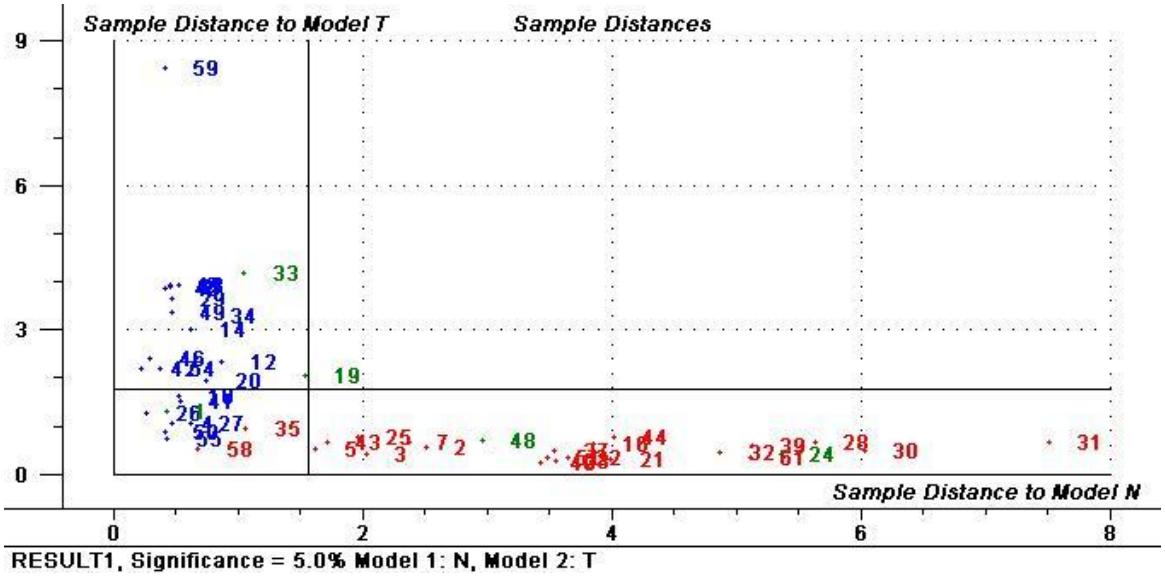

Fig. 3-26 Coomans plot, classification result (first subgroup)

The classification result is shown in Coomans plot (see Fig. 3-26). Samples 1, 19 and 33 are all among normal membership and are uniquely classified as normal. Samples 24 and 48 fell into tumour membership and are uniquely classified as tumour. Therefore, in this case SIMCA procedure classified all the unknown samples correctly.

Summary of the classification results for the elemental ratio data analyses are reviewed in table 3-12:

Elemental Ratio as Variables					
Subgroup	Sample	Classification Result		Histopathological Result	
		Normal	Tumour	Normal	Tumour
1	19	*		*	
	33	*		*	
	1	*		*	
	24		*		*
	48		*		*
2	13	*		*	
	20	*		*	
	7				*
	28		*		*
	51		*		*
3	14			*	
	41			*	
	55	*	*	*	
	16		*		*
	44		*		*
4	12	*		*	
	47	*		*	
	21		*		*
	30		*		*
	5		*		*

Table 3-12 Summary of classification results with elemental ratio variables and 5% confidence level

The score, loading and Coomans plots for the three other subgroups are presented in Appendix V.

3.4 Combined Data Study

Ultimately, all the elemental, coherent scattering and elemental ratio variables were combined and multivariate analysis was performed with the total of thirty five variables for the four unknown subgroups. PCA and SIMCA classification results for each subgroup will be reported in the following subsections.

3.4.1 First Subgroup Classification Results

The scores plot is illustrated in Fig. 3-27. Two separated clusters of normal and tumours can be seen evidently in score plot. PC1 explains 47% variation of raw data matrix and PC2 explains 10% and both together can explain 57% variation of data.

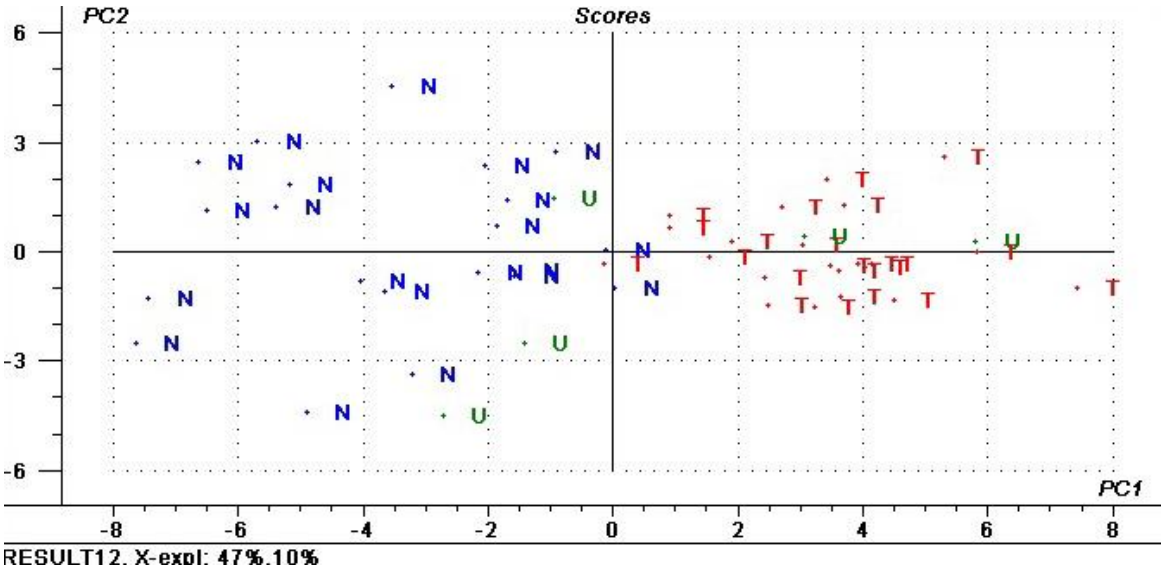

Fig. 3-27 Score Plot of PC1 vs. PC2 (first subgroup)

Loading plot which shows the similarities and differences of the samples is shown in Fig. 3-28. It can be seen that the variables which are similar between tumour samples are in the right side of PC1 line, and the variables which are similar between normal samples are in the left side of PC1 line. It is evident that all the variables lie far away from the origin. Since PC1 explains 47% and PC2 only 10%, then variables with large loadings in PC1 are much more important than those with large loadings in PC2, indeed 5 times as important.

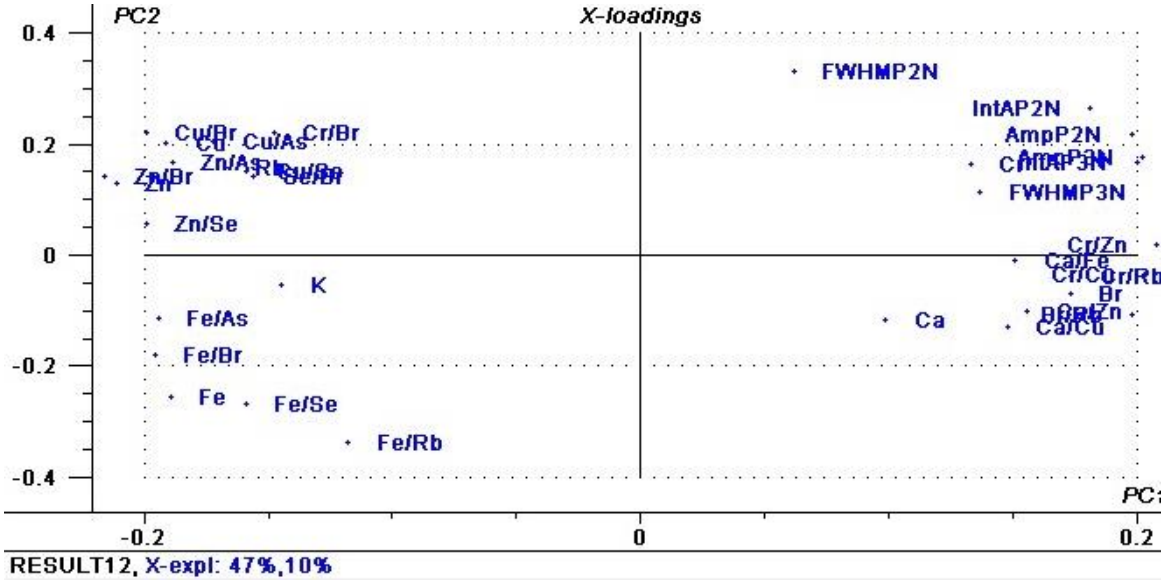

Fig. 3-28 Loading Plot of PC1 vs. PC2 (combined data as variables-first subgroup)

The SIMCA classification result is demonstrated by Coomans plot in Fig. 3-29. Explicitly it can be seen samples 1, 19 and 33 fell within the normal membership and therefore they accurately classified as normal. Likewise, samples 24 and 48 fell within the tumour membership distinctly, so classified precisely as tumour. In this case all the unknown samples were classified correctly.

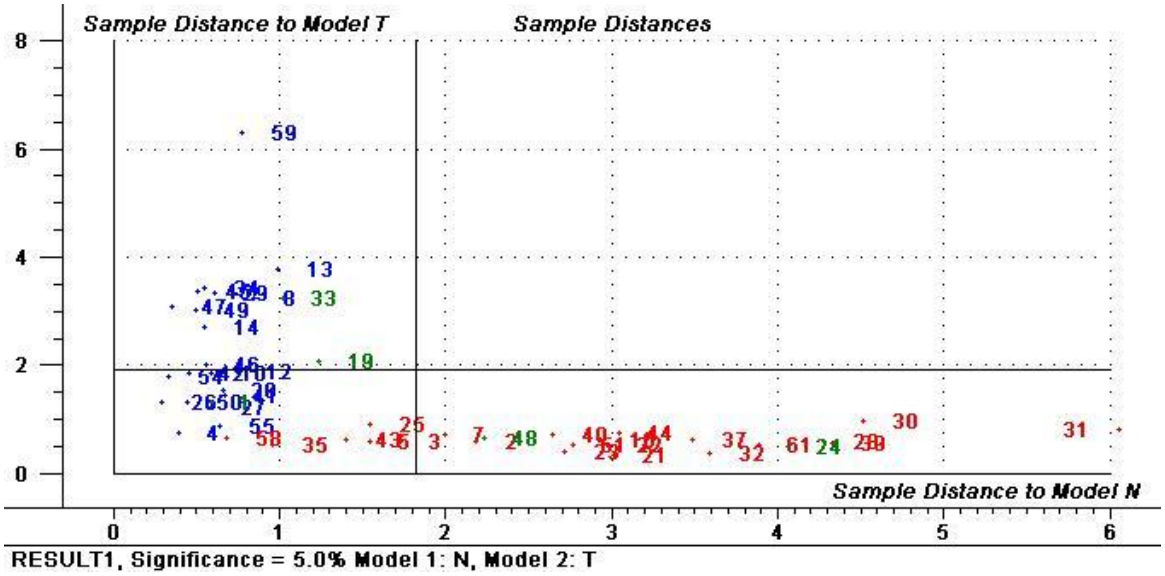

Fig. 3-29 Coomans plot, classification result (first subgroup)

Summary of the classification results for the combined data analyses are reviewed in table 3-13:

All combined as Variables					
Subgroup	Sample	Classification Result		Histopathological Result	
		Normal	Tumour	Normal	Tumour
1	19	*		*	
	33	*		*	
	1	*		*	
	24		*		*
	48		*		*
2	13	*		*	
	20	*		*	
	7	*			*
	28		*		*
	51		*		*
3	14			*	
	41	*		*	
	55	*	*	*	
	16		*		*
	44		*		*
4	12	*		*	
	47	*		*	
	21		*		*
	30		*		*
	5		*		*

Table 3-13 Summary of classification results with combined variables and 5% confidence level

The classification results for the four studies are summarized in table 3-14. It can be seen that combined variable study has the most correct classification and the Coherent scatter study has the least correct classification.

Study	Correct	Wrong	Both	None
XRF	10	1	7	2
Coherent Scatter	6	0	11	3
Elemental Ratios	16	0	1	3
Combined Variables	17	1	1	1

Table 3-14 Summary of classification results for four different studies

Chapter 4

Discussion and Conclusion

4.1 Discussion and Future Direction

4.2 Conclusion

4.1 Discussion

The bulk of the human body is comprised of hydrogen, carbon, nitrogen, oxygen and sulphur, which their concentration levels can be expressed in grams per kilograms. There are other elements in the periodic table called macrominerals, which act as structural components of tissue and the body fluids and are vital for the function of all cells. Na, Mg, P, Cl, K, and Ca are macrominerals and their concentration levels are lower than bulk elements, but still expressed in grams per kilograms (Merts, 1981). The rest of the elements in periodic table have much lower concentrations about milligrams or micrograms per kilogram of tissue. Since these elements were not readily quantified by the early analytical methods, and a very small amount of element could be detected, they were described as being present in "traces" and hence they have been called trace elements. They are categorized into essential and nonessential elements. In the absence of former ones, a deficiency syndrome develops however for the nonessential elements no proof of essentiality exists until now. Merely, seven essential trace elements were established until 1957: Mn, Fe, Cu, Zn, Co, Mo and I (Versieck, 1985). Several other elements have been added to the trace elements since then: F, Si, V, Cr, Ni, As (Schwartz, 1977), Se and Sb.

Elements of interest in this research are P, S, K, Ca, Cr, Fe, Cu, Zn, Ar, Se, Br and Rb (see table 2). However as it was presented in the results section, only K, Ca, Cr, Fe, Cu, Zn, Br and Rb were observed significantly different in human secondary colorectal liver tumour and normal surounding tissue. Hence, the focus is on these elements only.

The first element, potassium (K), has a substantial role in generating resting cell membranes and action potentials, sustaining intracellular osmalarity and in protein synthesis. Moreover, it is also a cofactor for acquiring maximum activity of the pyruvate kinase enzyme which is entangled in glycolysis energy production (Al-Abraheem *et al*, 2008). Ogawa *et al* (1999) reported an increased level of glycolysis in cancer cells in comparison to normal cell. This implies that K concentration level in cancerous tissue must be higher than in normal tissue, however, according to our result this is not the case for liver tissue. In Fig. 3-2 it can be clearly seen that the mean value in normal tissue is significantly higher than in tumour tissue (p=.046). This result is in agreement with Al-Abraheem *et al* (2008).

Over 90% of Calcium (Ca) in the body is restored in bone and about 19 mg/100 g is distributed in liver (Watts, 1990). It has a crucial role in skeletal structure and teeth. Barrage (1975) proved that Ca is a messenger, carrying signals through specific Ca channels within cells to target activities. In addition Ca ions are important for glycolytic enzyme activation and stability and affecting cell division and differentiation.

Malfunction of Ca^{2+} sensing receptor may lead to a progression of cancer disease. Kirchhoff and Geibel (2006) reported increased amount of extra cellular Ca^{2+} in colon carcinoma. Likewise, Al-Abraheem *et al* (2009) found higher Ca levels in tumour liver tissue. Our result for level of Ca supports this as well. According to table 3-1 and Fig. 3-2 Ca concentration level in secondary colorectal cancerous liver tissue is significantly ($p = .040$) higher compare to surrounding normal tissue.

In 1959, Cr was assumed as an essential element for mammals by Schwarz and Mertz (1959). It has an important role in keeping up proper carbohydrate and lipid metabolism. It is also important for the nucleid acids structure and metabolism. 5 to 6 mg is the total body content of Cr in adults; indeed it is higher at birth and decreases with age (Watts, 1989). Meat, whole grain, vegetable oil and beer are the good nutrition sources of Cr (Gross and Stosnach, 2009). Deficiency in Cr causes some disease: diabeties, peripheral neuropathy, cardiovascular heart disease, stress and depression (Watts, 1989). However Kristin *et al* (2011) published an article, using effects of a low-chromium diet, showed that Cr is no longer considered as an essential element in the body. In our study, it is found that Cr level is significantly higher ($p<.011$) in secondary colorectal liver tumour tissue compared to the surrounding normal tissue (see table 3-2 and Fig. 3-3).

Iron (Fe) is the trace element that exists in every cell. In the adult women body, the iron content is about 25 mg/kg and about 35 mg/kg in men (Watts, 1988). Electron transport via cytochromes in the Krebs cycle, oxidases, and oxygenates are the processes that Fe is involved with (Vitale, 1982). Moreover, it plays a major role in cell growth (Al-Ebraheem, 2008). Weinberg (1981, 1984, 1992a) found strong evidence for the dangerous effect of iron which is the ability to favour cancerous cell growth, and the fact that Fe can be carcinogenic. This was observed by Weinberg (1995). He explains the carcinogenic mechanism of Fe. Iron catalyses the development of hydroxyl radicals and suppresses activity of the host defence cells and advances cancer cells proliferation. In this study it is observed that the Fe level in tumour liver tissue was significantly lower ($p<.01$) than in normal surrounding liver tissue (see table 3-2 and Fig. 3-3). This result complies with the results reported by Al-Ebraheem *et al* (2009), Farquharson *et al* (2009) and Gurusamy *et al* (2008). The reduction in the level of Fe in tumour liver tissue could be justified by the fact that tumour cells consume more Fe for growth and results in the depletion of iron content in these tissues.

Copper (Cu) is the next essential element in the human body and its content in a healthy adult has been approximated to 80 mg/kg. Liver and brain are the two organs in the body with the highest level of copper. Cu has been accepted to be an essential factor of many enzymes including cytochrome c oxidase, superoxide dismutase (cytoplasm),

Ceruloplasmin, dopamine B-hydroxylase, lysyl oxidase, tyrosinase and monoamine oxidase (Watts, 1989). Copper is essential in protecting cells from damage via oxygen toxicity. Lower tissue copper contents are commonly observed in most metastatic cancers (Watts, 1989). Comparing tumour and normal liver tissue, it is found that copper level in tumour tissue is significantly lower ($p<.01$) than in normal liver tissue (see table 3-2 and Fig. 3-3). Supporting our result, lower level of copper in tumour liver tissue was reported by Gurusamy *et al* (2008) and Farquharson *et al* (2009) as well.

In 1869, the importance of Zinc (Zn) for the growth of living organisms was first discovered. Zinc has an important effect on human health and now it is confirmed that it is essential to over 300 enzymes in the human body. Zinc was discovered to be involved in the synthesis of RNA. (Watts, 1988) Furthermore, it has a role in anti-oxidation, immune function and inflammation (Tapiero, 2003). In our research, it is found that Zn is significantly lower ($p<.01$) in secondary colorectal liver tumour tissue than in surrounding normal liver tissue (see table 3-2 and Fig. 3-3). This result agrees with that reported by Al-Ebraheem *et al* (2008), Farquharson *et al* (2009) and Gurusamy *et al* (2008).

Bromine (Br) is not considered as an essential element for life functions. Br content in the human body is approximated to 260 mg. Bromine existence in the body is mostly due to the food intake, notably seafood. Br is easily absorbed by the body and it is particularly found in fluids around cells and in saliva. (Roza, 2009) In secondary colorectal liver tumour, it is found that Br levels were significantly higher ($p<.01$) when compared to normal surrounding normal liver tissue (see table 3-3 and Fig. 3-4).

Rubidium (Rb) is the 16^{th} most common element in the earth crust (Anderson, 1955), however in the human body there is little information about the biological importance of rubidium, and moreover evidence of Rb deficiency or intoxication has not been reported accurately. But, since it belongs to alkali metals and has close physiological relationship to potassium, there is huge interest in the biological properties of rubidium recently. Rb exists in all human tissues, however testis, liver, ovary, lymph node, kidney and muscle were found to have the highest concentrations (Selin *et al*, 1991 and Hamilton *et al*, 1972/1973). The biological role of rubidium is still unknown (Milman, 2006), although some observations imply that rubidium may be an essential trace element for human body (Schroeder, 1960). In our research it was found that Rb level was significantly ($p<.01$) lower in tumour tissue compared to normal liver tissue (see table 3-3 and Fig. 3-4).

The statistical differences between concentration levels of all these elements in normal and cancerous tissues can be due to the failure in the mechanism of chemical homeostasis. Cancer causes alteration in the permeability of cancerous cells` membranes

and leads to all of these differences in concentration of different elements between normal and cancerous tissues. (Majewska *et al*, 2007). The change of cell permeability is because of cancerous cells secretion of soluble factors into the cells (Payne *et al* , 1994).

Twenty one elemental ratios were found significantly different ($p < .001$) between normal and tumour liver tissue. These results suggest that ratio of the elements can be a more effective marker than the elements in liver tissue individually. For instance, in this study, As and Se were not significantly different ($p = .219$ and $p = .137$ respectively) between normal and cancerous liver tissue, however, their ratio was significant ($p = .04$). This result suggests that As/Se ratio could be a more effective marker of secondary colorectal liver cancer and a more important variable than changes in individual As and Se levels. With the intent of understanding the relationship of the trace elements and the mechanism related to tumour growth, the correlation between the eight elements in the normal and tumour liver tissue were checked using Spearman Rank-Order Correlation test. Correlation in normal liver tissue was found only for Zn and Se with the spearman coefficient of .521 and p value of .009. In addition, correlation between normal and tumour tissue was checked for all the pairs of elements. A strong correlation was found between Fe in tumour tissue and Br in normal tissue with spearman coefficient of .603 and p value of .001. This could be the reason behind the good classification result that was found with only these two elements. After extensive literature search, there is no work that represents a quantitative correlation between all these eight elements in the secondary colorectal liver tissue, so that the comparison would not be possible. However Silva *et al* (2009) observed a correlation between Ca and Zn in normal adjacent and tumour breast tissue with the coefficient of 0.551($p = .004$) and 0.482 ($p = .0.17$) respectively. They also found a correlation between Fe and Zn only in normal breast tissue and between Fe and Cu in tumour breast tissue. However in the liver tissue further study is required with different sets of tissues to verify our results or to investigate such a link.

In our coherent scattering study, four peaks were used in the samples spectra, which gave us useful information about the structure and composition of tissue samples. The first peak, appeared at 1.1 nm^{-1} momentum transfer, is related to the adipose (fat) content of tissue. As it can be seen in table 3-6, the three parameters of this peak were not significantly different ($p > .05$) between tumour and normal liver tissue (amplitude: $p = .051$, FWHM: $p = .950$ and Area: $p = .053$). The second peak, appeared at 1.6 nm^{-1} momentum transfer, and is related to the fibrous content of tissue. For this peak all the three peak parameters were significantly higher in tumour liver tissue compared to normal surrounding liver tissue (amplitude: $p < .01$, FWHM: $p = .039$ and Area: $p < .01$). The third peak, appeared at 2.2 nm^{-1} momentum transfer, and is related to the water content of

tissue. Similarly to the fibrous peak, all the three peak parameters for the water peak were significantly higher in tumour tissue when compared to normal liver tissue (amplitude: $p < .01$, FWHM: $p = .027$ and Area: $p < .01$). The position (momentum transfer) that each peak appeared at, are in agreement with results previously reported by Theodorakou and Farquharson (2009). They also found significant difference between tumour and normal tissue in amplitude and area for both fibrous and water content peaks ($p < .001$), however their result for the adipose peak showed a significant difference for adipose peak as well, contrarily to our adipose results.

The accuracy and repeatability of measuring the trace elements in liver and other human tissues using XRF are between 98 and 99% (Carvalho and Marques, 2001; Laursen *et al*, 2001 and Milman *et al*, 2000). The accuracy of our laboratory XRF for quantification of the trace elements in different tissues, including liver was checked in another study in this group (Moldovan, 2012) by analysing a standard reference material (homogenized lobster [LUTS-1, "Non defatted lobster hepatopancreas reference material for trace elements," National Research Council, Canada]) of the same samples weight. For instance Fe with the certified value = 11.6 ± 0.9 mg/kg and the experimental value = 12.4 ± 2.5 mg/kg (Moldovan, 2012). This validation indicates that our XRF method is accurate and reliable for trace elements measurement in human tissue samples.

Most of the problems around us are not univariate but multivariate in nature in which many variables contribute, and therefore there is a need of multivariate analysis which provides tools to mine the data, understand and visualize the relationships between samples and variables, either for pattern recognition, or to create models that can be used to classify new samples. The mean, median, standard deviation, normal distribution etc. are univariate statistics, which are useful but limited by only looking at one variable at a time. (CAMO Software white paper, 2011) For discriminating between normal and tumour liver tissue more than one variable is involved, so using only univariate analysis cannot tell the whole story and may lead to the wrong conclusions. In this study the difference in elemental content and structural composition between secondary colorectal liver tissue and the surrounding normal liver tissue were analyzed using multivariate analysis to develop normal and tumour models and classify the unknown samples based on the similarities to each model.

Multivariate analyses with different variables: elemental variables, coherent scattering variables, elemental ratio variables and combined variables, were carried out for twenty unknown samples. It was found that a two-element composite of Fe and Br correctly classified 7 of 10 normal and 8 of 10 tumour liver tissues for an overall accuracy of 75%. The best eight- and four-element PCA and SIMCA modelling for liver tissue

were less powerful, classifying with overall accuracy of 50% (6 of 10 normal and 4 of 10 tumour tissues) and 70% (8 of 10 normal and 6 of 10 tumour tissues).

It can be clearly noticed in tables 4-1 that classification results were improved prominently when all the elements, elemental ratios and coherent scattering parameters were employed for PCA and SIMCA modelling. If we consider "both" and "none" as a wrong classification result, then 50% of samples were classified correctly using 8 elements of interest as modelling variables (6 of 10 normal and 4 of 10 tumour liver tissue), 30% (3 of 10 normal and 3 of 10 tumour liver tissue) and 80% (7 of 10 normal and 9 of 10 tumour liver tissue) were classified correctly using coherent scattering parameters and elemental ratios respectively. However, when all these variables were combined in multivariate analysis, interestingly the percentage of correct classification increased to 85% (8 of 10 normal and 9 of 10 tumour liver tissue). All of the models have been performed with a 5% significance level. It is worth mentioning that all these samples were provided from a tissue bank, and the analyses relied on the labels which were written on the vials at the time of resection. So there is a possibility of mislabelling, or the fact that tissues were not precisely resected from the tumour or normal part of the tissue. For future work all the samples should histologically analysed over the measurement volume to have accurate information about the samples, and the classification results must be compared with the histological results.

a.

Elements as Variables			
Correct	**Wrong**	**Both**	**None**
19	7	1	13
33		48	41
24		28	
20		51	
14		55	
16		44	
12		5	
47			
21			
30			

b.

Coherent scattering as Variables			
Correct	**Wrong**	**Both**	**None**
19		1	14
33		48	47
24		13	30
16		20	
44		7	
12		28	
		51	
		41	
		55	
		21	
		5	

c.

Elemental Ratio as Variables			
Correct	**Wrong**	**Both**	**None**
19		55	7
33			14
1			41
24			
48			
13			
20			
28			
51			
16			
44			
12			
47			
21			
30			
5			

d.

All combined as Variables			
Correct	**Wrong**	**Both**	**None**
19	7	55	14
33			
24			
1			
48			
13			
20			
28			
51			
41			
16			
44			
12			
47			
21			
30			
5			

Table. 4-1 Summary of SIMCA classification results: **a.** Classification result with elements as variables (8 variables) in modelling. **b.** Classification result with coherent scattering parameters as variables (6 variables) in modelling. **c.** Classification result with elemental ratios as variables (21 variables) in modelling. **d.** Classification result with all combined parameters as variables in modelling.

Therefore SIMCA analysis has proven effective in differentiating between samples. This study is the indication of this fact that this technique has potential for creating effective tissue classification models. However it needs to be optimized clinical application. Optimization has to be performed to decrease the measurement time prominently to make it possible for use in the surgery room during the operation time. So far, the best method to differentiate between normal and tumour tissue is a histopathological test, which have to be carried out after the surgery and it takes time in order to provide an accurate result. Apart from detection of clear surgical margin, this method can be effectively used for diagnostic applications in different cancers such as breast or prostate cancers. The ideal and favourable cancer diagnostic method ought not to depend on the physician or patient characteristics. For instance, there are many factors that affect mammographic accuracy in diagnosing a breast cancer (Smith-Binman *et al*, 2005). Their results showed that the false-positive rate for the patients younger than 40 years old is lower (6.5%) than for the patients older than 70 years old (10.5%). Also, patients with the considerably fatty breast density, have lower false-positive rate. Furthermore, they founded that the mammographic accuracy not only depends on the patient characteristics but also in a large portion depends on the physician characteristics such as age, sex, annual mammographic volume, time since receipt of medical degree and a focus on screening mammography. Contrary to Beam *et al* (2003) their results support those of Elmore *et al* (1998) and Esserman *et al* (2002) that more experienced physicians have lower false-positive rates which are defined as:

> "No breast cancer was diagnosed within 12 months of a positive screening mammogram".

Statistically they found the mean sensitivity was 77%, and the mean false positive rate was 10% without adjusting for the patient characteristics. After adjustment their results showed higher specificity associated with three factors:

> "At least 25 years since receipt of a medical degree ([OR] = 1.54, 95% CI = 1.14 to 2.08; P =.006), interpretation of 2500 – 4000 (versus 481 – 750) screening mammograms annually (OR = 1.30, 95% CI = 1.06 to 1.59; P = .011) and a high focus on screening mammography compared with diagnostic mammography (OR = 1.59, 95% CI = 1.37 to 1.82; P <.001)."

However, if the method described in this work is optimized, its accuracy would not depend on the physician characteristics, hence it would be clinically favourable for diagnostic purposes as well.

One of the biggest sources of inaccuracy in this study comes from this fact that, there were not a constant calibrating normal and tumour samples to build the constant normal and tumour models. The unknown samples were picked out from the calibrating data samples; hence in the classification of each subgroup, the normal and tumour PCA models were built with the data from different samples. This cause a change in the model each time, so the decision to choose which variables (using discrimination and modelling power) help the improvement of modelling, would be hard and not accurate. For instance, in Fig. 3-8, K has a large discrimination power of more than 4 in subgroup 3, while it has a low discrimination power of less than 3 in subgroups 1 and 4. From all the discrimination powers it can be seen that subgroup 3 has a different trend compared to the other three subgroups, and this proves that changes in the data set, from which the normal and tumour PCA models were developed, would affect the accuracy of the classification result considerably. However this limitation is due to the number of samples used to develop each model. Ryan and Farquharson (2007) calculated the minimum required sample size for each tissue type should be 30. In this study the models built with 21 and 22 normal and tumour tissues. Hence, picking out subgroups out of this small sample size can really affect the models. Therefore in order to optimize and increase the accuracy of the classification result, for future work, much bigger sample size has to be used.

4.2 Conclusion

The main aim of presented research is to study the differences in elemental composition and structural information between normal and secondary colorectal cancer in human liver tissue. The results implied that XRF is a potent and effective technique to evaluate elemental composition of liver tissue. It was concluded that the level of P, S, As and Se were not statistically significant ($p > .05$) between tumour and normal liver tissue, however, the level of K ($p = .046$), Ca ($p = .040$), Cr ($p = .011$), Fe, Cu, Zn, Br and Rb were statistically significant ($p < 0.01$) between tumour and normal liver tissues. K, Fe, Cu, Zn and Rb were significantly higher in normal liver tissue than in secondary colorectal liver tumour tissue, while Ca, Cr and Br were significantly lower in normal liver tissue. These results are consistent with those obtained by the others. All the coherent scattering peak parameters were statistically significant ($p < .05$) for fibrous and water content peaks. It was found that amplitude; FWHM and area under these two peaks were significantly higher in secondary colorectal liver tumour tissue compared to surrounding normal liver tissue. However, the amplitude, FWHM and area under the adipose peaks were not seen to vary significantly different ($p >.05$) between tumour and normal liver tissue.

Using XRF data, elemental ratios and coherent scatter profiles separately in multivariate analyses, classification models have been built, and it was found that the classification accuracy for each set was 50%, 30% and 80% respectively. Ultimately, the classification results accuracy was improved to 85% when the amalgamation of all these variables was used in a final classification model.

This study proved that X-ray interaction techniques: XRF and coherent scattering, together with Principle Component Analysis and Soft Independent Modelling of Class Analogy approach can be used as a discriminator for human secondary colorectal liver cancer tissue samples and surrounding normal liver tissue samples. Since hepatic resection is still the best known therapeutic modality for patients with secondary colorectal liver metastasis, it would be our future goal to use this technique and optimize this model to develop a rapid, accurate diagnostic tool that can differentiate benign from malignant tissue at the time of surgery for this and other cancers.

REFERENCES

Al-Abraheem A, Farquharson M J, Ryan E. (2009). The evaluation of biologically important trace metals in liver, kidney and breast tissue. *Appl. Radiat. Isotopes. Doi:*10.1016/j.apradiso.2008.06.018

Al-Abraheem A, Mersov A, Gurusamy K, Farquharson M J. (2010). Distribution of Ca, Fe, Cu and Zn in primary colorectal cancer and secondary colorectal liver metastases . *Nucl. Instr. and Meth. A*. doi:10.1016/j.nima.2009.10.069

Anderson H M, and Mudge G H. (1955). The effect of potassium on intracellular bicarbonate in slices of kidney cortex. *J. clin. Invest.* 34, 1691-1697

Berridge M J. (1975). The interaction of cyclic nucleotides and calcium in the control of cellular activity. *Advances in Cyclic Nucleotide Researc.* Vol. 6. Greengard, P., Robi-son, G.A., Eds. Raven Press, N.Y.

CAMO Software. (2011). What is Multivariate analysis? An introduction to the principles and common models used in multivariate data analysis [White Paper]. Retrieved from CAMO Software: http://www.camo.com/

Canadian Cancer Society's Steering Committee on Cancer Statistics (2011). Canadian Cancer Statistics 2011. Toronto, ON: Canadian Cancer Society; 2011. May 2011 ISSN 0835-29761.5

Canadian Cancer Society, *What is Cancer?* Retrieved March 30, 2012 from: http://www.cancer.ca/Canada-wide/About%20cancer.aspx?sc_lang=en#ixzz1qcHMAk6n

Carvalho M L, Marques A F. (2001). X-ray fluorescence spectrometry: applications in trace elements studies in human tissues from patients with cirrhosis. *X-ray spectrum.* 30, 397-402

Castro C R F, Barroso R C and Lopes R T. (2005). Scattering Signatures for some human tissues using Synchrotron Radiation. *X-ray Spectrometry.* 34, 477-480

Changes V, Oghabian M A, Speller R, et al. (2005). Application of Small Angle X-ray Scattering (SAXS) for Differentiation between Normal and Cancerous Breast Tissue. *Int. J. Med. Sci.* 2(3), 118-121

Drake II E N, Sky-Peck H H. (1989). Discriminant Analysis of Trace Element Distribution in Normal and Malignant Human Tissues. *Cancer Research.* 49, 4210-4215

Dobrowolski Z, Drewniak T, Kwiatek W, et al. (2002). Trace Elements Distribution in Renal cell Carcinoma Depending on Stage of Disease. *European Urology.* 42, 475-480

Elmore JG, Wells CK, Howard DH. (1998). Does diagnostic accuracy in mammography depend on radiologists' experience? *Women's Health* 7, 443 – 9.

Esserman L, Cowley H, Eberle C, et al. (2002). Improving the accuracy of mammography: volume and outcome relationships. *Natl Cancer Inst* 94

Farquharson M J, Al-Abraham A, Theodorakou C, et al. (2009). Measurement of K, Fe, Cu and Zn levels in Secondary Colorectal Liver Cancer and Surrounding normal LiverTissue, and their Potential as a Tissue Classifier. *X-ray Spectroscopy.* 38, 81-88

Farquharson M J , Al-Abraham A, Geraki K, et al. (2009). Zinc presence in invasive ductal carcinoma of the breast and its correlation with oestrogen receptor status. *Phys. Med. Biol.* 54, 4213–4223

Geraki K, Farquharson MJ and Bradley DA. (2002). Concentration of Fe, Cu and Zn in breast tissue: a synchrotron XRF study. *Phys.Med.Biol.* 47, 2327-2339

Geraki K, Farquharson MJ and Bradley DA. (2004). X-ray fluorescence and energy dispersive x-ray diffraction for the quantification of elemental concentrations in breast tissue. *Phys.Med.Biol.* 49, 99-110

Gorry P A. (1990). General Least-Squares Smoothing and Differentiation by the Convolution (Savitzky-Golay) Method. *Anal Chem*. 62, 570-573

Gross A and Stosnach H. (2009). Lab Report XRF 434: S2 PICOFOX Trace Elements in Biological Matrices and their Impact in Clinical Chemistry. Bruker AXS Microanalysis GmbH, Berlin, Germany. Order No. L81-EXS034.

Gurusamy K S, Farquharson M J, Craig C, Davidson B R. (2008). An evaluation study of trace element content in colorectal liver metastases and surrounding normal livers by X-ray fluorescence. Bimetal. 21, 373-378

Hamilton E I, Minski M J, Cleary J J. (1972/1973). The concentration and distribution of some stable elements in healthy human tissues from the United Kingdom. *Sci Total Environ.* 1, 341–74

Health Metz. Retrieved March 30, 2012 from: http://healthmetz.com/2011/06/09/effects-and-how-treatment-of-liver-disease.html

Jemal A, Siegel R, Ward E, et al. (2009). Cancer statistics. *CA Cancer J Clin.* 59, 225–249

Kidane G, Speller R D, Royle G J and Hanby A M. (1999). X-ray Scatter Signature for Normal and Neoplastic Breast Tissues. *Phys.Med.Biol. 44, 1791-1802*

Kirchhoff P, Geibel J P. (2006). Role of Calcium and other trace elements in gastrointestinal Physilogy. *World J. Gastroenterol*. 12(20), 3229-3236

Knoll G F. (1979). Radiation Interaction. *Radiation detection and Measurement*. US. John Wiley & Sons Inc.

Kosanetzky J, Knoerr B, Harding G, Neitzel U. (1987). X-ray diffraction measurement of some plastic materials and body tissues. *Med Phys.* 14, 1811–1816

Kwiatek W M, Drewniak T, Gajda M, et al. (2002). Preliminary study on the distribution of selected elements in cancerous and non-cancerous kidney tissues. *Med. Biol.* 16, 155-160

Kwiatek W M, Hanson A L, Paluszkiewicz C, et al. (2004). Application of SRIXE and XANES to the determination of the oxidation state of iron in prostate tissue sections. *Alloys Comp.* 362, 83-87

Kwiatek W M, Ban´as A, Ban´as K, et al. (2005). Iron and other elements studies in cancerous and non-cancerous prostate tissues. *Alloys Comp.* 401, 178-183

Kubala-Kukus A, Braziewicz J, Banas D, et al. (1999). Trace Element Load in Cancer and Normal Tissue. *Nuclear Instruments and Methods in Physics Research B.* 150, 193-199

Lachance G R, Claisse F. (1995). X-ray Physics. *Quantitative X-ray Fluorescence Analysis.* US. John Wiley & Sons Ltd.

Laursen J, Milman N, Pederson HS, et al. (2001). Elements in autopsy liver tissue samples from Greenlandic Inuit and Danes. III. Zinc measured by X-ray fluorescence spectrometry. *Trace Elem Med Biol* 15(4), 209-214

Magalhães T., Carvalho M.L., Von Bohlen A., et al. (2010). Study on trace elements behaviour in cancerous and healthy tissues of colon, breast and stomach: Total reflection X-ray fluorescence applications. *Spectrochimica Acta Part B.* 65, 493–498

Majewska U, Banas D, Braziewicz J, et al. (2007). Trace Element Concentration distributions in Breast Lung and Colon Tissues. *Phys. Med. Boil*. 52, 3895-3911

Medindia. *Colorectal Cancer - Anatomy and Physiology.* Retrieved March 30, 2010 from: http://www.medindia.net/patients/patientinfo/ColorectalCancer-Anatomy.htm

Mertz W. (1981). The Essential Trace Elements. *Science.* 213, 1332-1338

Milman N, Laursen J, Sloth-Pederson H, et al. (2000). Elements in autopsy liver tissue samples from Greenlandic Inuit and Danes. II. Iron measured by X-ray fluorescence spectrometry. *Trace Elem Med Biol* 14(2), 100-107

Milman N, Laursen J, yBg K E, Peterson H S, Mulled G. (2006). Rubidium content in autopsy liver tissue samples from Greenlandic Inuit and Danes measured by X-ray fluorescence spectrometry. *Trace Elements in Medicine and Biology.* 20, 227–232

Moldovan N. (2012). Msc Thesis. Measurement of Transition Metals in the Rodent Brain using X-ray Fluorescence and Neutron Activation Analysis

Pawlik TM, Choti MA. (2007). Surgical therapy for colorectal metastases to the liver. *J Gastrointest Surg*. 11, 1057–1077.

Pereira G R, Rocha H S, Calza C, et al. (2010). Biological tissues analysis by XRF microtomography. *Applied Radiation and Isotopes*. 68, 704–708

Poletti M.E., Goncalves O.D., Mazzaro I., (2002a). Coherent and incoherent-scattering of 17.44 and 6.93 keV X-ray photons scattered from biological and biological-equivalent samples: characterization of tissues. *X-ray Spectrometry.* 31, 57–61

Poletti M.E., Goncalves O.D., Mazzaro I., (2002b). X-ray Scattering from Human Breast Tissues and Breast Equivalent materials.. *X-ray Spectrometry.* 47, 47–63.

Poletti M.E., Goncalves O.D., Perez C. A., et al. (2004). A preliminary study ofthe distribution oftrace elements in healthy and neoplastic breast tissues with synchrotron radiation X-ray fluorescence. *Radiation Physics and Chemistry*. 71, 975–976

Roza G. (2009). Bromine. *Understanding the elements of periodic table*. Rosen Publishing Group Inc. New York, NY.

Ryan E, Frquharson M J. (2004). Angular Dispersive X-ray Scattering from Breast tissue using Synchrotron Radiation. *Radiat. Phys. Chem.* 71, 971-972

Savitsky A, Golay M J A. (1964). Smoothing and differentiation of data by simplified least square procedure. *Anal Chem.* 36, 1627-1639

Schlot R and Uhlig S. (2000-2006). *An Overview of XRF Basics, An Introduction to X-ray Fluorescence (XRF).* Retrieved April 15, 2012 from: http://www.bruker-axs.de/fileadmin/user_upload/xrfintro/author.html

Schroeder HA. (1960). Possible relationships between trace metals and chronic diseases. In: Seven MJ, Johnson LA, editors. Metal-binding in medicine. Philadelphia: J.B. Lippincott Company. p. 59–65

Schwarz K, Mertz W. (1959). Chromium (III) and the glucose tolerance factor. *Arch Biochem Biophys* 85, 292–295

Schwarz K. (1977). Essentiality vs. toxicity of metals, in Clinical Chemistn and Chemical Toxicology of Metals. *Brown, S. S., Ed., Elsevier/North-Holland. Amsterdam*. 3

Selin E, Teeyasoontranont V. (1991). Rubidium: a companium of potassium or an essential trace element of its own. *Beitr Infusionsther*. 27, 86–103

Shilstein S Sh, Cortesi M, Breslin A, et al. (2006).Prostatic Zn determination for prostate cancer diagnosis *Atlanta.* 70, 914-921

Silva M P, Tomal A, Perez C A, et al. (2009). Determination of Ca, Fe, Cu and Zn and their correlations in breast cancer and normal adjacent tissues. *X-ray Spectrometry.* 38, 103-111

Smith-Bindman R , Chu P , Miglioretti DL, et al. (2005). Physician Predictors of Mammographic Accuracy. *National Cancer Institute* 97(5), 358-367

Steinier J, Termini Y, Deltour J. (1972). Smoothing and differentiation of data by simplified least square procedure. *Anal Chem.* 1;44(11), 1906-1909

Tapiero H, Tew K D. (2003). Trace elements in human physiology and pathology: zinc and metallothioneins. *Biomedicine & Pharmacotherapy* 57, 399–411

Theodorakou C, Farquharson M J. (2009). The classification of secondary colorectal liver cancer in human biopsy samples using angular dispersive x-ray diffraction and multivariate analysis. *Phys.Med.Biol*. 54, 4945-4957

Versieck J. (1985). Trace elements in human body fluids and tissues. *CRC Crit Rev Clin Lab Sci.* 22, 97–184

Vitale J J. (1982). Impact of nutrition on immune function. *Advances in Human Clinical Nutrition*. Broitman, S.A., Eds. John Wright, Inc. Boston

Watts D L. (1988). The Nutritional Relationships of Iron. *Orthomolecular Medicine*. 3 (3), 110-116

Watts D L. (1988). The Nutritional Relationships of Zinc. *Orthomolecular Medicine*. 3 (2), 63-67

Watts D L. (1989). The Nutritional Relationships of Chromium. Orthomolecular Medicine. 4 (1), 17-23

Watts D L. (1989). The Nutritional Relationships of Copper. *Orthomolecular Medicine.* 4 (2), 99-108

Watts D L. (1990). The Nutritional Relationships of Calcium. *Orthomolecular Medicine.* 5 (2), 61-66

Weinberg E D. (1981). Iron and neoplasia. *Boil Trace Element Res. 3, 55-80*

Weinberg E D. (1984). Iron withholding: a defense against infection and neoplasia. *Physiol Rev.* 64, 64-102

Weinberg E D. (1992a). Roles of iron metabolism in health and disease. *Drug Metab Rev.* 22, 531-579

Weinberg E D. (1996). The role of Iron in cancer. *European Journal of Cancer Prevention.* 5, 19-36

Zhang L, Lv J, Sun S. (2011). Elements in Lung Tissues of Patients from a High Lung Cancer Incidence Area of China. *Bio Trace Elem Res.* 10.1007/s12011-012-9336-6

APPENDIX I: RAW DATA: Normalized Peak Area (XRF)

Sample N	Sample T	K	K	K/Ca	K/Ca	K/Cr	K/Cr	K/Fe	K/Fe	K/Cu	K/Cu
		N	T	N	T	N	T	N	T	N	T
8	7	1.83E-03	1.03E-03	1.48E+01	9.41E+00	1.95E+01	1.54E+01	8.45E-01	1.85E+00	3.79E+00	1.69E+01
10	31	1.48E-03	5.54E-04	1.38E+01	7.54E-01	1.34E+01	3.71E+00	1.36E+00	9.21E-01	2.79E+00	3.54E+00
12	22	2.37E-03	1.80E-03	6.06E+00	5.71E+00	2.55E+01	1.14E+01	5.38E-01	2.77E+00	8.72E+00	1.04E+01
14	24	4.82E-04	3.16E-04	3.68E+00	3.38E+00	4.70E+00	1.80E+00	8.78E-01	5.95E-01	1.39E+00	2.59E+00
19	25	4.51E-04	1.23E-03	3.03E+00	1.25E+01	3.33E+00	8.73E+00	1.19E-01	7.13E-01	2.83E+00	8.33E+00
20	37	5.19E-04	1.73E-04	1.82E+01	2.46E+00	4.30E+00	1.27E+00	1.62E-01	1.19E-01	1.15E+00	2.03E+00
26	51	4.95E-04	1.39E-03	7.03E+00	5.76E+00	3.99E+00	9.98E+00	1.94E-01	1.99E+00	1.26E+00	1.26E+01
27	39	8.13E-04	1.45E-03	9.53E+00	1.55E+00	5.40E+00	1.11E+01	5.54E-01	1.16E+00	2.54E+00	8.93E+00
29	2	1.66E-03	3.08E-03	2.41E+01	8.74E+00	1.33E+01	2.53E+01	3.87E-01	3.52E+00	2.84E+00	1.71E+01
33	61	9.64E-04	2.90E-04	4.07E+00	3.72E+00	8.72E+00	1.53E+00	2.04E-01	1.53E+00	5.77E+00	1.87E+00
34	21	5.83E-04	1.12E-03	9.58E+00	3.37E+00	5.50E+00	6.63E+00	4.90E-01	9.72E-01	8.83E-01	6.58E+00
41	58	5.91E-04	1.55E-03	1.38E+00	1.23E+01	3.49E+00	1.47E+01	2.25E-01	7.92E-01	1.46E+00	5.43E+00
42	40	2.94E-03	3.81E-04	5.26E+01	1.76E+00	2.47E+01	2.73E+00	8.75E-01	5.62E-01	7.88E+00	2.92E+00
45	48	2.98E-03	6.31E-04	1.47E+01	1.47E+01	2.18E+01	4.82E+00	6.97E-01	9.48E-01	4.64E+00	2.57E+00
46	3	7.80E-04	1.17E-03	9.15E+00	4.37E+00	6.59E+00	1.01E+01	1.59E-01	8.38E-01	2.43E+00	9.36E+00
47	23	1.46E-03	1.27E-03	2.61E+01	3.28E+00	1.47E+01	6.97E+00	2.63E-01	1.45E+00	5.14E+00	4.29E+00
49	30	2.78E-03	2.94E-04	1.02E+01	2.79E+00	2.41E+01	1.37E+00	3.90E-01	3.02E-01	4.27E+00	1.81E+00
54	43	1.99E-03	4.08E-04	4.26E+01	1.82E+00	1.78E+01	3.03E+00	5.16E-01	2.55E-01	6.20E+00	2.68E+00
55	28	1.94E-03	7.15E-04	1.40E+01	1.66E+00	1.48E+01	5.54E+00	9.32E-01	7.46E-01	6.35E+00	3.25E+00
59	5	2.43E-03	7.05E-04	6.84E+01	1.65E+00	2.65E+01	5.38E+00	4.39E-01	7.75E-01	6.53E+00	4.08E+00
1	44	1.69E-03	7.32E-04	6.57E+00	5.05E+00	1.40E+01	4.08E+00	8.26E-01	1.02E+00	5.02E+00	5.55E+00
13	35	1.75E-03	2.46E-04	9.29E+00	1.44E+00	1.07E+01	1.86E+00	4.95E-01	3.12E-01	2.11E+00	6.60E-01
4	16	6.55E-04	6.27E-04	4.08E+00	3.13E+00	5.56E+00	5.58E+00	2.51E-01	3.37E-01	1.98E+00	7.46E+00
50	32	8.07E-04	7.27E-04	1.25E+01	2.65E+00	6.02E+00	4.22E+00	6.01E-01	8.51E-01	2.05E+00	2.28E+00

Table AI-1 a. Normalized Area under K Peak (peak area/scatter area ratio) and ratios of K peak area with other elements for both normal and tumor tissues

Sample N	Sample T	K/Zn	K/Zn	K/As	K/As	K/Se	K/Se	K/Br	K/Br	K/Rb	K/Rb
		N	T	N	T	N	T	N	T	N	T
8	7	3.47E-01	1.74E-01	9.25E+01	1.43E+01	2.57E+01	8.57E+00	2.58E+00	1.24E+00	1.13E+00	7.45E-01
10	31	3.90E-01	5.42E-01	2.87E+01	8.82E+00	1.43E+01	5.65E+00	2.91E+00	3.93E-01	1.01E+00	8.52E-01
12	22	6.06E-01	1.24E+00	4.01E+01	3.70E+01	3.02E+01	1.97E+01	3.67E+00	1.76E+00	1.66E+00	1.39E+00
14	24	5.27E-02	3.28E-01	1.37E+01	3.97E+00	2.42E+00	1.71E+00	1.09E+00	1.82E-01	2.32E-01	3.30E-01
19	25	1.61E-01	6.28E-01	4.29E+00	2.10E+01	3.94E+00	1.10E+01	6.07E-01	1.63E+00	1.99E-01	8.82E-01
20	37	1.14E-01	1.19E-01	6.94E+00	2.61E+00	3.38E+00	2.31E+00	7.61E-01	5.65E-02	7.75E-01	1.34E-01
26	51	8.37E-02	1.10E+00	7.45E+00	2.77E+01	3.38E+00	2.58E+01	7.56E-01	1.14E+00	3.87E-01	1.72E+00
27	39	9.69E-02	8.05E-01	9.69E+00	4.53E+01	4.16E+00	1.32E+01	1.07E+00	1.69E+00	4.91E-01	1.20E+00
29	2	2.19E-01	1.70E+00	5.25E+01	8.38E+01	1.39E+01	4.61E+01	2.96E+00	5.48E+00	5.51E-01	1.74E+00
33	61	3.14E-01	2.58E-01	1.06E+01	4.96E+00	1.15E+01	2.40E+00	1.96E+00	3.44E-01	1.22E+00	2.62E-01
34	21	1.17E-01	8.57E-01	8.75E+00	1.36E+01	5.01E+00	8.40E+00	1.61E+00	1.16E+00	3.15E-01	1.35E+00
41	58	8.84E-02	4.13E-01	1.17E+01	2.32E+01	4.36E+00	2.74E+01	6.32E-01	1.48E+00	8.64E-01	1.86E+00
42	40	5.76E-01	3.12E-01	5.14E+01	7.75E+00	2.02E+01	4.61E+00	5.35E+00	4.35E-01	1.67E+00	4.10E-01
45	48	4.35E-01	5.92E-01	6.10E+01	1.12E+01	2.30E+01	5.47E+00	6.57E+00	5.55E-01	1.48E+00	7.70E-01
46	3	1.95E-01	7.28E-01	1.03E+01	1.41E+01	6.88E+00	1.05E+01	1.07E+00	8.16E-01	4.51E-01	1.34E+00
47	23	3.20E-01	7.87E-01	1.98E+01	1.52E+01	9.00E+00	7.30E+00	2.50E+00	1.50E+00	1.11E+00	1.78E+00
49	30	3.56E-01	2.79E-01	4.53E+01	3.51E+00	3.04E+01	4.73E+00	3.84E+00	2.90E-01	1.54E+00	3.40E-01
54	43	4.11E-01	2.02E-01	4.11E+01	9.80E+00	1.55E+01	2.66E+00	3.21E+00	3.40E-01	1.16E+00	4.11E-01
55	28	4.88E-01	7.91E-01	2.67E+01	4.66E+00	2.21E+01	3.20E+00	2.83E+00	7.25E-01	1.22E+00	9.98E-01
59	5	3.76E-01	2.68E-01	4.03E+01	1.13E+01	2.36E+01	8.12E+00	8.44E+00	7.81E-01	1.85E+00	1.16E+00
1	44	4.18E-01	5.10E-01	5.11E+01	1.15E+01	1.72E+01	1.96E+01	2.96E+00	9.14E-01	1.64E+00	6.02E-01
13	35	1.53E-01	8.59E-02	2.14E+01	3.10E+00	4.88E+00	9.35E-01	3.23E+00	2.29E-01	1.15E+00	4.11E-01
4	16	2.10E-01	6.68E-01	9.85E+00	7.59E+00	5.18E+00	5.09E+00	7.87E-01	4.58E-01	9.01E-01	7.13E-01
50	32	1.92E-01	6.82E-01	1.17E+01	7.20E+00	9.72E+00	5.76E+00	1.34E+00	5.88E-01	4.65E-01	1.15E+00

Table AI-1 b. Normalized Area under K Peak (peak area/scatter area ratio) and ratios of K peak area with other elements for both normal and tumor tissues

Sample N	Sample T	Ca	Ca	Ca/Cr	Ca/Cr	Ca/Fe	Ca/Fe	Ca/Cu	Ca/Cu	Ca/Zn	Ca/Zn
		N	T	N	T	N	T	N	T	N	T
8	7	1.23E-04	1.09E-04	1.32E+00	1.64E+00	5.70E-02	1.96E-01	2.56E-01	1.79E+00	2.34E-02	1.84E-02
10	31	1.07E-04	7.35E-04	9.69E-01	4.92E+00	9.83E-02	1.22E+00	2.02E-01	4.69E+00	2.82E-02	7.18E-01
12	22	3.90E-04	3.15E-04	4.21E+00	2.00E+00	8.87E-02	4.85E-01	1.44E+00	1.83E+00	1.00E-01	2.18E-01
14	24	1.31E-04	9.35E-05	1.28E+00	5.33E-01	2.39E-01	1.76E-01	3.78E-01	7.66E-01	1.43E-02	9.70E-02
19	25	1.49E-04	9.88E-05	1.10E+00	7.00E-01	3.92E-02	5.72E-02	9.35E-01	6.68E-01	5.31E-02	5.03E-02
20	37	2.85E-05	7.03E-05	2.36E-01	5.16E-01	8.91E-03	4.83E-02	6.31E-02	8.23E-01	6.23E-03	4.83E-02
26	51	7.04E-05	2.41E-04	5.68E-01	1.73E+00	2.75E-02	3.46E-01	1.80E-01	2.18E+00	1.19E-02	1.91E-01
27	39	8.53E-05	9.39E-04	5.67E-01	7.18E+00	5.82E-02	7.52E-01	2.66E-01	5.77E+00	1.02E-02	5.20E-01
29	2	6.90E-05	3.53E-04	5.50E-01	2.90E+00	1.61E-02	4.03E-01	1.18E-01	1.96E+00	9.09E-03	1.94E-01
33	61	2.37E-04	7.80E-05	2.14E+00	4.12E-01	5.01E-02	4.12E-01	1.42E+00	5.04E-01	7.70E-02	6.94E-02
34	21	6.09E-05	3.34E-04	5.74E-01	1.97E+00	5.12E-02	2.89E-01	9.22E-02	1.95E+00	1.22E-02	2.55E-01
41	58	4.28E-04	1.26E-04	2.53E+00	1.20E+00	1.63E-01	6.46E-02	1.06E+00	4.43E-01	6.40E-02	3.37E-02
42	40	5.59E-05	2.17E-04	4.70E-01	1.55E+00	1.66E-02	3.20E-01	1.50E-01	1.66E+00	1.10E-02	1.77E-01
45	48	2.03E-04	4.30E-05	1.49E+00	3.28E-01	4.75E-02	6.45E-02	3.16E-01	1.75E-01	2.96E-02	4.03E-02
46	3	8.52E-05	2.69E-04	7.20E-01	2.32E+00	1.73E-02	1.92E-01	2.65E-01	2.14E+00	2.13E-02	1.67E-01
47	23	5.60E-05	3.86E-04	5.64E-01	2.12E+00	1.01E-02	4.43E-01	1.97E-01	1.31E+00	1.23E-02	2.40E-01
49	30	2.73E-04	1.05E-04	2.37E+00	4.93E-01	3.83E-02	1.08E-01	4.20E-01	6.50E-01	3.50E-02	1.00E-01
54	43	4.68E-05	2.25E-04	4.17E-01	1.67E+00	1.21E-02	1.40E-01	1.46E-01	1.47E+00	9.66E-03	1.11E-01
55	28	1.39E-04	4.32E-04	1.06E+00	3.35E+00	6.64E-02	4.51E-01	4.53E-01	1.96E+00	3.48E-02	4.78E-01
59	5	3.55E-05	4.28E-04	3.87E-01	3.27E+00	6.42E-03	4.71E-01	9.55E-02	2.48E+00	5.50E-03	1.63E-01
1	44	2.57E-04	1.45E-04	2.13E+00	8.08E-01	1.26E-01	2.02E-01	7.64E-01	1.10E+00	6.36E-02	1.01E-01
13	35	1.89E-04	1.71E-04	1.15E+00	1.29E+00	5.33E-02	2.16E-01	2.27E-01	4.57E-01	1.65E-02	5.96E-02
4	16	1.60E-04	2.01E-04	1.36E+00	1.78E+00	6.14E-02	1.08E-01	4.85E-01	2.38E+00	5.14E-02	2.14E-01
50	32	6.47E-05	2.74E-04	4.83E-01	1.59E+00	4.82E-02	3.21E-01	1.64E-01	8.60E-01	1.54E-02	2.57E-01

Table AI-2 a. Normalized Area under Ca Peak (peak area/scatter area ratio) and ratios of Ca peak area with other elements for both normal and tumor tissues

Sample N	Sample T	Ca/As	Ca/As	Ca/Se	Ca/Se	Ca/Br	Ca/Br	Ca/Rb	Ca/Rb
		N	T	N	T	N	T	N	T
8	7	6.24E+00	1.52E+00	1.74E+00	9.10E-01	1.74E-01	1.32E-01	7.60E-02	7.91E-02
10	31	2.08E+00	1.17E+01	1.04E+00	7.50E+00	2.11E-01	5.21E-01	7.31E-02	1.13E+00
12	22	6.61E+00	6.48E+00	4.97E+00	3.45E+00	6.05E-01	3.09E-01	2.73E-01	2.43E-01
14	24	3.74E+00	1.18E+00	6.58E-01	5.06E-01	2.96E-01	5.38E-02	6.32E-02	9.78E-02
19	25	1.42E+00	1.68E+00	1.30E+00	8.85E-01	2.01E-01	1.31E-01	6.58E-02	7.07E-02
20	37	3.81E-01	1.06E+00	1.86E-01	9.40E-01	4.18E-02	2.29E-02	4.25E-02	5.44E-02
26	51	1.06E+00	4.80E+00	4.80E-01	4.49E+00	1.08E-01	1.98E-01	5.51E-02	2.99E-01
27	39	1.02E+00	2.93E+01	4.37E-01	8.56E+00	1.12E-01	1.09E+00	5.15E-02	7.73E-01
29	2	2.18E+00	9.59E+00	5.76E-01	5.27E+00	1.23E-01	6.27E-01	2.28E-02	1.99E-01
33	61	2.61E+00	1.33E+00	2.82E+00	6.46E-01	4.80E-01	9.25E-02	2.99E-01	7.03E-02
34	21	9.13E-01	4.05E+00	5.23E-01	2.50E+00	1.68E-01	3.45E-01	3.29E-02	4.00E-01
41	58	8.43E+00	1.89E+00	3.16E+00	2.24E+00	4.57E-01	1.21E-01	6.25E-01	1.52E-01
42	40	9.76E-01	4.41E+00	3.84E-01	2.62E+00	1.02E-01	2.47E-01	3.17E-02	2.33E-01
45	48	4.16E+00	7.64E-01	1.57E+00	3.72E-01	4.48E-01	3.78E-02	1.01E-01	5.24E-02
46	3	1.12E+00	3.22E+00	7.51E-01	2.40E+00	1.17E-01	1.87E-01	4.93E-02	3.06E-01
47	23	7.58E-01	4.64E+00	3.44E-01	2.23E+00	9.56E-02	4.56E-01	4.27E-02	5.43E-01
49	30	4.46E+00	1.26E+00	2.99E+00	1.70E+00	3.78E-01	1.04E-01	1.52E-01	1.22E-01
54	43	9.65E-01	5.40E+00	3.64E-01	1.47E+00	7.53E-02	1.87E-01	2.74E-02	2.26E-01
55	28	1.90E+00	2.81E+00	1.57E+00	1.93E+00	2.02E-01	4.38E-01	8.70E-02	6.03E-01
59	5	5.90E-01	6.90E+00	3.45E-01	4.93E+00	1.23E-01	4.74E-01	2.70E-02	7.06E-01
1	44	7.78E+00	2.28E+00	2.62E+00	3.87E+00	4.51E-01	1.81E-01	2.49E-01	1.19E-01
13	35	2.30E+00	2.15E+00	5.25E-01	6.48E-01	3.47E-01	1.59E-01	1.24E-01	2.85E-01
4	16	2.41E+00	2.43E+00	1.27E+00	1.63E+00	1.93E-01	1.46E-01	2.21E-01	2.28E-01
50	32	9.38E-01	2.72E+00	7.79E-01	2.17E+00	1.07E-01	2.22E-01	3.73E-02	4.34E-01

Table AI-2 b. Normalized Area under Ca Peak (peak area/scatter area ratio) and ratios of Ca peak area with other elements for both normal and tumor tissues

Sample N	Sample T	Cr	Cr	Cr/Fe	Cr/Fe	Cr/Cu	Cr/Cu	Cr/Zn	Cr/Zn
		N	T	N	T	N	T	N	T
8	7	9.36E-05	6.67E-05	4.33E-02	1.20E-01	1.94E-01	1.09E+00	1.78E-02	1.12E-02
10	31	1.11E-04	1.49E-04	1.01E-01	2.48E-01	2.09E-01	9.54E-01	2.92E-02	1.46E-01
12	22	9.26E-05	1.57E-04	2.11E-02	2.42E-01	3.41E-01	9.13E-01	2.37E-02	1.09E-01
14	24	1.03E-04	1.75E-04	1.87E-01	3.30E-01	2.96E-01	1.44E+00	1.12E-02	1.82E-01
19	25	1.35E-04	1.41E-04	3.56E-02	8.17E-02	8.49E-01	9.55E-01	4.82E-02	7.19E-02
20	37	1.21E-04	1.36E-04	3.77E-02	9.37E-02	2.67E-01	1.60E+00	2.64E-02	9.38E-02
26	51	1.24E-04	1.39E-04	4.85E-02	2.00E-01	3.16E-01	1.26E+00	2.10E-02	1.10E-01
27	39	1.51E-04	1.31E-04	1.03E-01	1.05E-01	4.70E-01	8.04E-01	1.79E-02	7.25E-02
29	2	1.25E-04	1.22E-04	2.92E-02	1.39E-01	2.14E-01	6.77E-01	1.65E-02	6.71E-02
33	61	1.11E-04	1.89E-04	2.34E-02	1.00E+00	6.61E-01	1.22E+00	3.60E-02	1.68E-01
34	21	1.06E-04	1.70E-04	8.92E-02	1.47E-01	1.61E-01	9.93E-01	2.13E-02	1.29E-01
41	58	1.69E-04	1.06E-04	6.44E-02	5.40E-02	4.19E-01	3.70E-01	2.53E-02	2.81E-02
42	40	1.19E-04	1.40E-04	3.54E-02	2.06E-01	3.19E-01	1.07E+00	2.33E-02	1.14E-01
45	48	1.36E-04	1.31E-04	3.19E-02	1.97E-01	2.13E-01	5.34E-01	1.99E-02	1.23E-01
46	3	1.18E-04	1.16E-04	2.41E-02	8.26E-02	3.69E-01	9.23E-01	2.96E-02	7.18E-02
47	23	9.93E-05	1.82E-04	1.78E-02	2.09E-01	3.49E-01	6.15E-01	2.17E-02	1.13E-01
49	30	1.15E-04	2.14E-04	1.62E-02	2.19E-01	1.77E-01	1.32E+00	1.48E-02	2.03E-01
54	43	1.12E-04	1.34E-04	2.91E-02	8.41E-02	3.49E-01	8.82E-01	2.32E-02	6.66E-02
55	28	1.31E-04	1.29E-04	6.29E-02	1.35E-01	4.29E-01	5.87E-01	3.30E-02	1.43E-01
59	5	9.18E-05	1.31E-04	1.66E-02	1.44E-01	2.47E-01	7.57E-01	1.42E-02	4.97E-02
1	44	1.21E-04	1.79E-04	5.90E-02	2.50E-01	3.59E-01	1.36E+00	2.99E-02	1.25E-01
13	35	1.64E-04	1.33E-04	4.63E-02	1.68E-01	1.97E-01	3.56E-01	1.43E-02	4.63E-02
4	16	1.18E-04	1.12E-04	4.51E-02	6.04E-02	3.56E-01	1.34E+00	3.77E-02	1.20E-01
50	32	1.34E-04	1.72E-04	9.99E-02	2.02E-01	3.40E-01	5.41E-01	3.18E-02	1.62E-01

Table AI-3 a. Normalized Area under Cr Peak (peak area/scatter area ratio) and ratios of Cr peak area with other elements for both normal and tumor tissues

Sample N	Sample T	Cr/As	Cr/As	Cr/Se	Cr/Se	Cr/Br	Cr/Br	Cr/Rb	Cr/Rb
		N	T	N	T	N	T	N	T
8	7	4.74E+00	9.26E-01	1.32E+00	5.55E-01	1.32E-01	8.02E-02	5.77E-02	4.82E-02
10	31	2.15E+00	2.38E+00	1.07E+00	1.52E+00	2.18E-01	1.06E-01	7.55E-02	2.30E-01
12	22	1.57E+00	3.23E+00	1.18E+00	1.72E+00	1.44E-01	1.54E-01	6.49E-02	1.21E-01
14	24	2.92E+00	2.20E+00	5.14E-01	9.50E-01	2.31E-01	1.01E-01	4.94E-02	1.84E-01
19	25	1.29E+00	2.41E+00	1.18E+00	1.26E+00	1.82E-01	1.87E-01	5.97E-02	1.01E-01
20	37	1.61E+00	2.06E+00	7.86E-01	1.82E+00	1.77E-01	4.45E-02	1.80E-01	1.06E-01
26	51	1.87E+00	2.77E+00	8.46E-01	2.59E+00	1.89E-01	1.14E-01	9.70E-02	1.73E-01
27	39	1.79E+00	4.08E+00	7.70E-01	1.19E+00	1.98E-01	1.52E-01	9.08E-02	1.08E-01
29	2	3.96E+00	3.31E+00	1.05E+00	1.82E+00	2.23E-01	2.17E-01	4.15E-02	6.86E-02
33	61	1.22E+00	3.23E+00	1.32E+00	1.57E+00	2.25E-01	2.24E-01	1.40E-01	1.71E-01
34	21	1.59E+00	2.06E+00	9.11E-01	1.27E+00	2.93E-01	1.75E-01	5.73E-02	2.03E-01
41	58	3.34E+00	1.58E+00	1.25E+00	1.87E+00	1.81E-01	1.01E-01	2.47E-01	1.27E-01
42	40	2.08E+00	2.84E+00	8.18E-01	1.69E+00	2.16E-01	1.59E-01	6.75E-02	1.50E-01
45	48	2.79E+00	2.33E+00	1.05E+00	1.14E+00	3.01E-01	1.15E-01	6.76E-02	1.60E-01
46	3	1.56E+00	1.39E+00	1.04E+00	1.03E+00	1.62E-01	8.04E-02	6.85E-02	1.32E-01
47	23	1.34E+00	2.18E+00	6.11E-01	1.05E+00	1.69E-01	2.15E-01	7.57E-02	2.55E-01
49	30	1.88E+00	2.55E+00	1.26E+00	3.44E+00	1.59E-01	2.11E-01	6.40E-02	2.48E-01
54	43	2.31E+00	3.23E+00	8.73E-01	8.78E-01	1.81E-01	1.12E-01	6.56E-02	1.35E-01
55	28	1.80E+00	8.40E-01	1.49E+00	5.77E-01	1.91E-01	1.31E-01	8.25E-02	1.80E-01
59	5	1.52E+00	2.11E+00	8.91E-01	1.51E+00	3.19E-01	1.45E-01	6.98E-02	2.16E-01
1	44	3.65E+00	2.82E+00	1.23E+00	4.79E+00	2.12E-01	2.24E-01	1.17E-01	1.47E-01
13	35	2.00E+00	1.67E+00	4.56E-01	5.04E-01	3.02E-01	1.24E-01	1.08E-01	2.22E-01
4	16	1.77E+00	1.36E+00	9.30E-01	9.12E-01	1.41E-01	8.20E-02	1.62E-01	1.28E-01
50	32	1.94E+00	1.71E+00	1.61E+00	1.37E+00	2.22E-01	1.39E-01	7.72E-02	2.73E-01

Table AI-3 b. Normalized Area under Cr Peak (peak area/scatter area ratio) and ratios of Cr peak area with other elements for both normal and tumor tissues

Sample N	Sample T	Fe	Fe	Fe/Cu	Fe/Cu	Fe/Zn	Fe/Zn	Fe/As	Fe/As
		N	T	N	T	N	T	N	T
8	7	2.16E-03	5.57E-04	4.49E+00	9.12E+00	4.11E-01	9.39E-02	1.09E+02	7.73E+00
10	31	1.09E-03	6.01E-04	2.06E+00	3.84E+00	2.87E-01	5.88E-01	2.12E+01	9.58E+00
12	22	4.40E-03	6.49E-04	1.62E+01	3.78E+00	1.13E+00	4.49E-01	7.45E+01	1.34E+01
14	24	5.49E-04	5.31E-04	1.58E+00	4.35E+00	6.00E-02	5.51E-01	1.56E+01	6.68E+00
19	25	3.80E-03	1.73E-03	2.39E+01	1.17E+01	1.35E+00	8.81E-01	3.62E+01	2.95E+01
20	37	3.20E-03	1.46E-03	7.08E+00	1.70E+01	7.00E-01	1.00E+00	4.28E+01	2.20E+01
26	51	2.55E-03	6.96E-04	6.52E+00	6.31E+00	4.32E-01	5.51E-01	3.85E+01	1.39E+01
27	39	1.47E-03	1.25E-03	4.58E+00	7.67E+00	1.75E-01	6.92E-01	1.75E+01	3.89E+01
29	2	4.30E-03	8.75E-04	7.34E+00	4.87E+00	5.66E-01	4.82E-01	1.36E+02	2.38E+01
33	61	4.72E-03	1.89E-04	2.83E+01	1.22E+00	1.54E+00	1.68E-01	5.22E+01	3.23E+00
34	21	1.19E-03	1.15E-03	1.80E+00	6.76E+00	2.39E-01	8.82E-01	1.78E+01	1.40E+01
41	58	2.63E-03	1.96E-03	6.51E+00	6.86E+00	3.93E-01	5.21E-01	5.19E+01	2.93E+01
42	40	3.36E-03	6.79E-04	9.01E+00	5.19E+00	6.58E-01	5.54E-01	5.87E+01	1.38E+01
45	48	4.27E-03	6.66E-04	6.66E+00	2.71E+00	6.24E-01	6.24E-01	8.74E+01	1.18E+01
46	3	4.91E-03	1.40E-03	1.53E+01	1.12E+01	1.23E+00	8.68E-01	6.48E+01	1.68E+01
47	23	5.57E-03	8.70E-04	1.96E+01	2.95E+00	1.22E+00	5.41E-01	7.54E+01	1.05E+01
49	30	7.12E-03	9.74E-04	1.10E+01	6.01E+00	9.14E-01	9.26E-01	1.16E+02	1.16E+01
54	43	3.86E-03	1.60E-03	1.20E+01	1.05E+01	7.97E-01	7.92E-01	7.96E+01	3.84E+01
55	28	2.09E-03	9.57E-04	6.82E+00	4.36E+00	5.24E-01	1.06E+00	2.87E+01	6.24E+00
59	5	5.53E-03	9.09E-04	1.49E+01	5.26E+00	8.57E-01	3.45E-01	9.18E+01	1.46E+01
1	44	2.04E-03	7.18E-04	6.08E+00	5.44E+00	5.06E-01	5.00E-01	6.19E+01	1.13E+01
13	35	3.54E-03	7.89E-04	4.26E+00	2.12E+00	3.10E-01	2.76E-01	4.32E+01	9.95E+00
4	16	2.61E-03	1.86E-03	7.90E+00	2.21E+01	8.37E-01	1.98E+00	3.93E+01	2.25E+01
50	32	1.34E-03	8.54E-04	3.40E+00	2.68E+00	3.19E-01	8.02E-01	1.94E+01	8.47E+00

Table AI-4 a. Normalized Area under Fe Peak (peak area/scatter area ratio) and ratios of Fe peak area with other elements for both normal and tumor tissues

Sample N	Sample T	Fe/Se	Fe/Se	Fe/Br	Fe/Br	Fe/Rb	Fe/Rb
		N	T	N	T	N	T
8	7	3.04E+01	4.63E+00	3.05E+00	6.70E-01	1.33E+00	4.03E-01
10	31	1.05E+01	6.13E+00	2.15E+00	4.26E-01	7.44E-01	9.25E-01
12	22	5.61E+01	7.10E+00	6.82E+00	6.37E-01	3.08E+00	5.02E-01
14	24	2.75E+00	2.88E+00	1.24E+00	3.06E-01	2.64E-01	5.56E-01
19	25	3.32E+01	1.55E+01	5.12E+00	2.29E+00	1.68E+00	1.24E+00
20	37	2.08E+01	1.95E+01	4.69E+00	4.75E-01	4.77E+00	1.13E+00
26	51	1.74E+01	1.30E+01	3.90E+00	5.73E-01	2.00E+00	8.64E-01
27	39	7.51E+00	1.14E+01	1.93E+00	1.45E+00	8.85E-01	1.03E+00
29	2	3.59E+01	1.31E+01	7.66E+00	1.56E+00	1.42E+00	4.93E-01
33	61	5.62E+01	1.57E+00	9.59E+00	2.24E-01	5.98E+00	1.71E-01
34	21	1.02E+01	8.64E+00	3.28E+00	1.19E+00	6.42E-01	1.38E+00
41	58	1.94E+01	3.46E+01	2.81E+00	1.87E+00	3.84E+00	2.35E+00
42	40	2.31E+01	8.20E+00	6.11E+00	7.73E-01	1.91E+00	7.30E-01
45	48	3.30E+01	5.77E+00	9.42E+00	5.86E-01	2.12E+00	8.12E-01
46	3	4.33E+01	1.25E+01	6.73E+00	9.73E-01	2.84E+00	1.60E+00
47	23	3.43E+01	5.02E+00	9.50E+00	1.03E+00	4.24E+00	1.22E+00
49	30	7.81E+01	1.57E+01	9.86E+00	9.63E-01	3.96E+00	1.13E+00
54	43	3.00E+01	1.04E+01	6.21E+00	1.33E+00	2.26E+00	1.61E+00
55	28	2.37E+01	4.28E+00	3.03E+00	9.71E-01	1.31E+00	1.34E+00
59	5	5.37E+01	1.05E+01	1.92E+01	1.01E+00	4.21E+00	1.50E+00
1	44	2.08E+01	1.92E+01	3.59E+00	8.96E-01	1.99E+00	5.90E-01
13	35	9.85E+00	3.00E+00	6.52E+00	7.36E-01	2.33E+00	1.32E+00
4	16	2.06E+01	1.51E+01	3.14E+00	1.36E+00	3.59E+00	2.12E+00
50	32	1.62E+01	6.78E+00	2.22E+00	6.91E-01	7.73E-01	1.35E+00

Table AI-4 b. Normalized Area under Fe Peak (peak area/scatter area ratio) and ratios of Fe peak area with other elements for both normal and tumor tissues

Sample N	Sample T	Cu	Cu	Cu/Zn	Cu/Zn	Cu/As	Cu/As	Cu/Se	Cu/Se	Cu/Br	Cu/Br	Cu/Rb	Cu/Rb
		N	T	N	T	N	T	N	T	N	T	N	T
8	7	4.82E-04	6.11E-05	9.17E-02	1.03E-02	2.44E+01	8.48E-01	6.79E+00	5.08E-01	6.81E-01	7.35E-02	2.97E-01	4.42E-02
10	31	5.31E-04	1.56E-04	1.40E-01	1.53E-01	1.03E+01	2.49E+00	5.12E+00	1.60E+00	1.04E+00	1.11E-01	3.61E-01	2.41E-01
12	22	2.71E-04	1.72E-04	6.95E-02	1.19E-01	4.60E+00	3.54E+00	3.46E+00	1.88E+00	4.21E-01	1.69E-01	1.90E-01	1.33E-01
14	24	3.47E-04	1.22E-04	3.79E-02	1.27E-01	9.88E+00	1.53E+00	1.74E+00	6.61E-01	7.82E-01	7.02E-02	1.67E-01	1.28E-01
19	25	1.59E-04	1.48E-04	5.68E-02	7.54E-02	1.52E+00	2.52E+00	1.39E+00	1.33E+00	2.14E-01	1.96E-01	7.03E-02	1.06E-01
20	37	4.52E-04	8.54E-05	9.88E-02	5.87E-02	6.04E+00	1.29E+00	2.94E+00	1.14E+00	6.62E-01	2.79E-02	6.74E-01	6.61E-02
26	51	3.92E-04	1.10E-04	6.63E-02	8.73E-02	5.90E+00	2.20E+00	2.68E+00	2.06E+00	5.99E-01	9.08E-02	3.07E-01	1.37E-01
27	39	3.20E-04	1.63E-04	3.82E-02	9.02E-02	3.82E+00	5.08E+00	1.64E+00	1.48E+00	4.22E-01	1.89E-01	1.93E-01	1.34E-01
29	2	5.86E-04	1.80E-04	7.71E-02	9.90E-02	1.85E+01	4.89E+00	4.89E+00	2.69E+00	1.04E+00	3.20E-01	1.94E-01	1.01E-01
33	61	1.67E-04	1.55E-04	5.44E-02	1.38E-01	1.85E+00	2.64E+00	1.99E+00	1.28E+00	3.39E-01	1.84E-01	2.12E-01	1.40E-01
34	21	6.60E-04	1.71E-04	1.33E-01	1.30E-01	9.91E+00	2.07E+00	5.67E+00	1.28E+00	1.82E+00	1.77E-01	3.57E-01	2.05E-01
41	58	4.04E-04	2.85E-04	6.04E-02	7.60E-02	7.96E+00	4.27E+00	2.98E+00	5.05E+00	4.32E-01	2.73E-01	5.90E-01	3.43E-01
42	40	3.73E-04	1.31E-04	7.31E-02	1.07E-01	6.52E+00	2.66E+00	2.57E+00	1.58E+00	6.79E-01	1.49E-01	2.12E-01	1.41E-01
45	48	6.42E-04	2.45E-04	9.37E-02	2.30E-01	1.31E+01	4.36E+00	4.96E+00	2.13E+00	1.42E+00	2.16E-01	3.18E-01	2.99E-01
46	3	3.21E-04	1.25E-04	8.03E-02	7.78E-02	4.23E+00	1.50E+00	2.83E+00	1.12E+00	4.40E-01	8.72E-02	1.86E-01	1.43E-01
47	23	2.85E-04	2.95E-04	6.23E-02	1.84E-01	3.86E+00	3.55E+00	1.75E+00	1.70E+00	4.86E-01	3.49E-01	2.17E-01	4.15E-01
49	30	6.50E-04	1.62E-04	8.35E-02	1.54E-01	1.06E+01	1.93E+00	7.13E+00	2.61E+00	9.00E-01	1.60E-01	3.62E-01	1.88E-01
54	43	3.21E-04	1.52E-04	6.63E-02	7.54E-02	6.62E+00	3.66E+00	2.50E+00	9.95E-01	5.17E-01	1.27E-01	1.88E-01	1.53E-01
55	28	3.06E-04	2.20E-04	7.69E-02	2.43E-01	4.20E+00	1.43E+00	3.47E+00	9.83E-01	4.45E-01	2.23E-01	1.92E-01	3.07E-01
59	5	3.72E-04	1.73E-04	5.76E-02	6.57E-02	6.18E+00	2.78E+00	3.61E+00	1.99E+00	1.29E+00	1.91E-01	2.83E-01	2.85E-01
1	44	3.36E-04	1.32E-04	8.32E-02	9.18E-02	1.02E+01	2.07E+00	3.42E+00	3.53E+00	5.90E-01	1.65E-01	3.26E-01	1.08E-01
13	35	8.32E-04	3.73E-04	7.27E-02	1.30E-01	1.02E+01	4.70E+00	2.31E+00	1.42E+00	1.53E+00	3.48E-01	5.47E-01	6.23E-01
4	16	3.31E-04	8.41E-05	1.06E-01	8.96E-02	4.98E+00	1.02E+00	2.61E+00	6.82E-01	3.97E-01	6.14E-02	4.55E-01	9.56E-02
50	32	3.94E-04	3.19E-04	9.36E-02	2.99E-01	5.71E+00	3.16E+00	4.75E+00	2.53E+00	6.53E-01	2.58E-01	2.27E-01	5.05E-01

Table AI-5. Normalized Area under Cu Peak (peak area/scatter area ratio) and ratios of Cu peak area with other elements for both normal and tumor tissues

Sample N	Sample T	Zn	Zn	Zn/As	Zn/As	Zn/Se	Zn/Se	Zn/Br	Zn/Br	Zn/Rb	Zn/Rb
		N	T	N	T	N	T	N	T	N	T
8	7	5.26E-03	5.94E-03	2.66E+02	8.24E+01	7.40E+01	4.94E+01	7.42E+00	7.14E+00	3.24E+00	4.29E+00
10	31	3.80E-03	1.02E-03	7.37E+01	1.63E+01	3.67E+01	1.04E+01	7.47E+00	7.25E-01	2.59E+00	1.57E+00
12	22	3.90E-03	1.45E-03	6.61E+01	2.98E+01	4.98E+01	1.58E+01	6.06E+00	1.42E+00	2.74E+00	1.12E+00
14	24	9.15E-03	9.64E-04	2.60E+02	1.21E+01	4.59E+01	5.22E+00	2.06E+01	5.55E-01	4.40E+00	1.01E+00
19	25	2.81E-03	1.96E-03	2.67E+01	3.35E+01	2.45E+01	1.76E+01	3.78E+00	2.60E+00	1.24E+00	1.41E+00
20	37	4.57E-03	1.45E-03	6.12E+01	2.19E+01	2.98E+01	1.94E+01	6.71E+00	4.75E-01	6.83E+00	1.13E+00
26	51	5.91E-03	1.26E-03	8.90E+01	2.52E+01	4.04E+01	2.35E+01	9.03E+00	1.04E+00	4.63E+00	1.57E+00
27	39	8.39E-03	1.81E-03	1.00E+02	5.63E+01	4.29E+01	1.65E+01	1.10E+01	2.09E+00	5.06E+00	1.49E+00
29	2	7.59E-03	1.82E-03	2.40E+02	4.94E+01	6.34E+01	2.72E+01	1.35E+01	3.23E+00	2.51E+00	1.02E+00
33	61	3.07E-03	1.12E-03	3.39E+01	1.92E+01	3.66E+01	9.31E+00	6.24E+00	1.33E+00	3.89E+00	1.01E+00
34	21	4.97E-03	1.31E-03	7.46E+01	1.59E+01	4.27E+01	9.80E+00	1.37E+01	1.35E+00	2.68E+00	1.57E+00
41	58	6.68E-03	3.75E-03	1.32E+02	5.62E+01	4.94E+01	6.64E+01	7.15E+00	3.59E+00	9.77E+00	4.51E+00
42	40	5.10E-03	1.22E-03	8.92E+01	2.49E+01	3.51E+01	1.48E+01	9.29E+00	1.39E+00	2.90E+00	1.32E+00
45	48	6.86E-03	1.07E-03	1.40E+02	1.90E+01	5.30E+01	9.24E+00	1.51E+01	9.39E-01	3.40E+00	1.30E+00
46	3	4.00E-03	1.61E-03	5.27E+01	1.93E+01	3.52E+01	1.44E+01	5.48E+00	1.12E+00	2.31E+00	1.84E+00
47	23	4.57E-03	1.61E-03	6.19E+01	1.93E+01	2.81E+01	9.27E+00	7.80E+00	1.90E+00	3.48E+00	2.26E+00
49	30	7.79E-03	1.05E-03	1.27E+02	1.26E+01	8.54E+01	1.69E+01	1.08E+01	1.04E+00	4.33E+00	1.22E+00
54	43	4.84E-03	2.02E-03	9.99E+01	4.85E+01	3.77E+01	1.32E+01	7.79E+00	1.68E+00	2.83E+00	2.03E+00
55	28	3.98E-03	9.04E-04	5.47E+01	5.89E+00	4.52E+01	4.04E+00	5.79E+00	9.16E-01	2.50E+00	1.26E+00
59	5	6.46E-03	2.63E-03	1.07E+02	4.24E+01	6.27E+01	3.04E+01	2.24E+01	2.92E+00	4.91E+00	4.34E+00
1	44	4.03E-03	1.44E-03	1.22E+02	2.26E+01	4.11E+01	3.84E+01	7.08E+00	1.79E+00	3.92E+00	1.18E+00
13	35	1.14E-02	2.86E-03	1.40E+02	3.61E+01	3.18E+01	1.09E+01	2.11E+01	2.67E+00	7.52E+00	4.79E+00
4	16	3.12E-03	9.38E-04	4.69E+01	1.14E+01	2.47E+01	7.61E+00	3.75E+00	6.85E-01	4.29E+00	1.07E+00
50	32	4.21E-03	1.07E-03	6.10E+01	1.06E+01	5.07E+01	8.46E+00	6.98E+00	8.62E-01	2.43E+00	1.69E+00

Table AI-6. Normalized Area under Zn Peak (peak area/scatter area ratio) and ratios of Zn peak area with other elements for both normal and tumor tissues

Sample N	Sample T	As	As	As/Se	As/Se	As/Br	As/Br	As/Rb	As/Rb
		N	T	N	T	N	T	N	T
8	7	1.98E-05	7.21E-05	2.78E-01	5.99E-01	2.79E-02	8.66E-02	1.22E-02	5.21E-02
10	31	5.16E-05	6.27E-05	4.98E-01	6.40E-01	1.01E-01	4.45E-02	3.51E-02	9.65E-02
12	22	5.90E-05	4.86E-05	7.53E-01	5.32E-01	9.16E-02	4.77E-02	4.14E-02	3.76E-02
14	24	3.51E-05	7.96E-05	1.76E-01	4.31E-01	7.91E-02	4.58E-02	1.69E-02	8.32E-02
19	25	1.05E-04	5.87E-05	9.16E-01	5.26E-01	1.41E-01	7.77E-02	4.63E-02	4.20E-02
20	37	7.48E-05	6.62E-05	4.87E-01	8.86E-01	1.10E-01	2.16E-02	1.12E-01	5.13E-02
26	51	6.64E-05	5.01E-05	4.53E-01	9.34E-01	1.01E-01	4.13E-02	5.20E-02	6.23E-02
27	39	8.39E-05	3.21E-05	4.30E-01	2.92E-01	1.10E-01	3.72E-02	5.06E-02	2.64E-02
29	2	3.17E-05	3.68E-05	2.64E-01	5.50E-01	5.64E-02	6.54E-02	1.05E-02	2.07E-02
33	61	9.05E-05	5.86E-05	1.08E+00	4.85E-01	1.84E-01	6.95E-02	1.15E-01	5.28E-02
34	21	6.66E-05	8.24E-05	5.72E-01	6.16E-01	1.84E-01	8.52E-02	3.60E-02	9.87E-02
41	58	5.07E-05	6.68E-05	3.74E-01	1.18E+00	5.42E-02	6.38E-02	7.41E-02	8.02E-02
42	40	5.72E-05	4.92E-05	3.94E-01	5.95E-01	1.04E-01	5.61E-02	3.25E-02	5.30E-02
45	48	4.89E-05	5.62E-05	3.78E-01	4.88E-01	1.08E-01	4.95E-02	2.42E-02	6.86E-02
46	3	7.58E-05	8.35E-05	6.68E-01	7.45E-01	1.04E-01	5.80E-02	4.39E-02	9.52E-02
47	23	7.39E-05	8.31E-05	4.54E-01	4.80E-01	1.26E-01	9.83E-02	5.63E-02	1.17E-01
49	30	6.12E-05	8.38E-05	6.71E-01	1.35E+00	8.47E-02	8.29E-02	3.41E-02	9.71E-02
54	43	4.85E-05	4.16E-05	3.77E-01	2.72E-01	7.80E-02	3.47E-02	2.84E-02	4.19E-02
55	28	7.29E-05	1.54E-04	8.27E-01	6.87E-01	1.06E-01	1.56E-01	4.57E-02	2.14E-01
59	5	6.02E-05	6.21E-05	5.85E-01	7.16E-01	2.09E-01	6.88E-02	4.58E-02	1.02E-01
1	44	3.30E-05	6.36E-05	3.36E-01	1.70E+00	5.79E-02	7.94E-02	3.21E-02	5.23E-02
13	35	8.19E-05	7.93E-05	2.28E-01	3.01E-01	1.51E-01	7.40E-02	5.38E-02	1.33E-01
4	16	6.65E-05	8.27E-05	5.25E-01	6.71E-01	7.98E-02	6.03E-02	9.15E-02	9.40E-02
50	32	6.90E-05	1.01E-04	8.31E-01	8.00E-01	1.14E-01	8.16E-02	3.98E-02	1.60E-01

Table AI-7. Normalized Area under As Peak (peak area/scatter area ratio) and ratios of As peak area with other elements for both normal and tumor tissues

Sample N	Sample T	Se	Se	Se/Br	Se/Br	Se/Rb	Se/Rb
		N	T	N	T	N	T
8	7	7.10E-05	1.20E-04	1.00E-01	1.45E-01	4.38E-02	8.69E-02
10	31	1.04E-04	9.80E-05	2.04E-01	6.95E-02	7.06E-02	1.51E-01
12	22	7.84E-05	9.14E-05	1.22E-01	8.97E-02	5.50E-02	7.06E-02
14	24	1.99E-04	1.85E-04	4.49E-01	1.06E-01	9.60E-02	1.93E-01
19	25	1.14E-04	1.12E-04	1.54E-01	1.48E-01	5.06E-02	7.99E-02
20	37	1.54E-04	7.48E-05	2.25E-01	2.44E-02	2.29E-01	5.79E-02
26	51	1.46E-04	5.36E-05	2.24E-01	4.42E-02	1.15E-01	6.67E-02
27	39	1.95E-04	1.10E-04	2.57E-01	1.27E-01	1.18E-01	9.03E-02
29	2	1.20E-04	6.69E-05	2.13E-01	1.19E-01	3.97E-02	3.77E-02
33	61	8.40E-05	1.21E-04	1.71E-01	1.43E-01	1.06E-01	1.09E-01
34	21	1.16E-04	1.34E-04	3.21E-01	1.38E-01	6.29E-02	1.60E-01
41	58	1.35E-04	5.65E-05	1.45E-01	5.40E-02	1.98E-01	6.79E-02
42	40	1.45E-04	8.27E-05	2.65E-01	9.43E-02	8.25E-02	8.90E-02
45	48	1.29E-04	1.15E-04	2.85E-01	1.02E-01	6.41E-02	1.41E-01
46	3	1.13E-04	1.12E-04	1.55E-01	7.79E-02	6.56E-02	1.28E-01
47	23	1.63E-04	1.73E-04	2.77E-01	2.05E-01	1.24E-01	2.44E-01
49	30	9.12E-05	6.21E-05	1.26E-01	6.14E-02	5.07E-02	7.19E-02
54	43	1.28E-04	1.53E-04	2.07E-01	1.28E-01	7.51E-02	1.54E-01
55	28	8.81E-05	2.24E-04	1.28E-01	2.27E-01	5.53E-02	3.12E-01
59	5	1.03E-04	8.67E-05	3.58E-01	9.61E-02	7.84E-02	1.43E-01
1	44	9.81E-05	3.74E-05	1.72E-01	4.67E-02	9.54E-02	3.08E-02
13	35	3.59E-04	2.63E-04	6.62E-01	2.45E-01	2.36E-01	4.40E-01
4	16	1.27E-04	1.23E-04	1.52E-01	9.00E-02	1.74E-01	1.40E-01
50	32	8.30E-05	1.26E-04	1.38E-01	1.02E-01	4.78E-02	2.00E-01

Table AI-8. Normalized Area under Se Peak (peak area/scatter area ratio) and ratios of Se peak area with other elements for both normal and tumor tissues

Sample N	Sample T	Br	Br	Rb	Rb	Rb/Br	Rb/Br
		N	T	N	T	N	T
8	7	7.08E-04	8.32E-04	1.62E-03	1.38E-03	2.29E+00	1.66E+00
10	31	5.09E-04	1.41E-03	1.47E-03	6.50E-04	2.88E+00	4.61E-01
12	22	6.44E-04	1.02E-03	1.43E-03	1.29E-03	2.21E+00	1.27E+00
14	24	4.44E-04	1.74E-03	2.08E-03	9.56E-04	4.68E+00	5.50E-01
19	25	7.42E-04	7.55E-04	2.26E-03	1.40E-03	3.05E+00	1.85E+00
20	37	6.82E-04	3.06E-03	6.70E-04	1.29E-03	9.83E-01	4.22E-01
26	51	6.54E-04	1.21E-03	1.28E-03	8.05E-04	1.95E+00	6.63E-01
27	39	7.60E-04	8.62E-04	1.66E-03	1.22E-03	2.18E+00	1.41E+00
29	2	5.61E-04	5.63E-04	3.02E-03	1.77E-03	5.38E+00	3.15E+00
33	61	4.92E-04	8.43E-04	7.90E-04	1.11E-03	1.60E+00	1.32E+00
34	21	3.62E-04	9.67E-04	1.85E-03	8.35E-04	5.11E+00	8.63E-01
41	58	9.35E-04	1.05E-03	6.84E-04	8.32E-04	7.32E-01	7.95E-01
42	40	5.49E-04	8.78E-04	1.76E-03	9.30E-04	3.20E+00	1.06E+00
45	48	4.54E-04	1.14E-03	2.02E-03	8.19E-04	4.45E+00	7.22E-01
46	3	7.30E-04	1.44E-03	1.73E-03	8.77E-04	2.37E+00	6.10E-01
47	23	5.86E-04	8.46E-04	1.31E-03	7.11E-04	2.24E+00	8.41E-01
49	30	7.23E-04	1.01E-03	1.80E-03	8.64E-04	2.49E+00	8.54E-01
54	43	6.21E-04	1.20E-03	1.71E-03	9.92E-04	2.75E+00	8.28E-01
55	28	6.88E-04	9.86E-04	1.59E-03	7.16E-04	2.32E+00	7.26E-01
59	5	2.88E-04	9.03E-04	1.31E-03	6.06E-04	4.57E+00	6.71E-01
1	44	5.69E-04	8.01E-04	1.03E-03	1.22E-03	1.81E+00	1.52E+00
13	35	5.43E-04	1.07E-03	1.52E-03	5.98E-04	2.80E+00	5.58E-01
4	16	8.33E-04	1.37E-03	7.27E-04	8.80E-04	8.73E-01	6.42E-01
50	32	6.04E-04	1.24E-03	1.74E-03	6.31E-04	2.88E+00	5.10E-01

Table AI-9. Normalized Area under Br and Rb Peaks (peak area/scatter area ratio)

APPENDIX II : RAW DATA : Normalized Peak Area (Coherent Scatter)

Adipose peak							
parameters	parameters	Amplitude	Amplitude	FWHM	FWHM	Int Area	Int Area
Samples	Samples	N	T	N	T	N	T
8	7	5.46E-02	4.67E-02	2.94E-01	2.88E-01	1.71E-02	1.43E-02
10	31	4.89E-02	4.58E-02	3.04E-01	3.09E-01	1.58E-02	1.51E-02
12	22	5.83E-02	5.27E-02	3.06E-01	2.59E-01	1.90E-02	1.46E-02
14	24	3.23E-02	5.08E-02	2.99E-01	3.03E-01	1.03E-02	1.64E-02
19	25	6.03E-02	5.47E-02	3.08E-01	2.98E-01	1.98E-02	1.74E-02
20	37	5.25E-02	4.46E-02	3.01E-01	3.01E-01	1.68E-02	1.43E-02
26	51	5.48E-02	4.83E-02	3.02E-01	2.98E-01	1.76E-02	1.53E-02
27	39	5.35E-02	4.55E-02	2.95E-01	3.06E-01	1.68E-02	1.48E-02
29	2	4.65E-02	4.62E-02	3.00E-01	2.95E-01	1.48E-02	1.45E-02
33	61	5.07E-02	5.04E-02	2.96E-01	3.07E-01	1.60E-02	1.65E-02
34	21	4.52E-02	4.78E-02	3.00E-01	3.02E-01	1.44E-02	1.54E-02
41	58	4.67E-02	4.75E-02	3.08E-01	3.00E-01	1.53E-02	1.52E-02
42	40	5.25E-02	5.86E-02	3.01E-01	3.01E-01	1.68E-02	1.88E-02
45	48	5.74E-02	4.63E-02	2.92E-01	3.12E-01	1.79E-02	1.54E-02
46	3	4.57E-02	4.81E-02	3.11E-01	3.03E-01	1.51E-02	1.55E-02
47	23	6.19E-02	4.94E-02	2.95E-01	3.02E-01	1.95E-02	1.59E-02
49	30	5.77E-02	3.89E-02	2.99E-01	3.06E-01	1.84E-02	1.27E-02
54	43	5.59E-02	5.42E-02	3.03E-01	2.98E-01	1.80E-02	1.72E-02
55	28	5.77E-02	4.96E-02	2.96E-01	3.00E-01	1.82E-02	1.58E-02
59	5	5.21E-02	4.54E-02	3.02E-01	3.16E-01	1.68E-02	1.53E-02
1	44	4.65E-02	4.35E-02	3.05E-01	3.03E-01	1.51E-02	1.40E-02
13	35	5.78E-02	5.18E-02	2.90E-01	3.02E-01	1.78E-02	1.67E-02
4	16	5.15E-02	5.03E-02	2.98E-01	3.05E-01	1.63E-02	1.63E-02
50	32	4.43E-02	5.18E-02	3.03E-01	2.98E-01	1.43E-02	1.65E-02

Table AII-1. Normalized Area under Adipose Peak (normalized to unity and attenuation coefficient)

Fibrous Peak							
parameters	parameters	Amplitude	Amplitude	FWHM	FWHM	Int Area	Int Area
Samples	Samples	N	T	N	T	N	T
8	7	2.18E-02	2.58E-02	5.31E-01	5.83E-01	1.23E-02	1.60E-02
10	31	2.46E-02	2.96E-02	5.18E-01	5.24E-01	1.36E-02	1.65E-02
12	22	2.03E-02	2.68E-02	4.85E-01	5.88E-01	1.05E-02	1.67E-02
14	24	1.49E-02	2.90E-02	5.31E-01	5.03E-01	8.44E-03	1.56E-02
19	25	1.88E-02	2.80E-02	4.74E-01	4.86E-01	9.46E-03	1.45E-02
20	37	2.39E-02	3.13E-02	5.25E-01	5.36E-01	1.34E-02	1.78E-02
26	51	2.44E-02	2.65E-02	5.18E-01	5.61E-01	1.34E-02	1.58E-02
27	39	2.29E-02	2.91E-02	5.30E-01	5.49E-01	1.29E-02	1.70E-02
29	2	2.29E-02	2.68E-02	5.54E-01	5.48E-01	1.35E-02	1.56E-02
33	61	1.88E-02	2.62E-02	5.17E-01	5.24E-01	1.03E-02	1.46E-02
34	21	2.50E-02	2.59E-02	5.65E-01	5.21E-01	1.50E-02	1.44E-02
36	62	2.06E-02	2.94E-02	4.89E-01	5.26E-01	1.07E-02	1.64E-02
41	58	2.54E-02	2.60E-02	5.21E-01	5.42E-01	1.41E-02	1.50E-02
42	40	1.98E-02	2.21E-02	4.87E-01	4.84E-01	1.03E-02	1.14E-02
45	48	2.11E-02	2.72E-02	5.11E-01	5.13E-01	1.15E-02	1.49E-02
46	3	2.57E-02	2.69E-02	5.24E-01	5.31E-01	1.43E-02	1.52E-02
47	23	1.49E-02	2.50E-02	4.69E-01	5.22E-01	7.46E-03	1.39E-02
49	30	1.86E-02	3.25E-02	5.10E-01	5.95E-01	1.01E-02	2.06E-02
54	43	2.11E-02	2.66E-02	5.10E-01	5.28E-01	1.15E-02	1.50E-02
55	28	2.17E-02	2.42E-02	5.13E-01	5.30E-01	1.19E-02	1.36E-02
56	17	2.11E-02	2.49E-02	5.17E-01	5.22E-01	1.16E-02	1.38E-02
59	5	2.20E-02	2.78E-02	5.18E-01	5.11E-01	1.21E-02	1.51E-02
60	38	2.70E-02	2.81E-02	5.41E-01	5.27E-01	1.55E-02	1.58E-02
1	44	2.55E-02	2.97E-02	5.35E-01	5.62E-01	1.45E-02	1.78E-02
13	35	2.32E-02	2.32E-02	5.21E-01	5.39E-01	1.28E-02	1.33E-02
4	16	2.45E-02	2.85E-02	5.24E-01	5.23E-01	1.37E-02	1.59E-02
50	32	2.68E-02	2.54E-02	5.54E-01	5.10E-01	1.58E-02	1.38E-02

Table AII-2. Normalized Area under Fibrous Peak (normalized to unity and attenuation coefficient)

Water Content Peak							
parameters Samples	parameters Samples	Amplitude N	Amplitude T	FWHM N	FWHM T	Int Area N	Int Area T
8	7	1.41E-02	1.67E-02	5.30E-01	5.35E-01	7.97E-03	9.51E-03
10	31	1.66E-02	1.97E-02	5.78E-01	5.87E-01	1.02E-02	1.23E-02
12	22	1.39E-02	1.70E-02	5.69E-01	5.30E-01	8.44E-03	9.57E-03
14	24	1.04E-02	1.99E-02	5.63E-01	5.95E-01	6.21E-03	1.26E-02
19	25	1.41E-02	1.94E-02	5.58E-01	6.01E-01	8.39E-03	1.24E-02
20	37	1.63E-02	2.08E-02	5.54E-01	6.02E-01	9.58E-03	1.33E-02
26	51	1.63E-02	1.76E-02	5.63E-01	5.48E-01	9.78E-03	1.02E-02
27	39	1.56E-02	1.85E-02	5.41E-01	5.81E-01	9.00E-03	1.14E-02
29	2	1.53E-02	1.75E-02	5.44E-01	5.58E-01	8.87E-03	1.04E-02
33	61	1.32E-02	1.79E-02	5.30E-01	5.62E-01	7.41E-03	1.07E-02
34	21	1.65E-02	1.75E-02	5.68E-01	5.77E-01	9.98E-03	1.08E-02
36	62	1.48E-02	1.91E-02	5.09E-01	5.93E-01	8.03E-03	1.20E-02
41	58	1.68E-02	1.76E-02	5.87E-01	5.54E-01	1.05E-02	1.04E-02
42	40	1.39E-02	1.55E-02	5.64E-01	5.61E-01	8.34E-03	9.27E-03
45	48	1.48E-02	1.84E-02	5.40E-01	5.85E-01	8.53E-03	1.14E-02
46	3	1.72E-02	1.70E-02	6.00E-01	5.42E-01	1.10E-02	9.83E-03
47	23	1.21E-02	1.71E-02	5.17E-01	5.70E-01	6.64E-03	1.04E-02
49	30	1.31E-02	2.03E-02	5.20E-01	5.67E-01	7.26E-03	1.22E-02
54	43	1.51E-02	1.79E-02	5.33E-01	5.35E-01	8.54E-03	1.02E-02
55	28	1.47E-02	1.65E-02	5.14E-01	5.50E-01	8.02E-03	9.64E-03
56	17	1.46E-02	1.67E-02	5.31E-01	5.44E-01	8.25E-03	9.68E-03
59	5	1.50E-02	1.88E-02	5.61E-01	5.79E-01	8.98E-03	1.16E-02
60	38	1.81E-02	1.90E-02	5.85E-01	5.69E-01	1.12E-02	1.15E-02
1	44	1.68E-02	1.93E-02	5.63E-01	5.76E-01	1.01E-02	1.18E-02
13	35	1.60E-02	1.55E-02	5.22E-01	5.39E-01	8.87E-03	8.89E-03
4	16	1.68E-02	1.93E-02	5.60E-01	5.77E-01	1.00E-02	1.18E-02
50	32	1.78E-02	1.77E-02	5.71E-01	5.71E-01	1.08E-02	1.08E-02

Table AII-3. Normalized Area under Water Content Peak (normalized to unity and attenuation coefficient)

APPENDIX III : Score, Loading and Coomans Plots for Second, Third and Fourth Subgroup (XRF Study)

AIII. 1 Second subgroup classification results

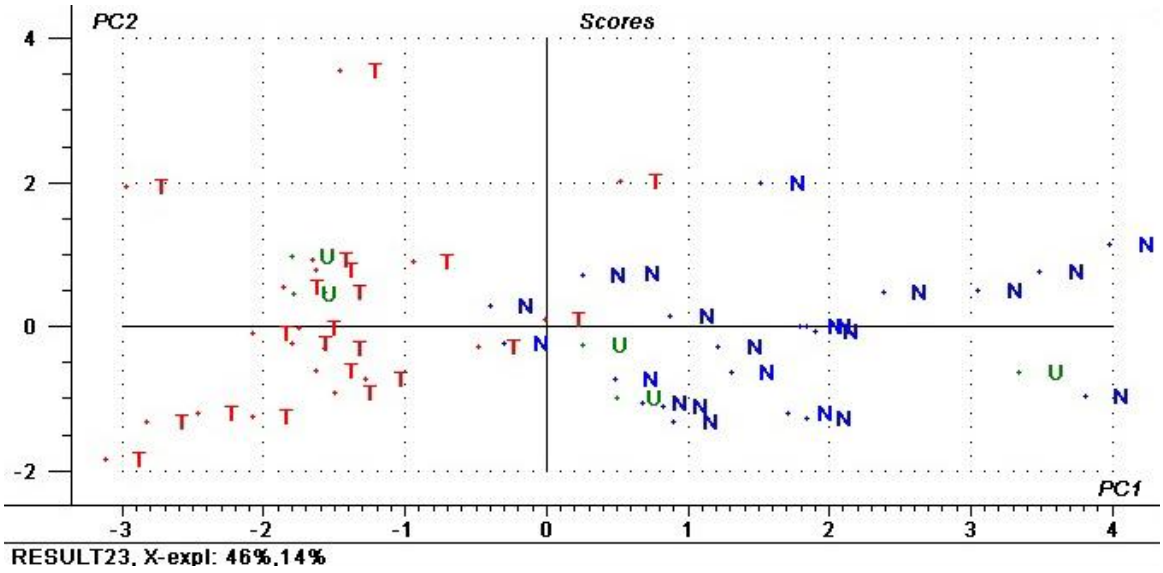

Fig. AIII 1-1 Score Plot of PC1 vs. PC2

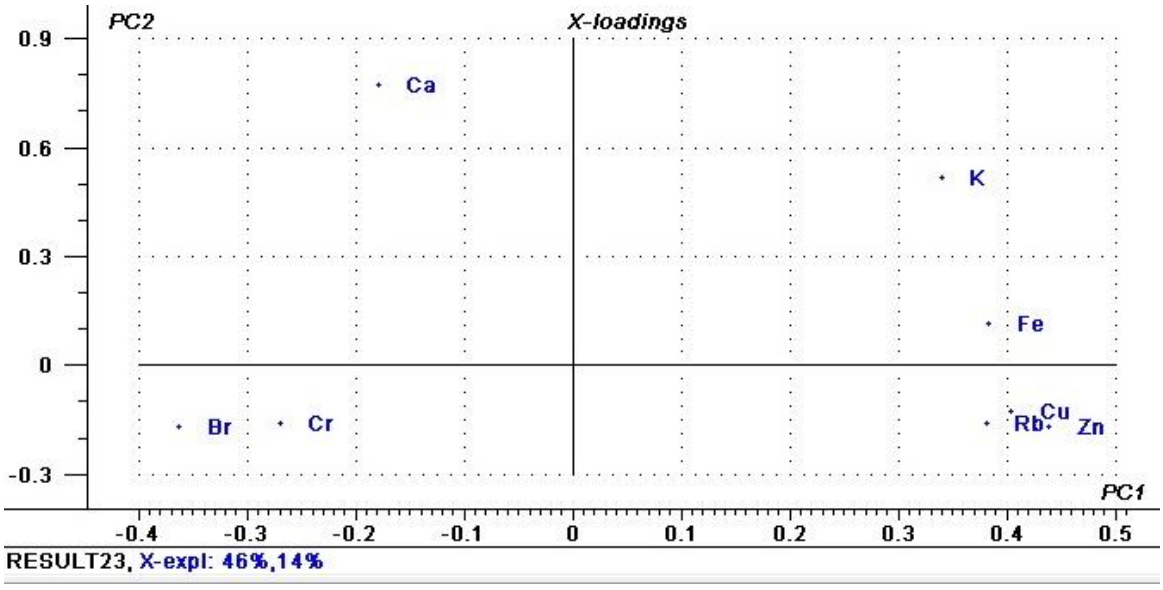

Fig. AIII 1-2 Loading Plot of PC1 vs. PC2

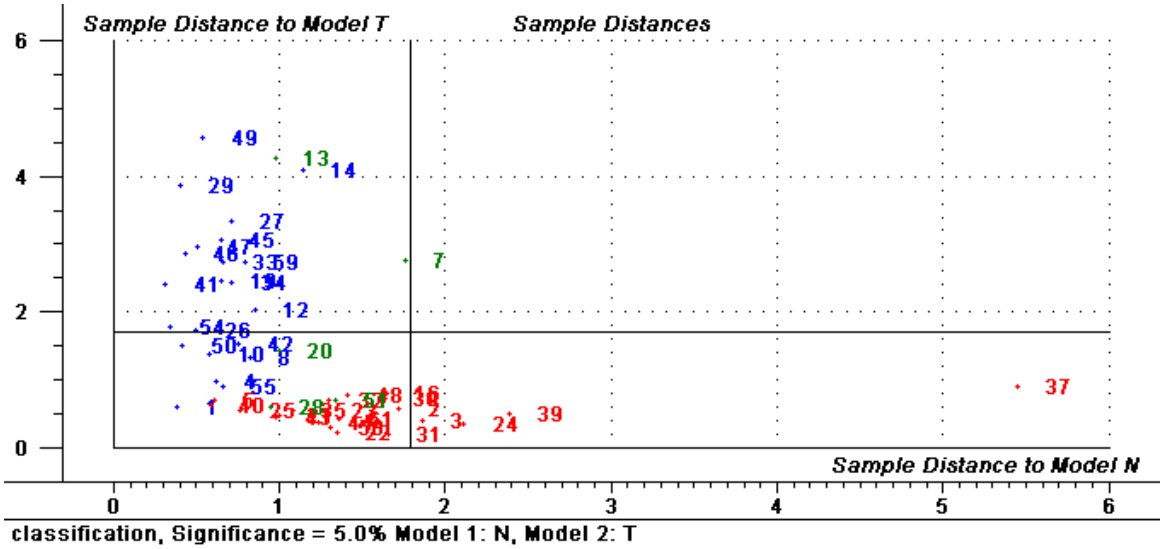

Fig. AIII 1-3 Coomans Plot, classification result

AIII. 2 Third subgroup classification results

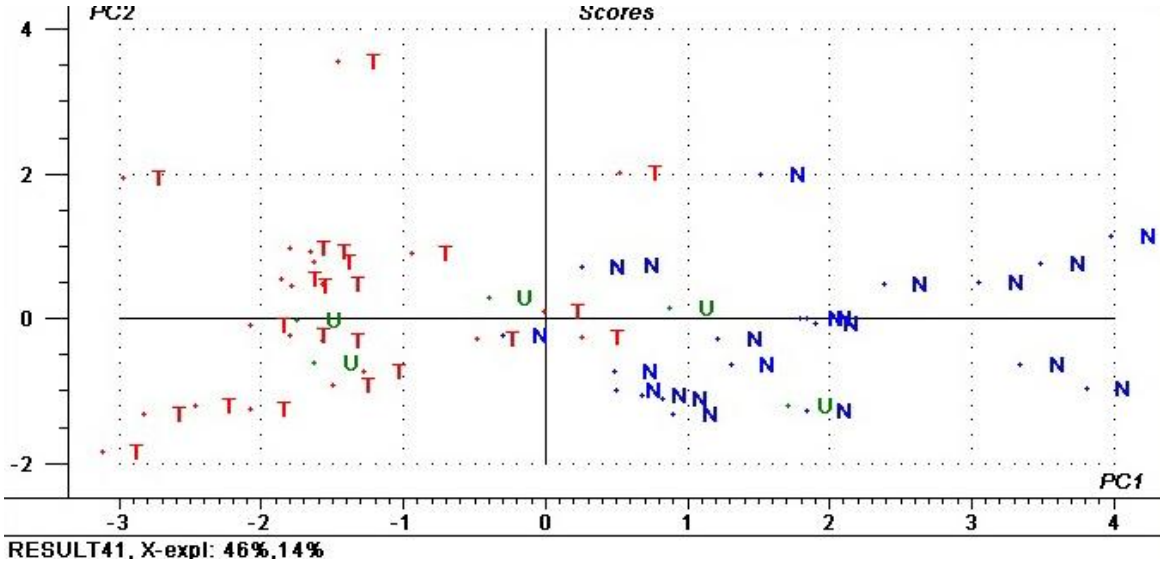

Fig. AIII 2-1 Score Plot of PC1 vs. PC2

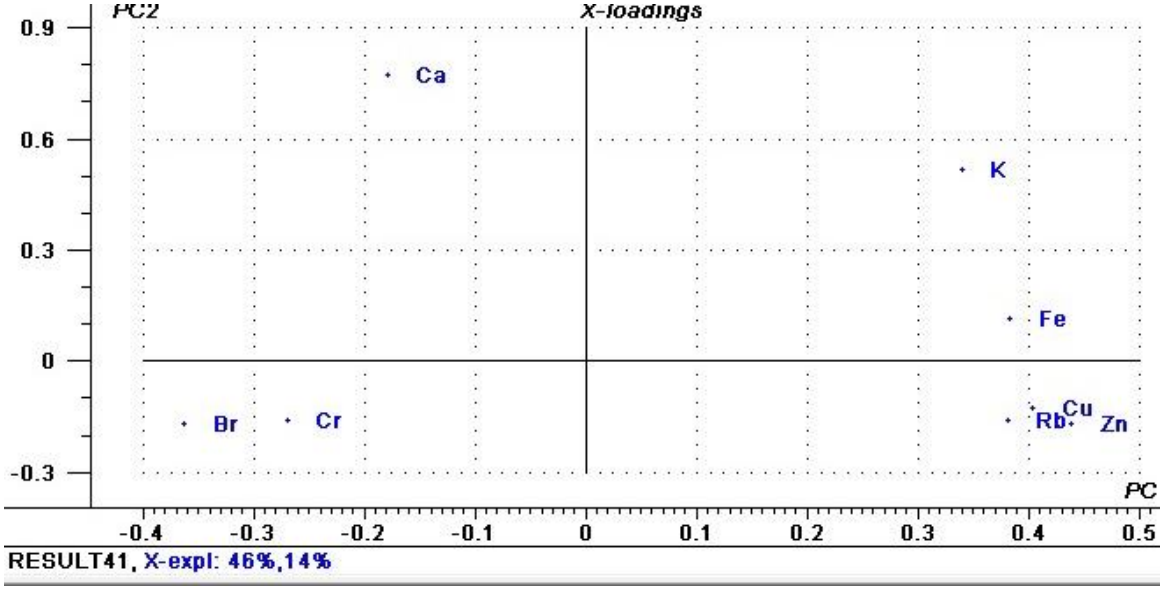

Fig. AIII 2-2 Loading Plot of PC1 vs. PC2

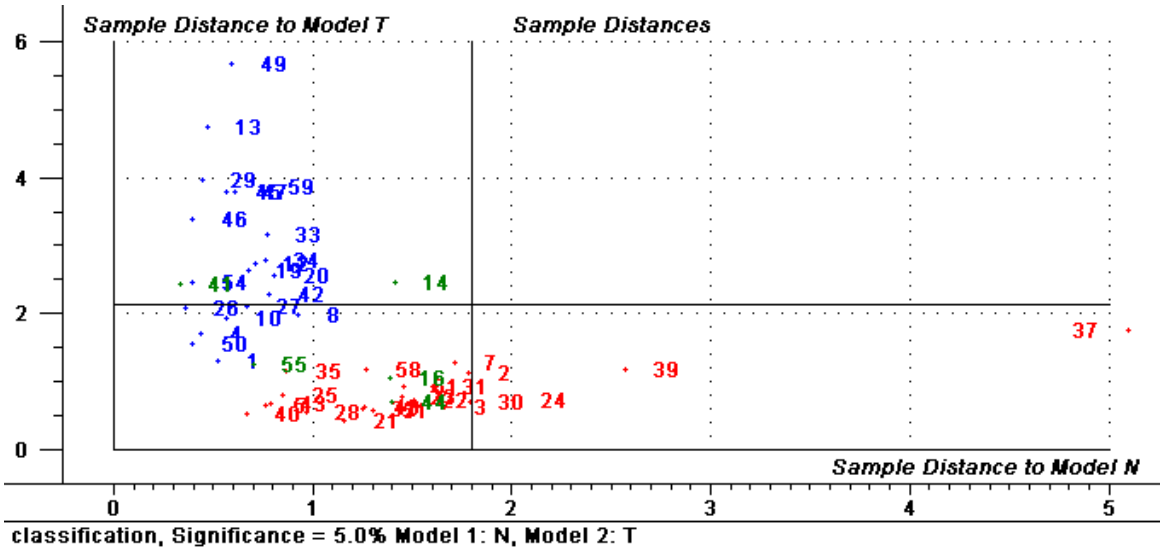

Fig. AIII 2-3 Coomans Plot, classification result

AIII. 3 Fourth subgroup classification results

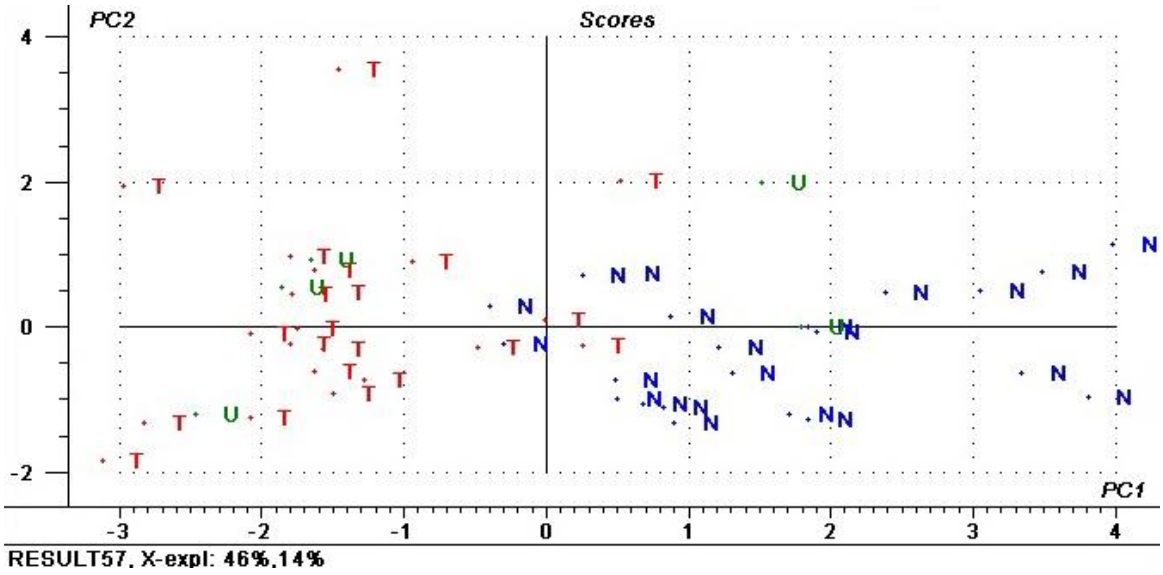

Fig. AIII 3-1 Score Plot of PC1 vs. PC2

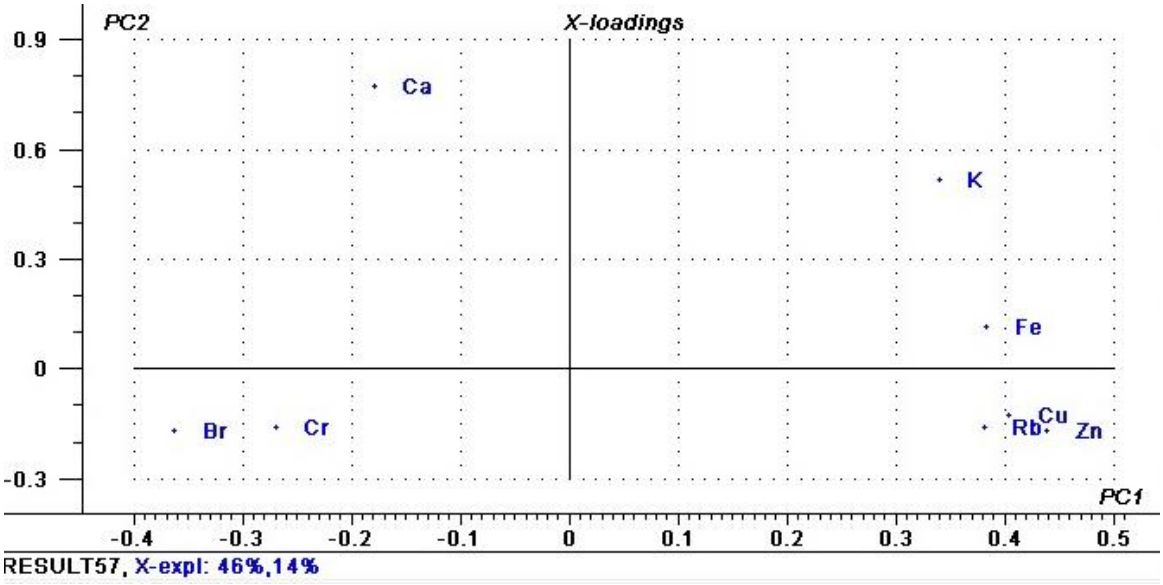

Fig. AIII 3-2 Loading Plot of PC1 vs. PC2

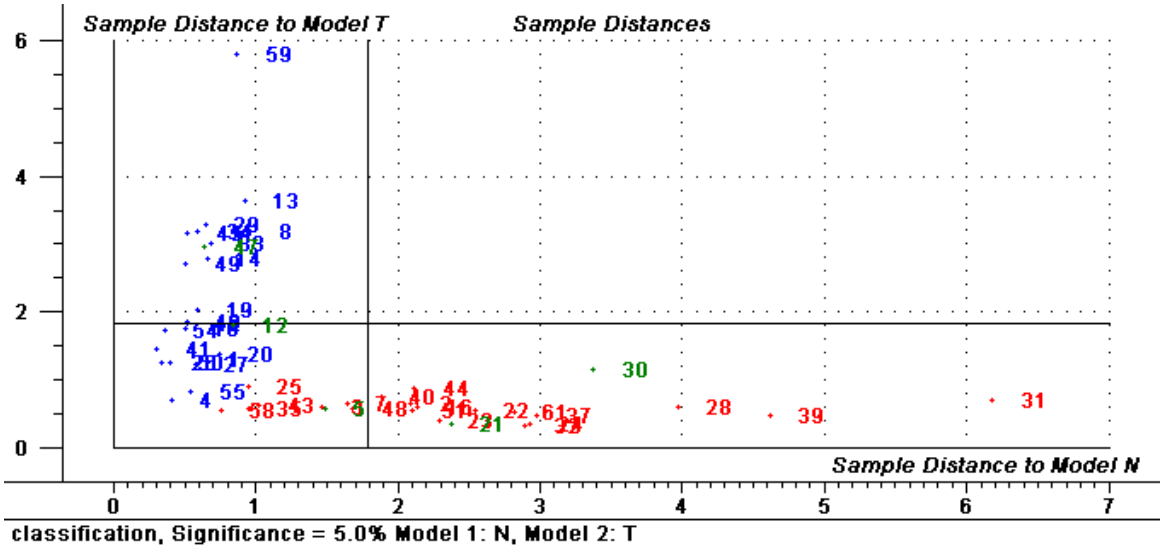

Fig. AIII 3-3 Coomans Plot, classification result

APPENDIX IV : Score, Loading and Coomans Plots for Second, Third and Fourth Subgroup (Coherent Scatter)

AIV. 1 Second subgroup classification results

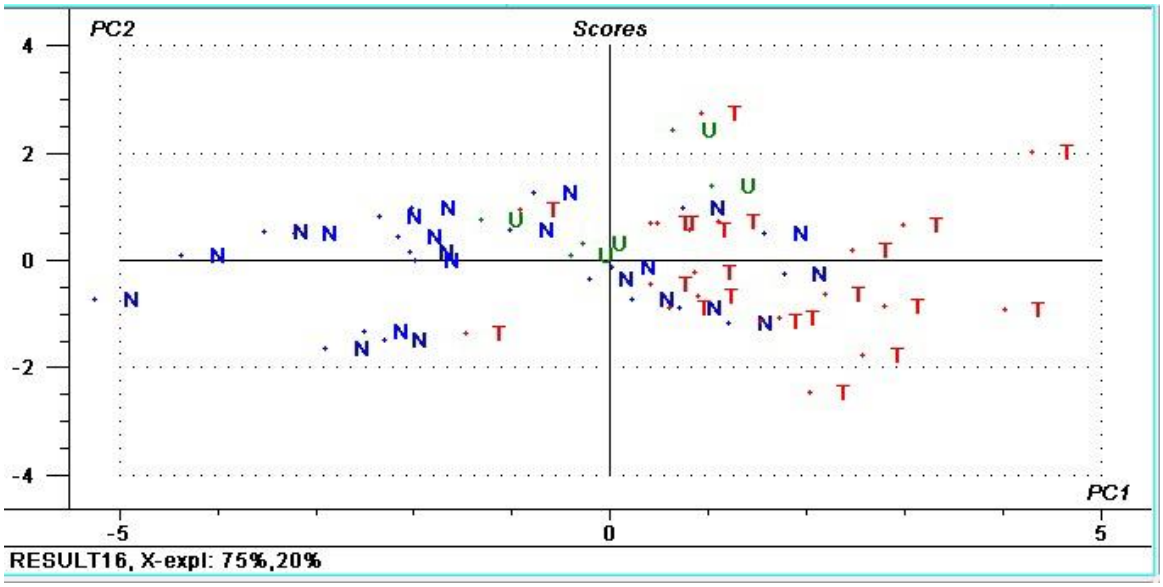

Fig. IV 1-1 Score Plot of PC1 vs. Pc2

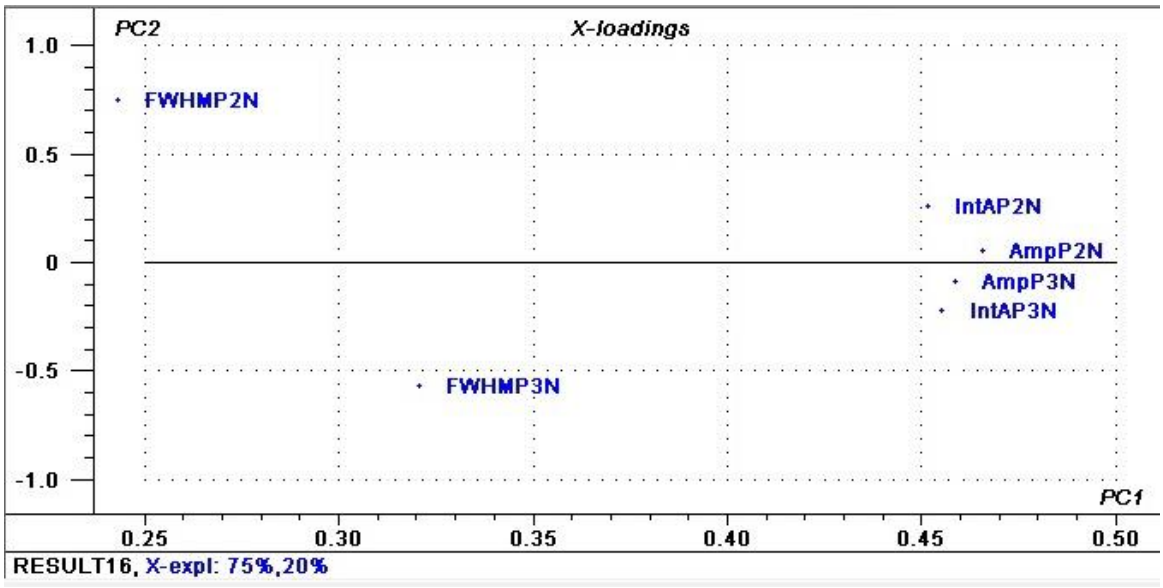

Fig. IV 1-2 Loading Plot of PC1 vs. PC2

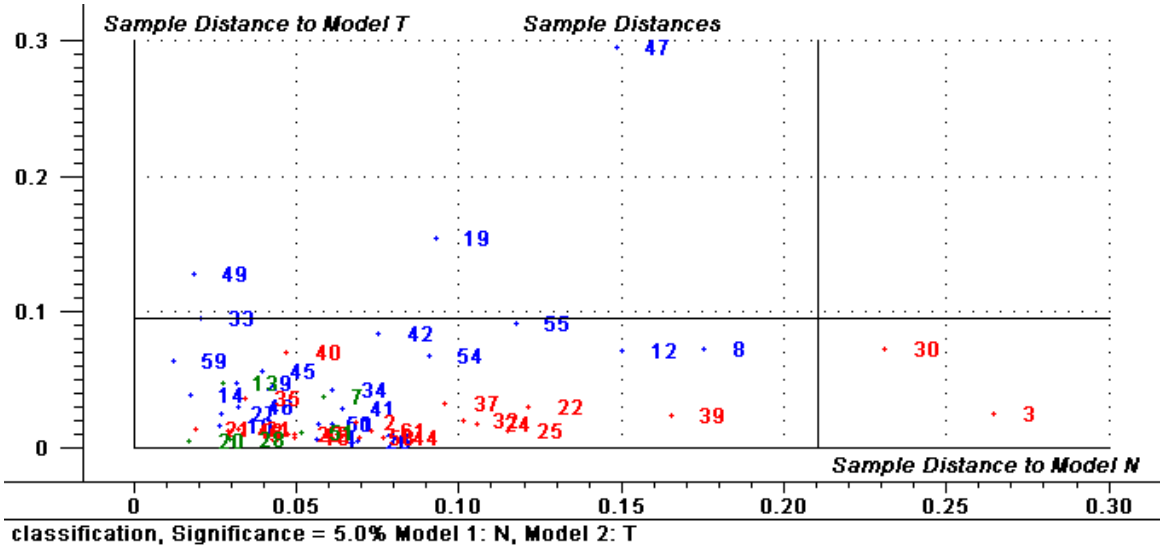

Fig. IV 1-3 Coomans plot, classification result

AIV. 2 Third subgroup classification results

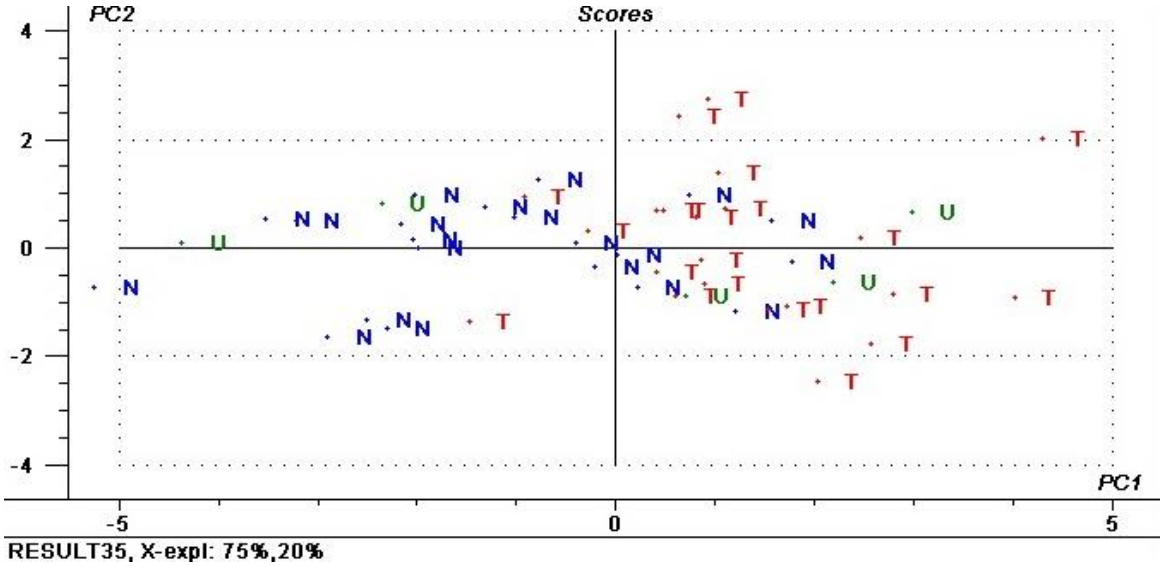

Fig. IV 2-1 Score Plot of PC1 vs. PC2

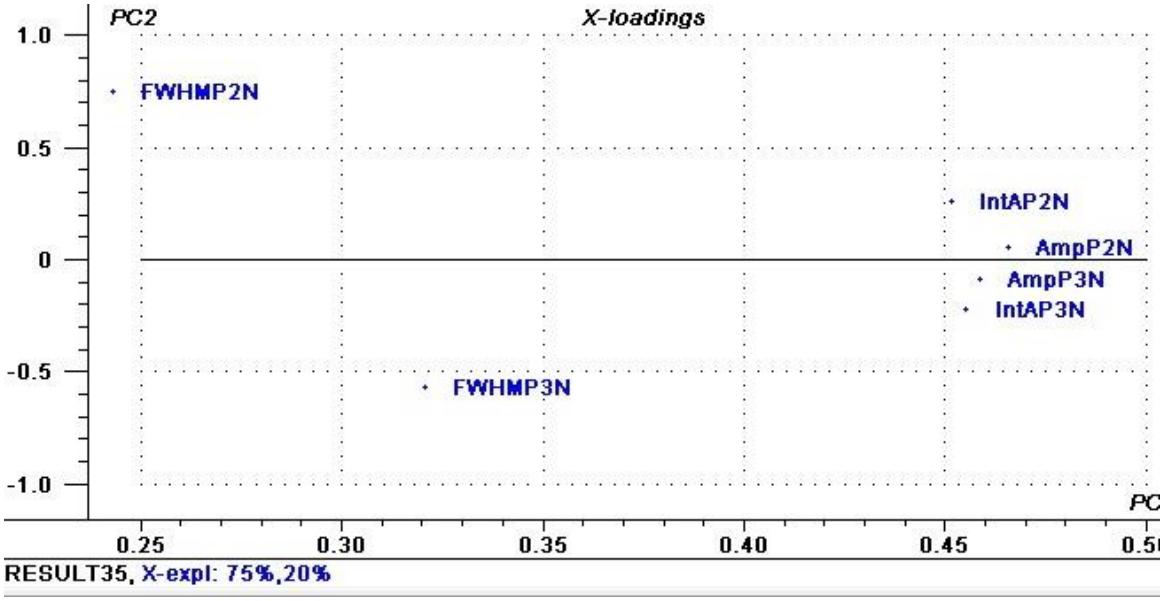

Fig. IV 2-2 Loading Plot of PC1 vs. PC2

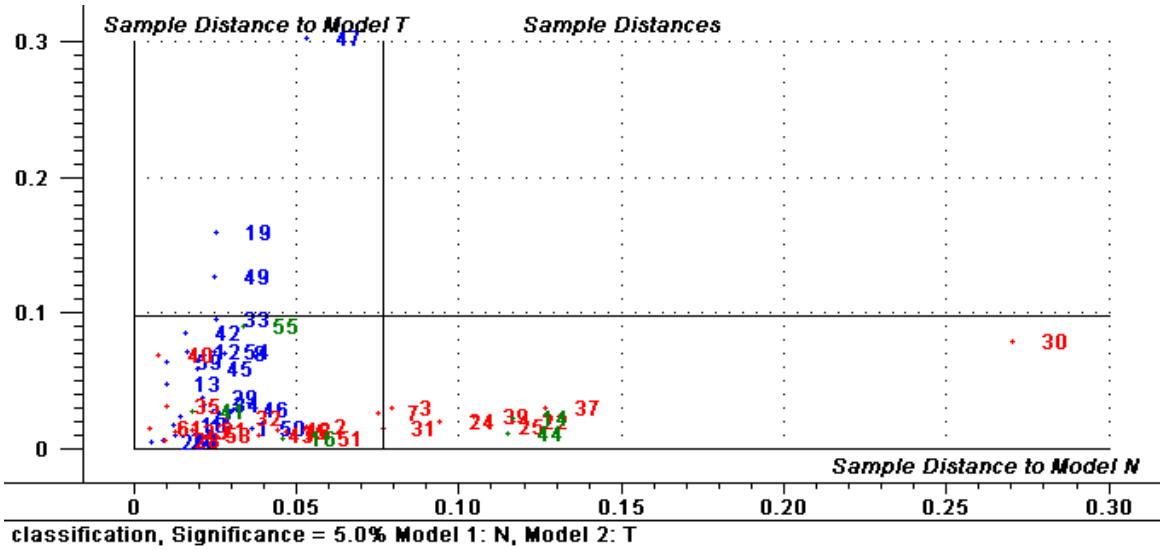

Fig. IV 2-3 Coomans plot, classification result

AIV. 3 Fourth subgroup classification results

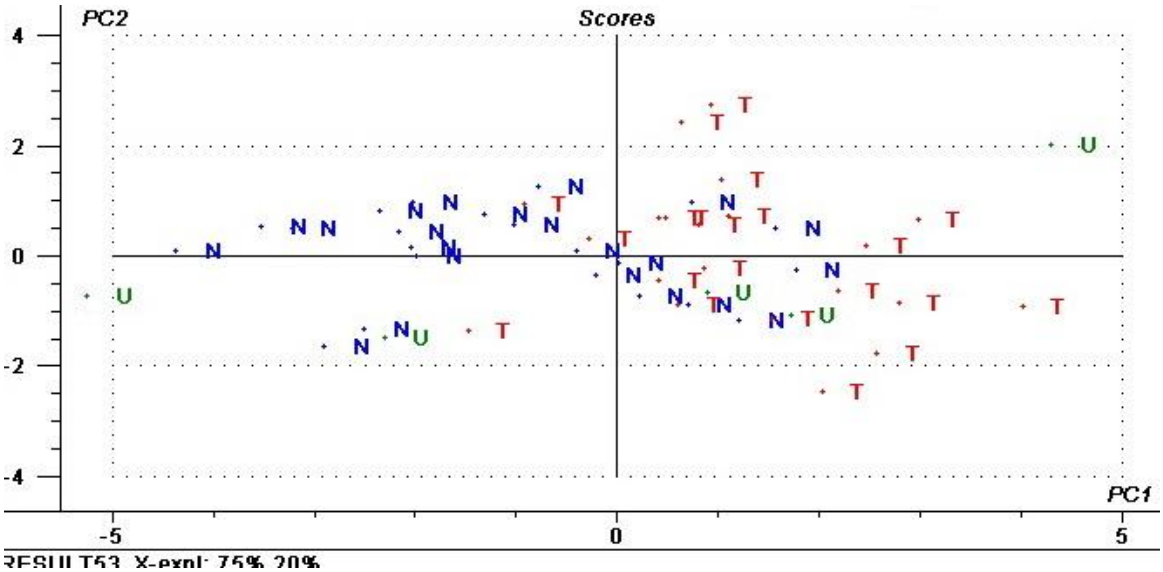

Fig. IV 3-1 Score Plot of PC1 vs. PC2

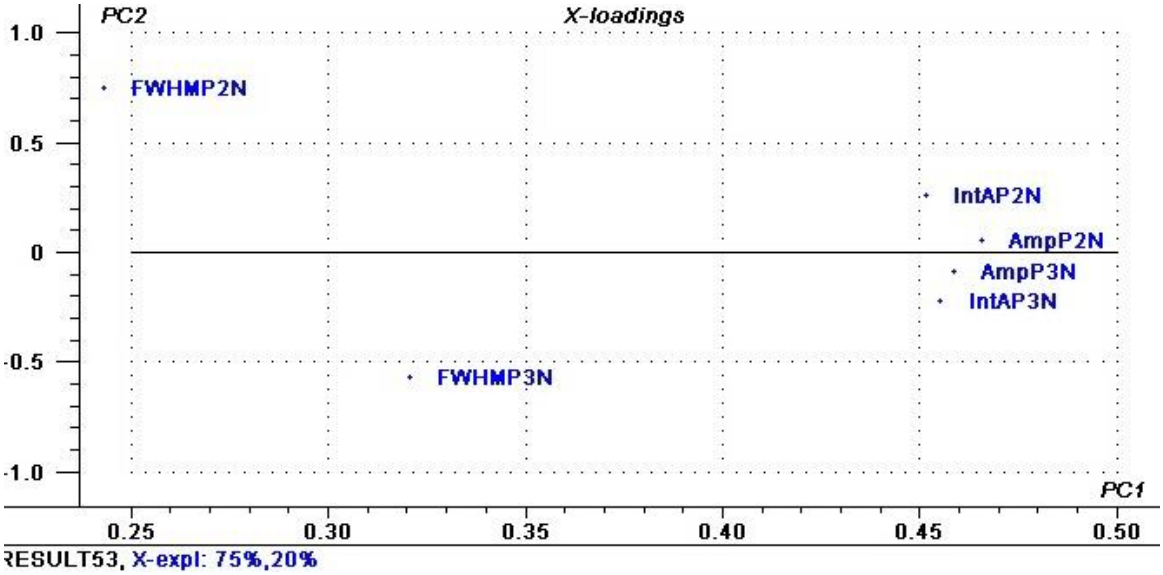

Fig. IV 3-2 Loading Plot of PC1 vs. PC2

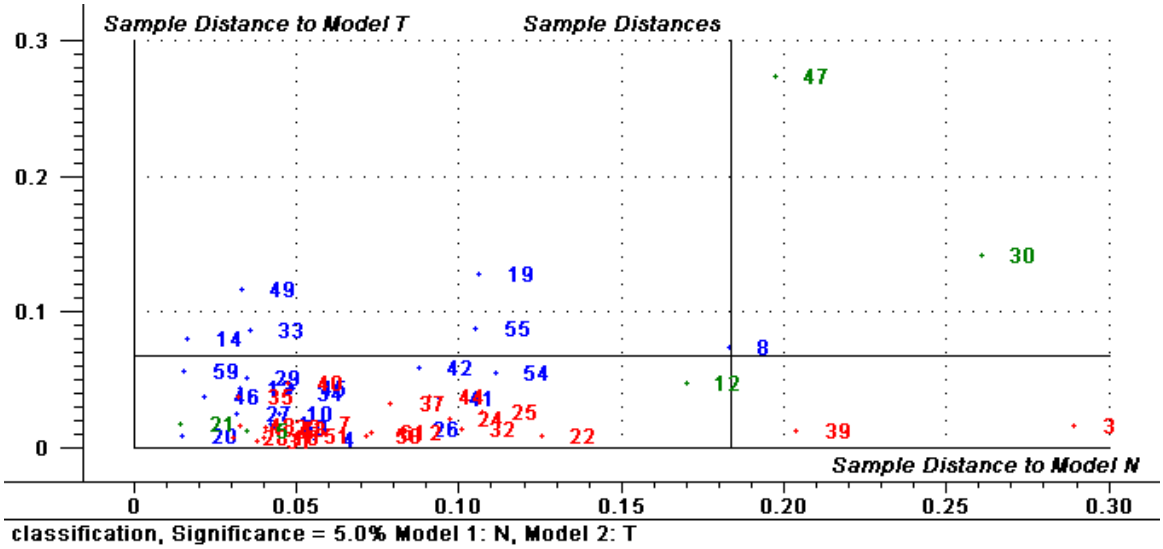

Fig. IV 3-3 Coomans plot, classification result

APPENDIX V : Score, Loading and Coomans Plots for Second, Third and Fourth Subgroup (Elemental Ratio study)

AV. 1 Second subgroup classification results

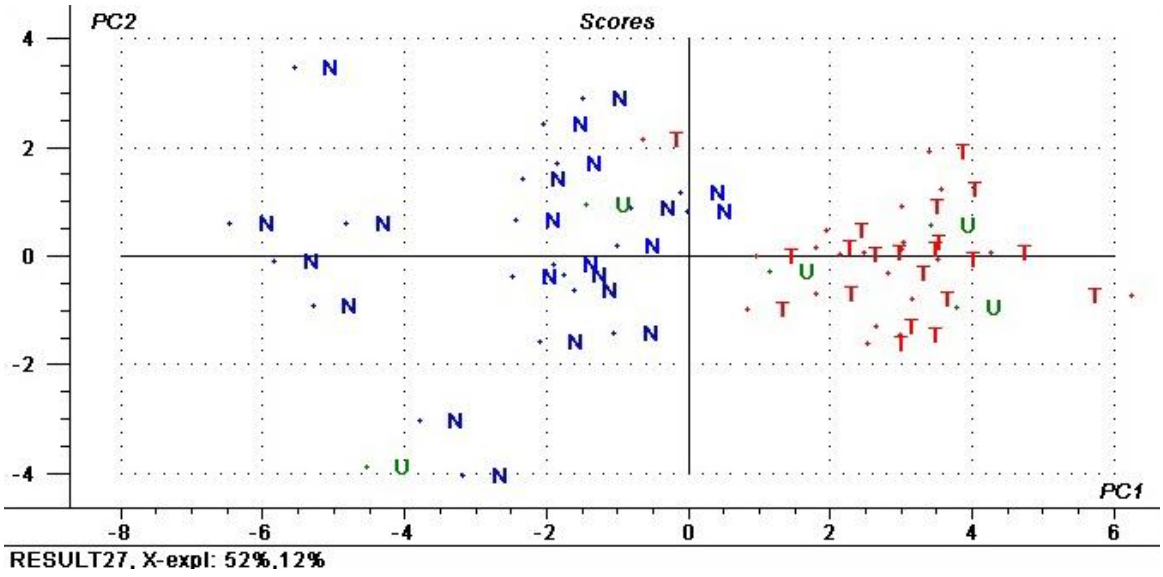

Fig. AV 1-1 Score Plot of PC1 vs. PC2

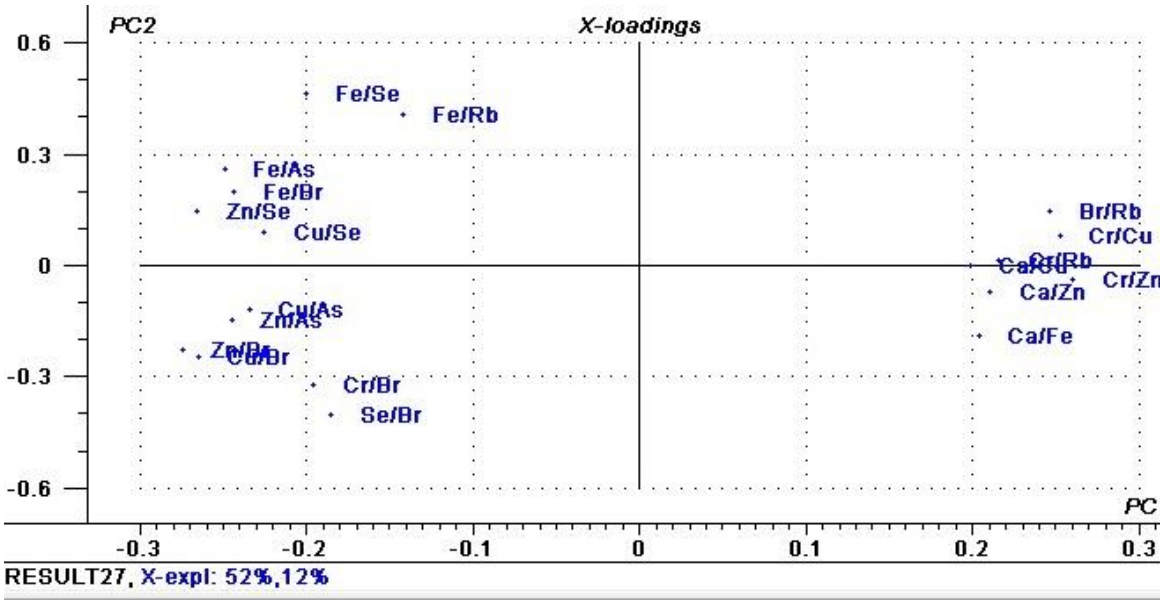

Fig. AV 1-2 Loading Plot of PC1 vs. PC2

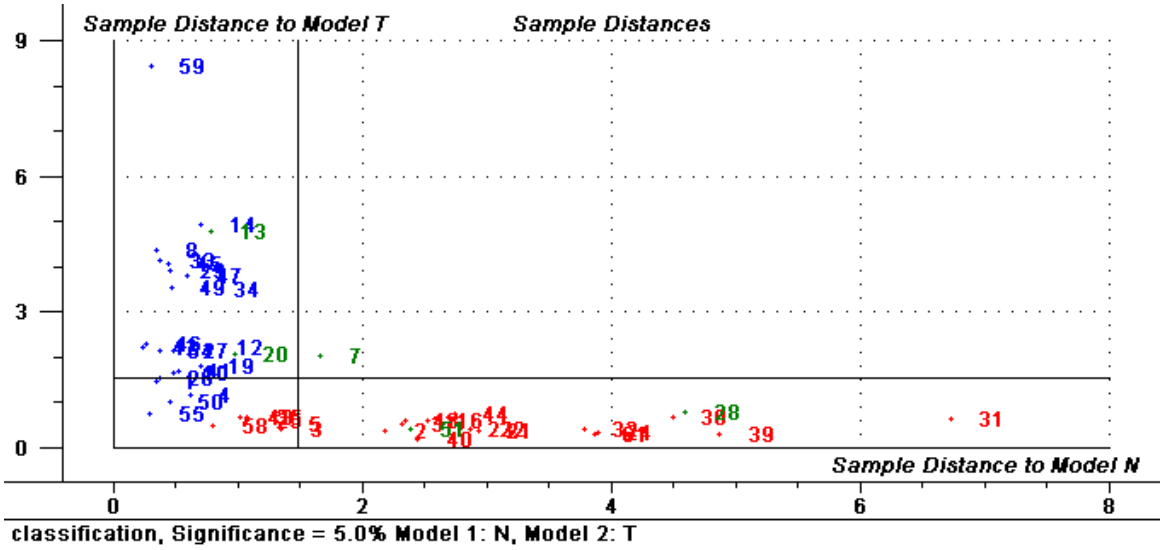

Fig. AV 1-2 Coomans plot, classification result

AV. 2 Third subgroup classification results

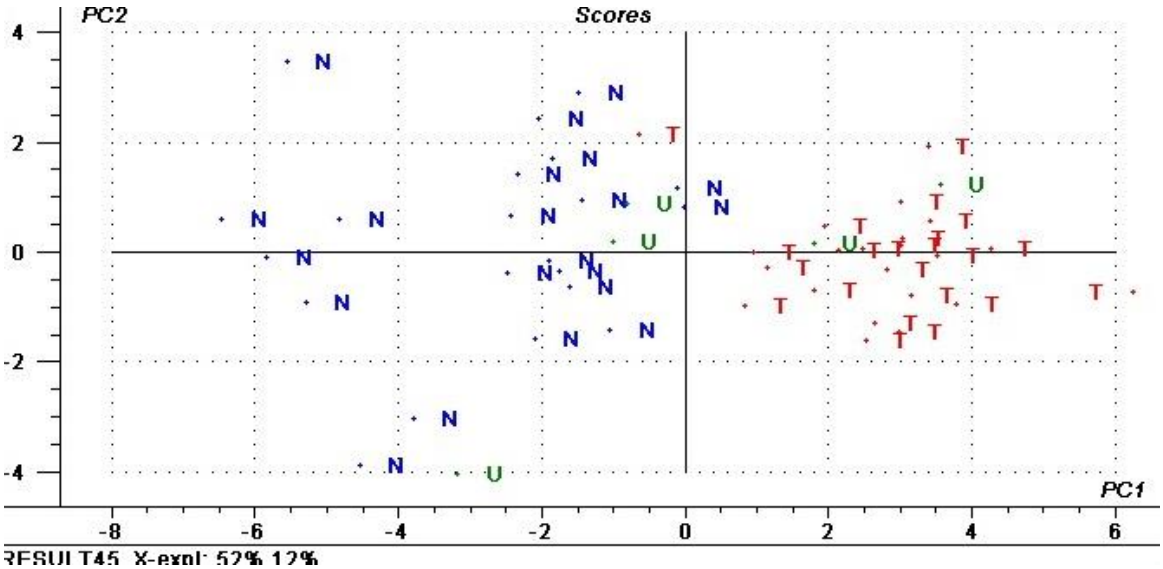

Fig. AV 2-1 Score Plot of PC1 vs. PC2

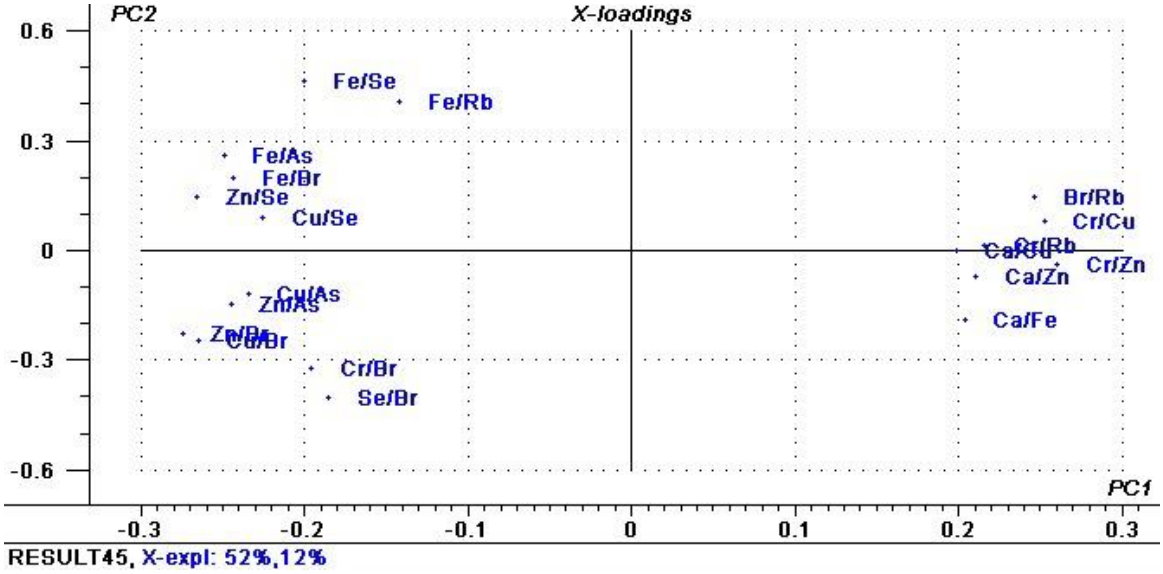

Fig. AV 2-2 Loading Plot of PC1 vs. PC2

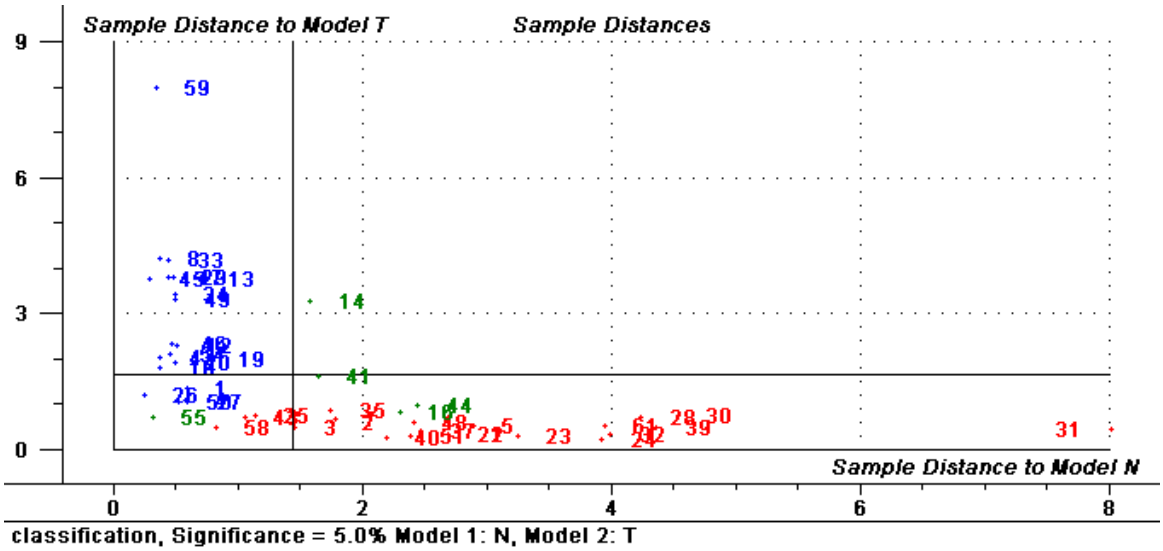

Fig. AV 2-3 Coomans plot, classification result

AV. 3 Fourth subgroup classification results

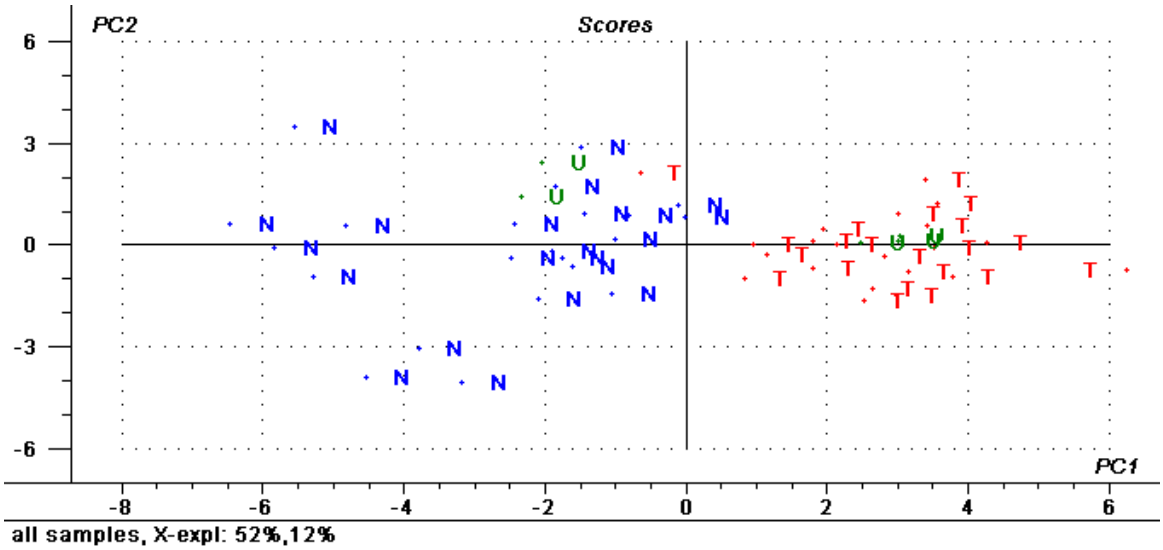

Fig. AV 3-1 Score Plot of PC1 vs. PC2

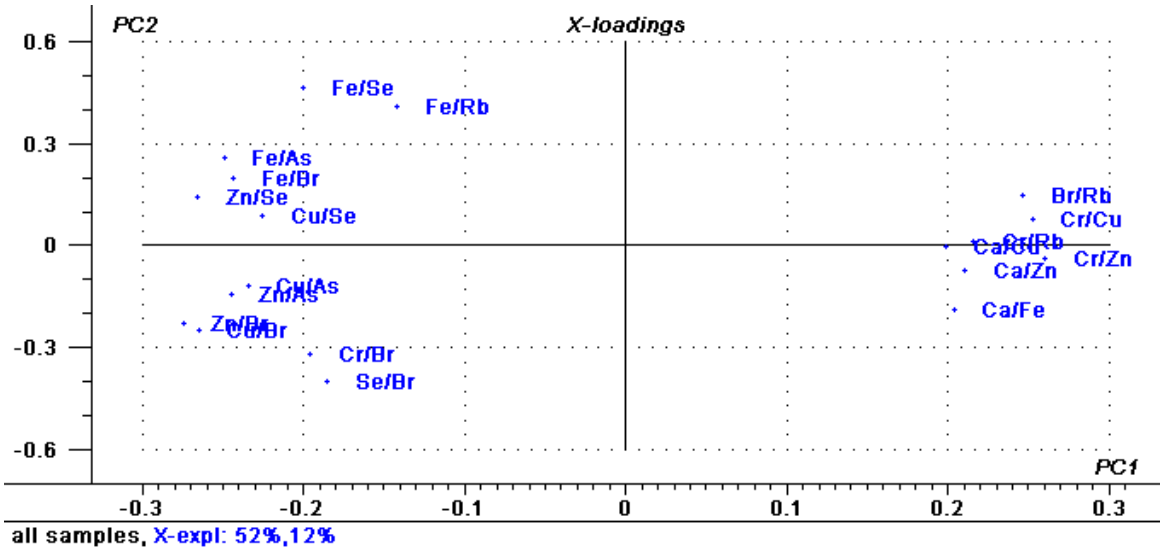

Fig. AV 3-2 Loading Plot of PC1 vs. PC2

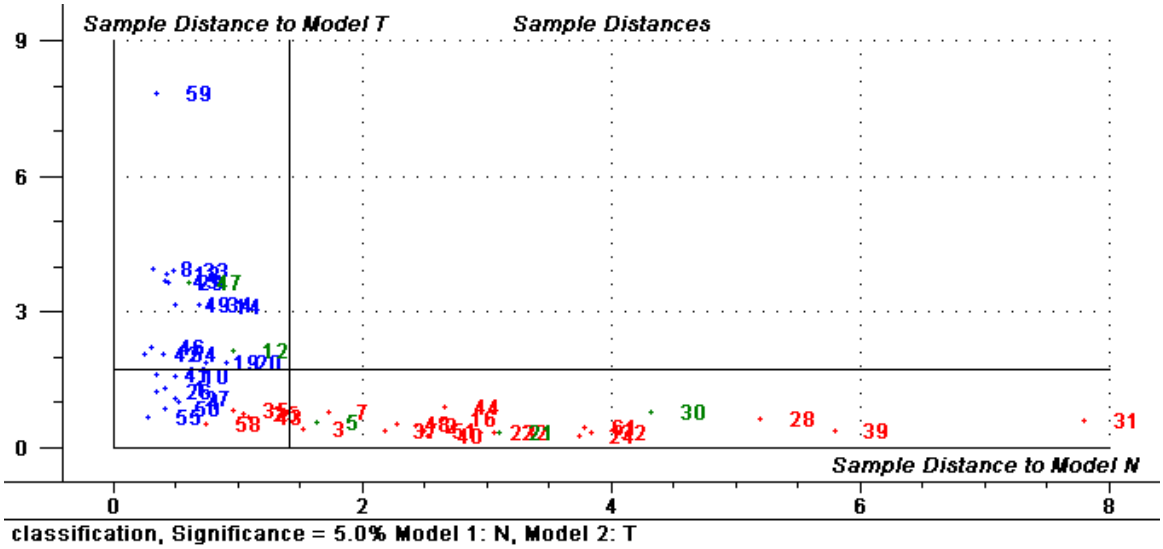

Fig. AV 3-3 Coomans plot, classification result

APPENDIX VI : Score, Loading and Coomans Plots for Second, Third and Fourth Subgroup (Combined Data Study)

AVI. 1 Second Subgroup Classification Results

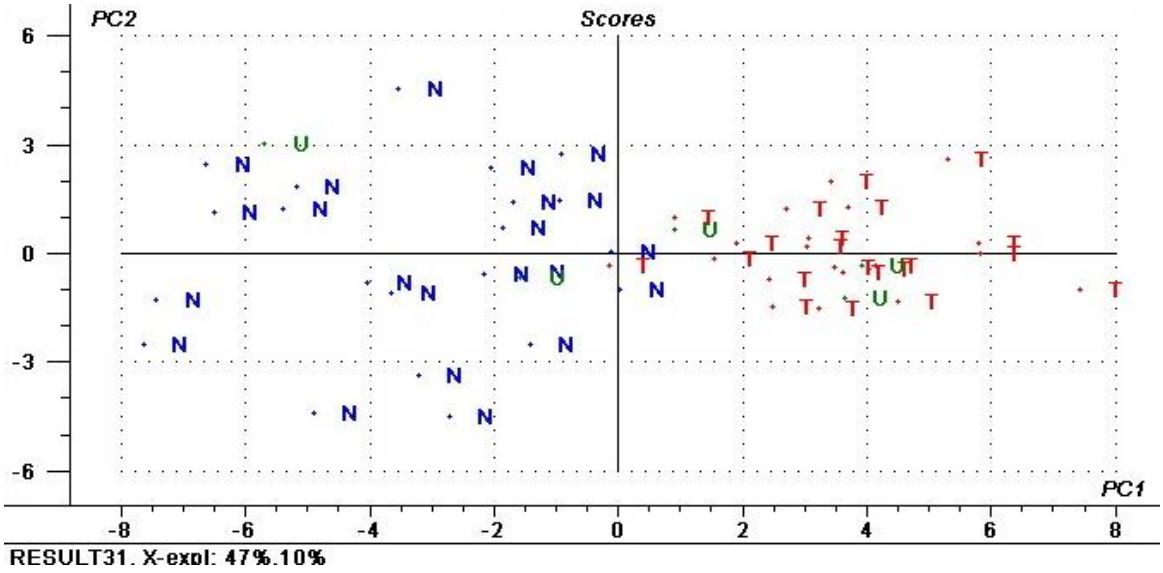

Fig. AVI 1-1 Score Plot of PC1 vs. PC2

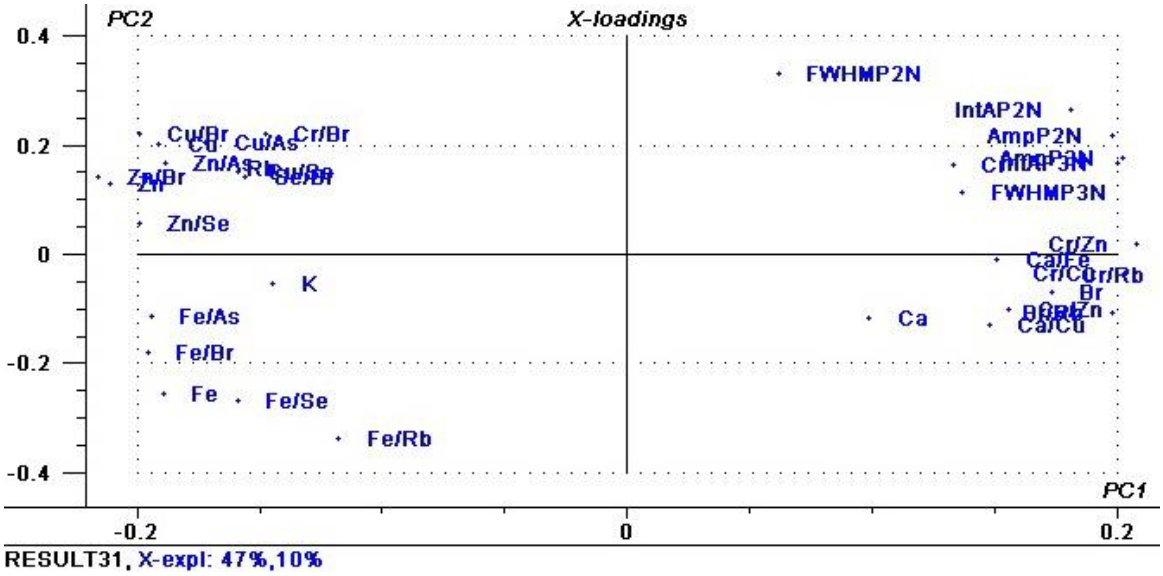

Fig. AVI 1-2 Loading Plot of PC1 vs. PC2 (combined data as variables-second subgroup)

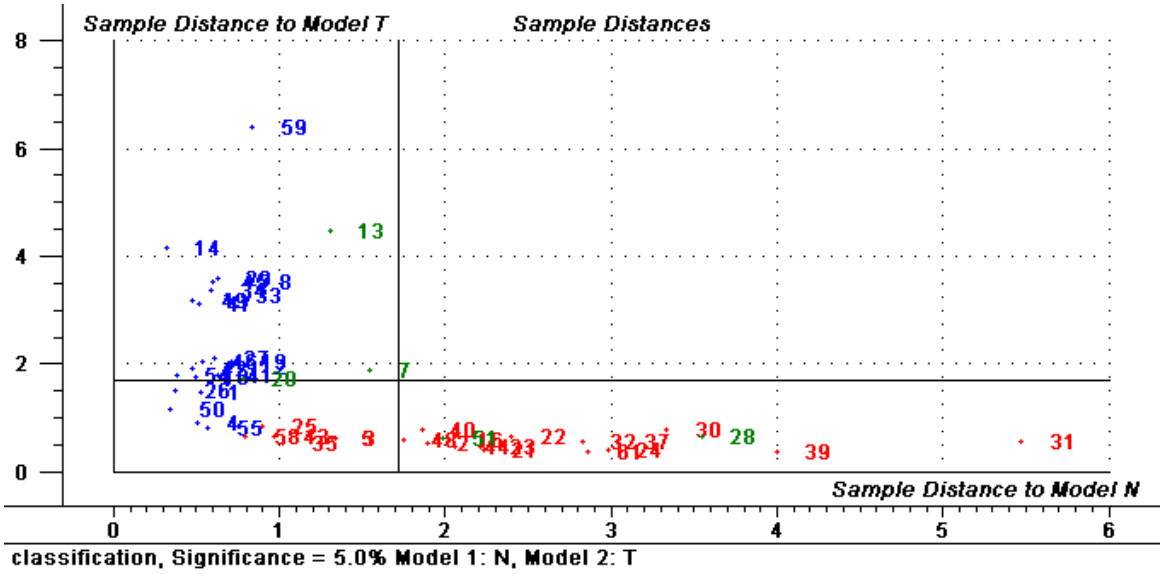

Fig. AVI 1-3 Coomans plot, classification result

AVI. 2 Third Subgroup Classification Results

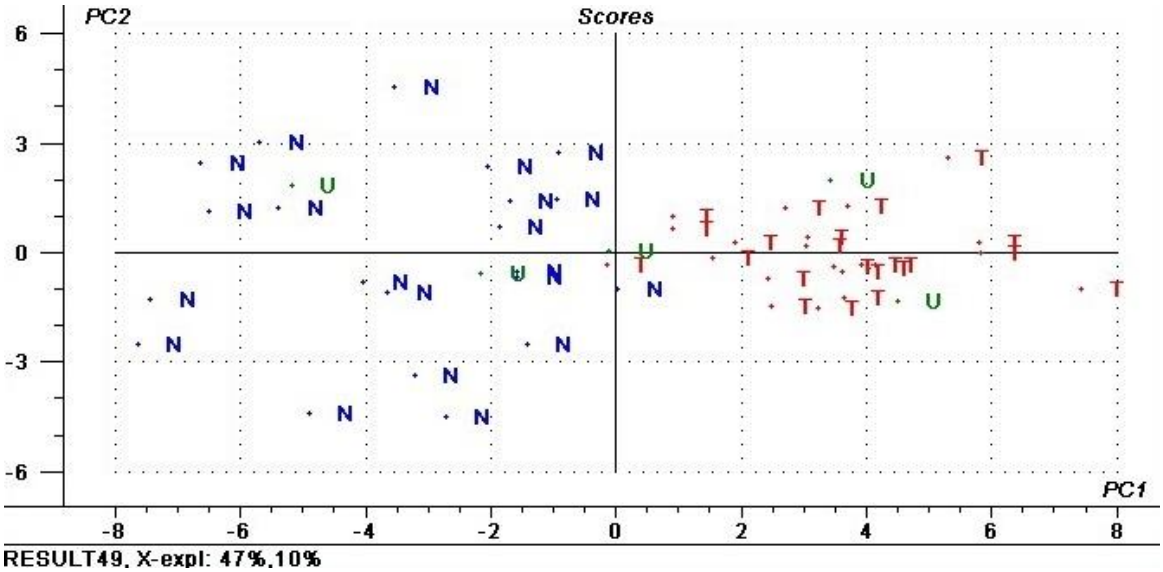

Fig. AVI 2-1 Score Plot of PC1 vs. PC2

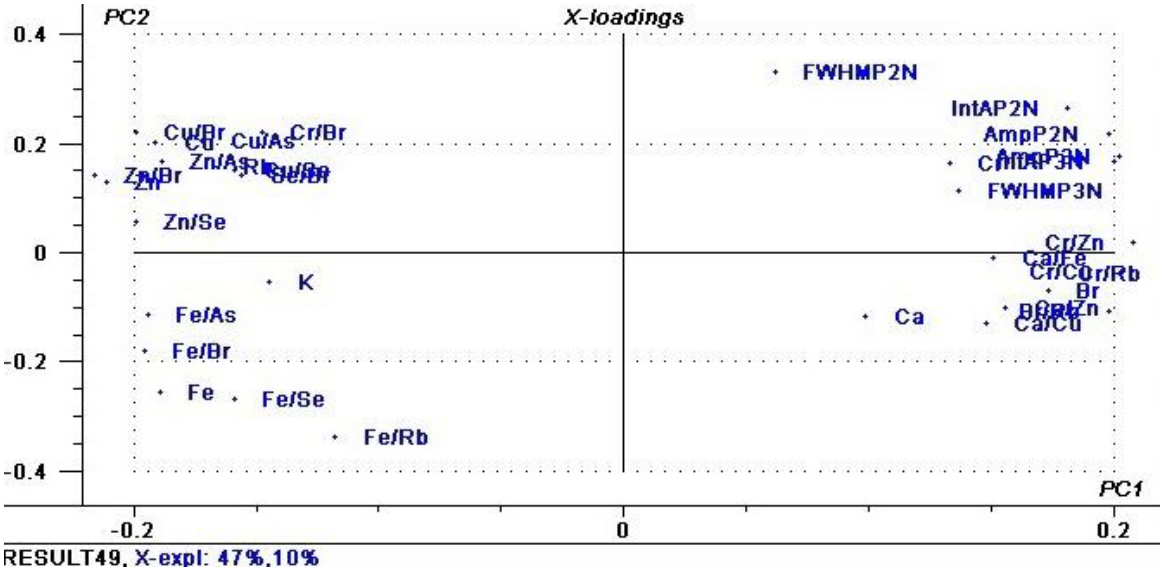

Fig. AVI 2-2 Loading Plot of PC1 vs. PC2

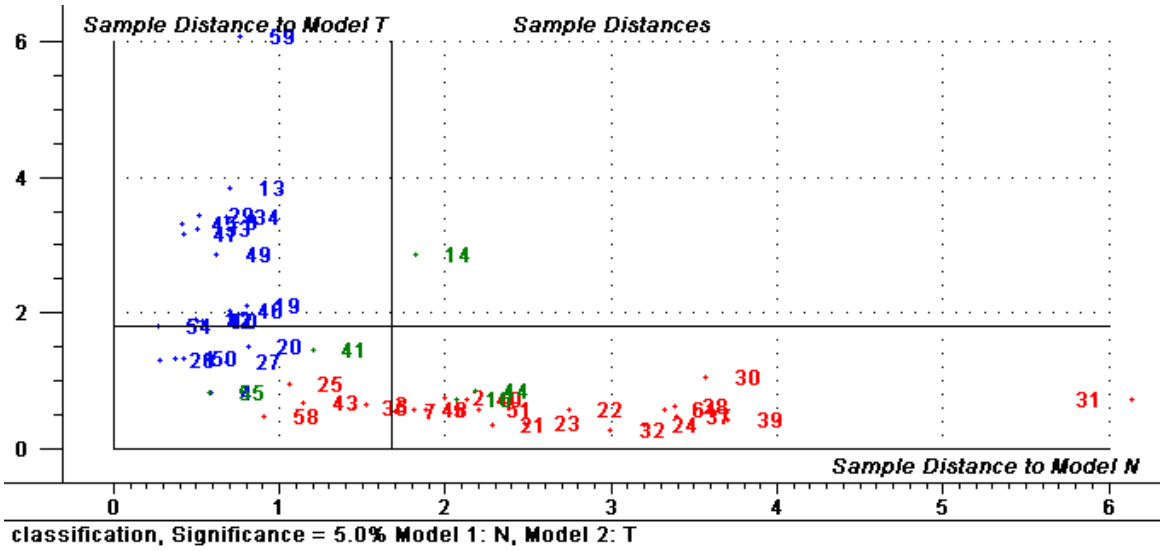

Fig. AVI 2-3 Coomans plot, classification result

AVI. 3 Fourth Subgroup Classification Results

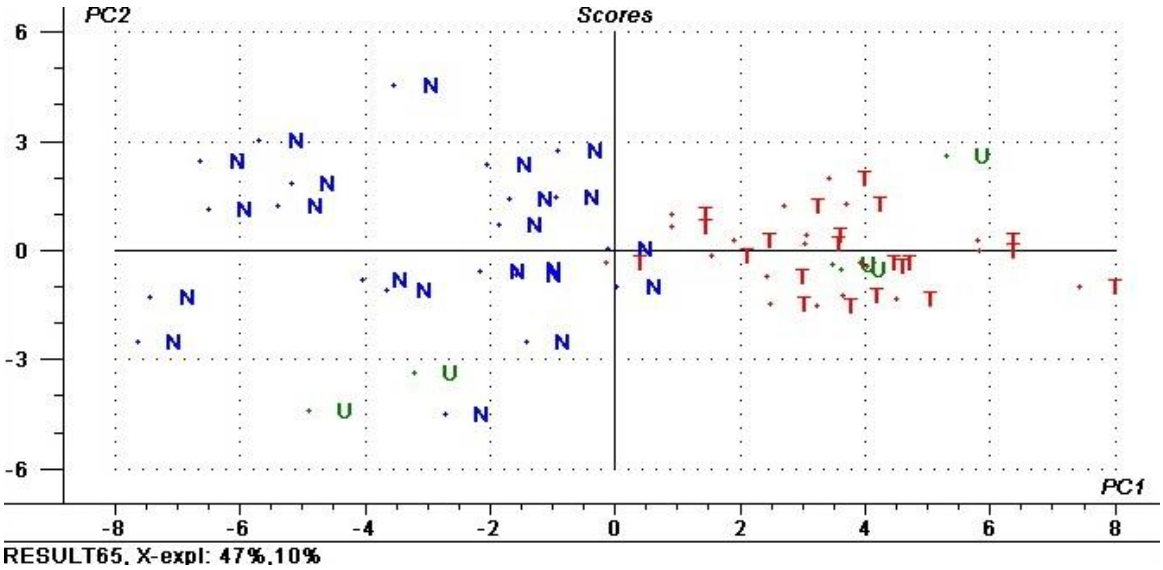

Fig. AVI 3-1 Score Plot of PC1 vs. PC2

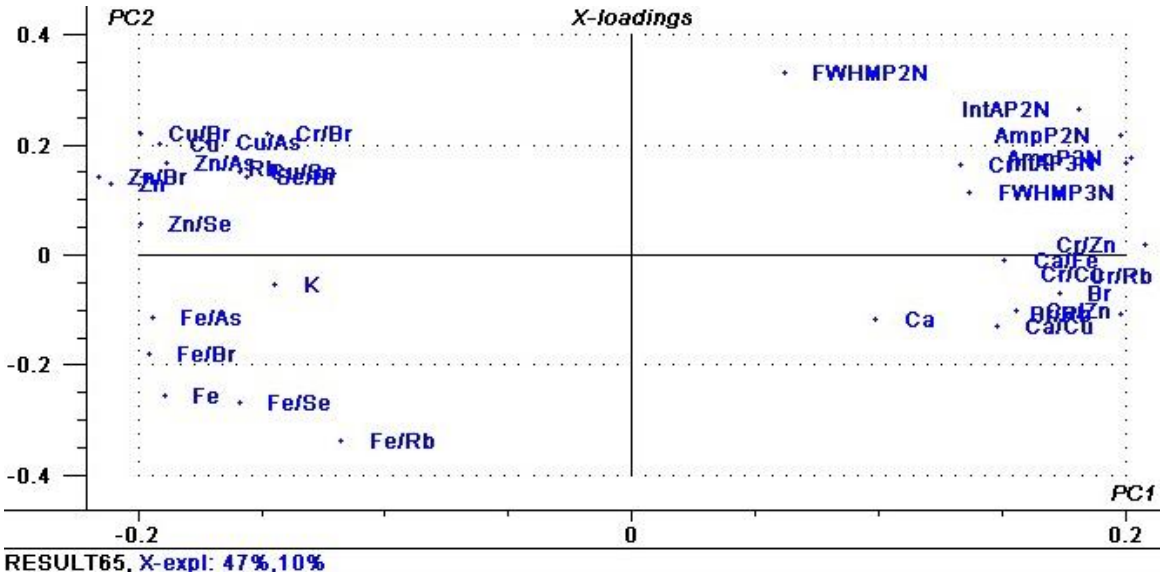

Fig. AVI 3-2 Loading Plot of PC1 vs. PC2

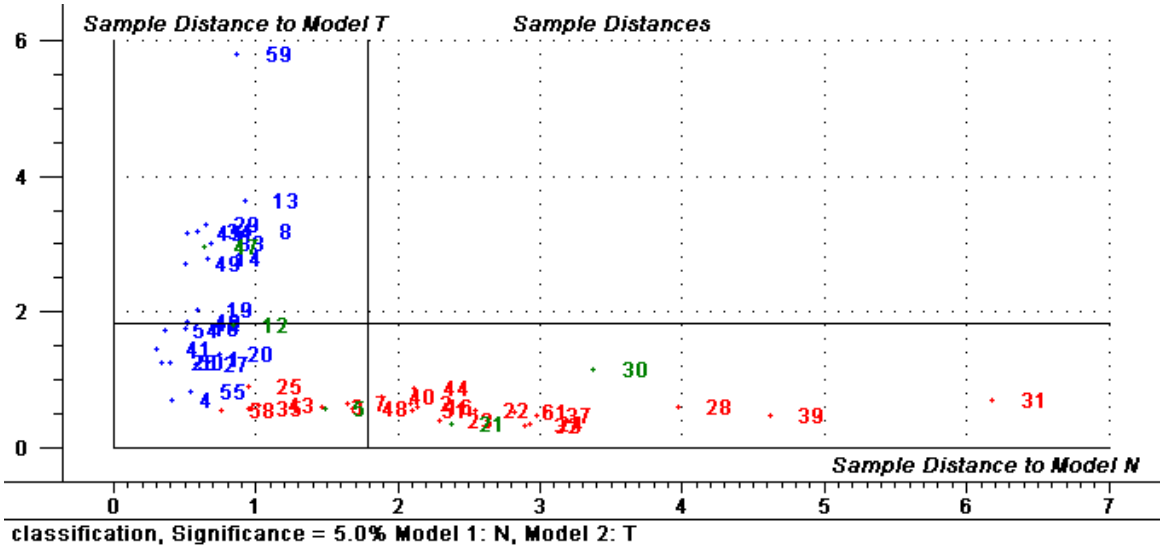

Fig. AVI 3-3 Coomans plot, classification result